THEORETICAL AND EXPERIMENTAL INVESTIGATIONS OF THE INCEPTION OF CAVITATION

By

GLENNON MAPLES

Bachelor of Science
Mississippi State University
State College, Mississippi
1955

Master of Science
Mississippi State University
State College, Mississippi
1961

Submitted to the faculty of the Graduate College of the Oklahoma State University in partial fulfillment of the requirements for the degree of DOCTOR OF PHILOSOPHY
May, 1967

THEORETICAL AND EXPERIMENTAL INVESTIGATIONS OF THE INCEPTION OF CAVITATION

Thesis Approved:

Thesis Adviser

Dean of the Graduate College

ACKNOWLEDGMENT

The writer would like to extend sincere appreciation to the following individuals who have had a part, in one way or another, in aiding me during my doctoral program:

Particularly my graduate committee, composed of Dr. J. D. Parker, Chairman, Dr. J. A. Wiebelt, Professor F. C. McQuiston, and Dr. L. W. Johnson, who provided invaluable guidance.

For their day-to-day assistance, encouragement, and discussions throughout the course of this work, the author is indebted to two of his brothers, Dupree and Dago.

Mr. H. C. Hewitt for his technical discussions throughout this research.

Mrs. Margaret Estes and Mr. E. J. Hardy for their expert assistance in preparing the manuscript.

Mr. D. D. Fry, Mr. L. E. Wallace, and Mr. T. D. Mathis for their technical assistance throughout the course of this study.

Mr. R. A. Williams for his assistance during the latter part of the experimental program.

Most of all, to my mother and father, who made the effort worthwhile and to whom this work is dedicated.

In addition, I would like to thank the George C.

Marshall Space Flight Center, Huntsville, Alabama, for financial support during this study.

TABLE OF CONTENTS

LIST OF TABLES

LIST OF FIGURES

NOMENCLATURE

A	cross-sectional area
a_v/a_ℓ	cavitation form parameter based on areas
c	speed of sound in fluid
C	chord length
C_D	discharge coefficient
C_i	$369\ n_1 T$ $(ft - lbs_f)$
C_p	pressure coefficient
C_{p_ℓ}	specific heat of liquid
$C_{p_{min_s}}$	minimum-pressure coefficient of a smooth surface
$\overline{d}$	pipe diameter
D	diameter
D^*	critical bubble diameter
F_L	Froude number
g	acceleration of gravity
g_c	gravitational constant
h	height of roughness element
h_c	p_i/ρ_o
h_v	p_v/ρ_o
h_∞	p_∞/ρ_o
H	boundary layer shape parameter
H_1, H_2, H_3, H_4	height of mercury or water

H_{tap}	distance from tap opening in test section to "0" point of manometer "1"
k	coefficient of heat conduction
K	cavitation number
K_d	desinent cavitation number evaluated at plane of desinent cavitation
K_i	incipient cavitation number evaluated at plane of incipient cavitation
K_o	cavitation number evaluated at reference plane "0"
K_t	cavitation number evaluated at reference plane "t"
K_{d_o}	desinent cavitation number evaluated at reference plane "0"
K_{i_o}	incipient cavitation number evaluated at reference plane "0"
K_{i_t}	incipient cavitation number evaluated near plane of incipient cavitation
K_{r_o}	incipient cavitation number of roughness element evaluated at reference plane "0"
$\overline{K}_o$	modified cavitation number (equation (2-9))
L_1	length or any linear dimension
L_v	latent heat of vaporization
M	Mach number
m_g	mass of inert gas in bubble
n	polytropic constant
n_1	number of moles of gas
N	number of nuclei per unit volume of the fluid
p, p_x	local pressure
p_A	constant pressure part of forcing function
p_b	back pressure or pressure at an arbitrary position upstream of plane of incipient cavitation (see Figure 59)

p_b'	pressure at same position as p_b (see Figure 59)
p_c	minimum pressure in test section with cavitation present (equation (6-4))
p_c'	minimum pressure in test section without cavitation present (see Figure 59)
p_d	stream pressure at plane of desinent cavitation
p_e	exit pressure
p_g	partial pressure of inert gas
p_i	stream pressure at plane of incipient cavitation
p_o	pressure within liquid at reference "0"
p_t	pressure at throat of test section
p_v	vapor pressure
p_{d_o}	stream pressure for desinent cavitation evaluated at reference "0"
p_{g_o}	initial inert gas pressure
p_{i_o}	stream pressure for incipient cavitation evaluated at reference "0"
p_{i_t}	pressure near plane of incipient cavitation
p^*	$(p_\infty - p_v)_{min}$
p_∞	pressure within liquid far from bubble
P	total pressure within bubble
Pe	Peclet number
P_{min}	minimum pressure in flow field
q_f	energy dissipated through friction heating
r	radius in spherical coordinate system
R	bubble radius
$\overline{R}$	radius of centerline of elbow
$\underline{R}$	radius of circular arc
$\dot{R}$	velocity of bubble's wall

$\ddot{R}$	acceleration of bubble's wall
R^*	critical bubble radius
R_o	initial bubble radius
R_E	Reynolds number
R_g	gas constant for inert gas
R_{ms}	maximum stable bubble radius
R_v	radius of a vapor bubble
t	time
$\overline{t}_{max}$	maximum thickness of hydrofoil
T	temperature
T_i	temperature within bubble
T_o	initial temperature
v	specific volume of mixture within bubble
v_ℓ	specific volume of liquid
v_v	specific volume of vapor
V	mass velocity
$\underline{V}$	volume of bubble
V_o	mass velocity at reference "O"
V_r	velocity in radial direction
V_t	mass velocity at throat "t"
V_x	mass velocity at location "x"
V_{d_o}	mass velocity evaluated at reference "O" during incipient cavitation
V_{i_t}	mass velocity at throat during incipient cavitation
W	Weber number
x	distance measured along axis
z	elevation

Z	arbitrary function of time

Greek

α	air content of liquid
α/α_s	relative air content
$\overline{\beta}$	1.03 psi/PPM (PPM is parts per million)
γ/γ_s	relative dissolved oxygen content of water (where γ is quantity of dissolved oxygen in water and γ_s is quantity of dissolved oxygen in saturated water at the same temperature)
δ	boundary layer thickness
δ^*	displacement thickness
θ	momentum thickness, coordinate angle
μ	dynamic viscosity
ν	kinematic viscosity
ρ_o, ρ_L	mass density of liquid
σ	surface tension
$\sigma_{rr}, \sigma_{\theta\theta}, \sigma_{\Phi\Phi}, \sigma_{\theta\Phi}, \sigma_{\Phi r}, \sigma_{r\theta}$	stress components
Ψ	arbitrary function of time
ω	angular velocity

CHAPTER I

INTRODUCTION

In the latter half of the nineteenth century, the screw propeller began to replace the paddle wheel as the most efficient means of ship propulsion. As the speed of the shaft revolution was increased, a point was reached where the propellers "raced," the efficiency deteriorated, and the power needed could not be delivered to the water. As early as 1873, Osborne Reynolds attributed racing to what he described as the admission of air to the propeller which would interfere with the supply of water to the blades. While this turned out not to be the explanation for the observations of the time, such air admission would indeed result in what we now call "ventilation," with the same effects.

The mystery was finally cleared up in the 1890's to the extent that the source of the trouble was identified and given a name. The new phenomenon was called "cavitation" by R. E. Froude.

Cavitation has long been of interest and importance in the fields of shipbuilding and hydraulic machinery. In recent years cavitation has become of increasing interest and importance in a number of other applications and technologies. Among the latter are such diverse disciplines as

chemical processing (acceleration of reactions and industrial cleaning), nuclear physics (use of bubble chambers for research on high-energy particles), and handling of highly volatile liquid rocket fuels and cryogenic liquids.

Cavitation is defined as the process of formation of the vapor phase of a liquid when it is subjected to reduced pressures at constant liquid temperature. In general a liquid is said to cavitate when vapor bubbles are observed to form and grow as a consequence of pressure reduction. When the phase transition is a result of pressure change by hydrodynamic means, a two-phase flow composed of a liquid and its vapor is called a cavitating flow. These definitions imply a distinction between phase transitions associated with reduction of pressure (cavitation) and addition of heat (boiling). Heat-transfer effects may play an important role in many cases of cavitating liquids. Such effects are especially important in liquids near their boiling points. From a purely physical-chemical point of view, of course, no distinction need be made between boiling and cavitation, at least in so far as the question of inception is concerned.

It is now the generally accepted view that the inception of cavitation is associated with the growth of nuclei (sub-microscopic in size) which contain vapor, undissolved gas, or both, and which are present either within the liquid or in crevices on suspended particle matter or on boundary walls. Some insight into the many variables that affect the inception of cavitation may be gained through a theoretical

investigation of the growth of small nuclei. The theoretical investigation consists of solving the differential equation which describes the motion of small nuclei under transient pressures. The nuclei content and initial radii are unknowns; nevertheless, important trends can be obtained by making the necessary assumptions which are needed to obtain solutions to the equation of motion. The effects of viscosity, surface tension, density, velocity, inert gas content, polytropic changes within nuclei, and vapor pressure upon nuclei growth are shown in this paper.

Extensive past experimentation concerning the true liquid pressure at the occurrence of cavitation has shown that, in general, the pressure at the initiation of cavitation is not the equilibrium vapor pressure, and in many instances is not even representative of the vapor pressure. Lehman and Young [3]* measured pressures near the plane of incipient cavitation for water flowing through venturi type test sections. They reported only one pressure which was below the liquid vapor pressure. This is not in agreement with the experimental investigation reported by Ruggeri and Gelder [33]. Ruggeri and Gelder observed the pressure at the plane of incipient cavitation to be below the liquid vapor pressure and to decrease with an increase in stream velocity.

---

*Numbers in brackets designate References listed in Bibliography.

An experimental investigation was made in order to determine the validity of reported experimental data concerning the conditions at the inception of cavitation. The objectives of the experimental investigation were two-fold. First, the necessary tests were performed to determine the validity of recent reported experimental data. This required the construction of a hydrodynamic tunnel so that venturi-type test sections could be installed and the inception of cavitation studied. Second, a comparison between the conditions at the inception of cavitation for different test sections were made. The test sections used in this investigation were axisymmetric (circular cross-section) and two-dimensional (rectangular cross-section) with converging-diverging shapes.

CHAPTER II

LITERATURE REVIEW

The literature on cavitation has grown to great proportions since studies began in the late nineteenth century. This is due to the large number of variables involved and to the wide range of the aspects of cavitation, any one of which may happen to be of prime interest to investigators in different fields. The literature reviewed on cavitation was that literature directed toward vaporous cavitation as might be expected to occur in fluids flowing through conduits.

In order to clearly bring out the problem to be discussed, it is necessary to distinguish between two broad types of cavitation. Vaporous cavitation is the sudden expansion of a vapor bubble due to vaporization of the liquid at the bubble wall, whereas gaseous cavitation is the relatively slow expansion of a gas bubble due to diffusion. Strasberg [1] showed that the critical pressure needed for vaporous cavitation would be equal to or less than the vapor pressure, whereas gaseous cavitation could occur at pressures above the vapor pressure.

Vaporous cavitation, a phenomenon caused by a decrease in the stream pressure, may occur as a result of any one or combination of the following: (1) friction in the conduit,

(2) reduction of the flow area, (3) centrifugal effects (flow in bends), (4) vibration, etc. However, pressure alone does not specify the conditions under which a flowing fluid will cavitate. It might be said that pressure below the vapor pressure is a necessary condition for vaporous cavitation; however, this is not sufficient because of other variables.

Variables Affecting Cavitation

The variables which affect the onset of cavitation may be divided into four major groups. These groups together with the individual group variables are:

I. Fluid Properties

1. Vapor pressure
2. Surface tension
3. Wettability of liquid
4. Viscosity
5. Thermal conductivity
6. Mass diffusion coefficient
7. Pressure

II. Foreign Variables

1. Dissolved gases
2. Undissolved gases
3. Impurities (solids, dissolved solids, etc.)

III. Conduit Variables

1. Surface roughness
2. Material of conduit

IV. Dynamic Variables

1. Turbulence level
2. Pressure distribution
3. Velocity
4. Vibration

Because of the large number of variables involved, the efforts to find similarity or scaling laws encompassing all of these variables has not been successful.

The problem of determining the conditions under which a fluid will cavitate is not impossible because of the relatively minor role most of these variables play and the

dominant role of a few. Vapor pressure is the most important single variable because it gives an indication of the pressure necessary to cause cavitation. Several investigators have considered the nuclei (small invisible bubbles filled with a mixture of inert gas and vapor) present in the fluid and conduit as an important variable. The role of the nuclei in producing cavitation will be discussed in a following section.

Incipient and Desinent Cavitation

Incipient cavitation is defined as that phenomena which occurs when the stream pressure progresses from a condition of no cavitation to one supporting cavitation. It marks the onset of cavitation. Desinent cavitation, on the other hand, identifies the condition when the stream passes from a condition supporting cavitation to one in which there is no cavitation. It defines the cessation of cavitation. Many investigators in the past called both the beginning and the cessation "incipient" cavitation. Holl [2], in 1960 named these two different occurrences of cavitation.

For incipient cavitation there will correspond a particular value of pressure called the "inception pressure," p_i, whereas for desinent cavitation there is the "desinence pressure," p_d. From these definitions there follows the incipient-cavitation number K_{i_o} and desinent-cavitation number K_{d_o} defined by

$$K_{i_o} = \frac{p_{i_o} - p_v}{\frac{1}{2} \rho_o V_{i_o}^2}, \tag{2-1}$$

and

$$K_{d_o} = \frac{p_{d_o} - p_v}{\frac{1}{2} \rho_o V_{d_o}^2}. \tag{2-2}$$

The subscript "o" designates a reference state which is usually taken upstream of the minimum pressure section.

The experimental investigations by Lehman and Young [3] and Kermeen [4] indicate that the desinence pressure, p_d, is greater than or equal to the inception pressure, p_i. The pressure difference $p_d - p_i$ is often referred to as the "cavitation hysteresis." Thus, for the same vapor pressure the following relation between equations (2-1) and (2-2) can be written:

$$K_{i_o} \leq K_{d_o}. \tag{2-3}$$

For a given flow condition K_{d_o} appears to be the upper limit for K_{i_o}. Holl [2] pointed out that investigators in the past referred to desinent cavitation as incipient cavitation because of its repeatable nature. However, in some cases the only difference between incipient and desinent cavitation is in the definitions.

Inception of Cavitation

Some insight into the inception of cavitation can be gained by examining the theory of nuclei, sources of nuclei,

and scale effects.

Nuclei Theory for Cavitation Inception

It is now the generally accepted view that the inception of cavitation in ordinary liquids is associated with the growth of nuclei which contain vapor, undissolved gas, or both, and which are present either within the liquid or in crevices on boundary walls. On the basis of physical arguments made by Eisenberg [5], it is unlikely that completely dissolved gases can play a dominant role in inception, although in certain cases such dissolved gases may become important during the inception process. The work of Harvey, McElroy, and Whiteley [6] is of particular importance in this connection. They demonstrated that air-saturated water, after having been "denucleated" by prior application of large pressures, exhibited very high fracture strength. Thus, the presence of large nuclei is taken to account for cavitation onset at pressures of the order of vapor pressure.

Cavitation inception is a dynamic phenomenon; however, the basic principles can be revealed by a static analysis. For static equilibrium the following equation for a spherical bubble must be satisfied:

$$p_v + p_g = p_\infty + \frac{2\sigma}{R} \quad . \tag{2-4}$$

For a constant weight of a perfect gas at constant temperature, $p_g = \frac{C_i}{R^3}$, where C_i is proportional to the number of molecules or weight of the gas and R refers to the radius

of the sphere. Hence equation (2-4) becomes

$$p_\infty - p_v = \frac{C_i}{R^3} - \frac{2\sigma}{R} \quad . \tag{2-5}$$

The minimum value of $p_\infty - p_v = p^*$ occurs at a radius

$$R = R^* = \left[\frac{3C_i}{2\sigma}\right]^{\frac{1}{2}}$$

or

$$(p_\infty - p_v)_{min} = -\frac{4\sigma}{3R^*} \quad . \tag{2-6}$$

In this relation the negative sign indicates that the critical fluid pressure is actually below the vapor pressure. If the pressure is decreased slightly from the condition of $(p_\infty - p_v)_{min} = p^*$ at $R = R^*$, the bubble becomes unstable and tends to grow without bound. At pressures greater than the critical pressure, the bubble is stable and assumes an equilibrium radius which satisfies equation (2-4). The relation between $p_\infty - p_v$ and diameter for different values of C_i and an assumed surface tension value of 0.005 lbs. per ft. for 68°F water are shown in Figure 1. The corresponding relation between pressure and critical diameter is shown in Figure 2.

It may be observed from equation (2-6) that the critical radius for a bubble containing only vapor ($C_i = 0$) is zero and, consequently, that the fluid pressure must be infinitely negative in order to cavitate such a bubble. This requirement for infinite pressure to cause instability of a vapor bubble must be modified when the bubble radius

approaches molecular size and the continuum theory becomes invalid.

The previous analysis has considered only the static stability of the cavitation nuclei. It appears reasonable to expect that if nuclei are subjected to transient pressure reductions the critical pressure for instability might be considerably less than the value given by equation (2-6). Noltingk and Neppiras [8], [9] were able to show, in the majority of cases, that the critical pressure predicted by the static analysis is not significantly altered by the

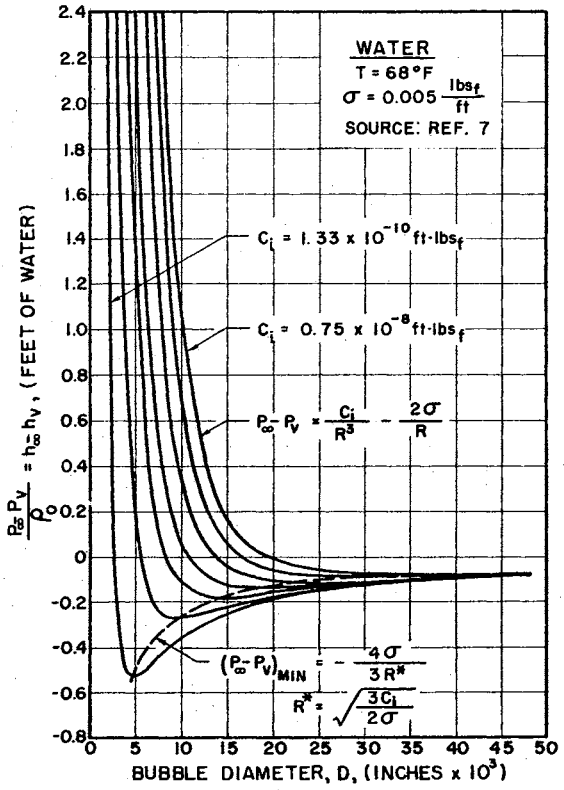

Figure 1. Results of Static Analysis for Isothermal Changes Within Bubble

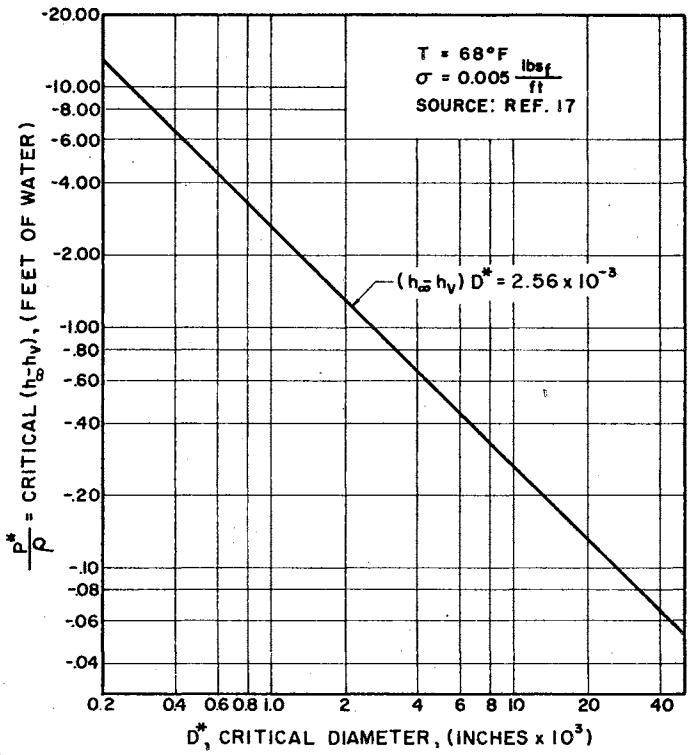

Figure 2. Pressure Required to Cause Instability of Critical-Size Gas Nuclei

duration of the transient. The investigations performed by Noltingk and Neppiras revealed that the pressure need only stay at the critical pressure for a time slightly greater than the natural period of oscillation of the bubble. For a bubble diameter of 0.001 inches, the pressure need remain at the critical value for approximately 10 microseconds. On the other hand, cavitation experiments conducted at high velocities on small scale models with short low pressure regions (flow through venturi-type nozzles) can be misleading if it is assumed that dynamic effects do not influence the critical nuclei size and pressure.

Sources of Nuclei

In the previous section a spherical gas bubble was assumed as the nuclei for cavitation. Such nuclei do exist near the surface of agitated liquids as continuously entrained air bubbles. However, at greater depths or in a confined fluid, it appears that the gas should dissolve in the fluid. The partial pressure of the gas within the bubble is higher than the surrounding fluid pressure because of surface tension and thus some gas should diffuse into the liquid. The loss of gas decreases the size of the bubble and thus increases the surface tension pressure which increases the gas partial pressure and increases the rate of diffusion into the liquid, and so forth. From equation (2-6) we have seen that stable spherical vapor nuclei cannot exist. Consequently, some nuclei source other than free gas bubbles must be postulated in order to explain the cavitation that is observed in fluids in which free gas bubbles of the required size for instability are not observed.

When new glass which has been cleaned with acid is immersed in water, the water tends to fill all the microscopic cracks and crevices. Such a surface is often referred to ashydrophyllic. Schweitzer and Szebehely [10] ran some gas evolution tests by placing the fluid to be tested in steel and lucite containers. No precaution was

made to clean the containers chemically. With water they were unable to produce any appreciable supersaturation without observing bubble formation. However, with petroleum hydrocarbons, which wet both steel and lucite, they observed considerable supersaturations without bubble release, provided the liquid was kept in a static state. This illustrates that the properties of the liquid are important when studying cavitation.

A material in which water does not tend to fill microscopic cracks and crevices is classified as hydrophobic. This type of material includes almost everything and thus gas volumes are easily contained in the crevices of foreign particles entrained in the fluid or in the crevices of the boundary material itself. It is presently believed that the nuclei needed for the cavitation process (other than free gas bubbles) are located in the crevices and cracks of such hydrophobic materials. Harvey, McElroy, and, Whiteley [6] were able to show that in a crevice of a hydrophobic material it is possible to have contact angles between the liquid, solid, and gas, such that the surface tension pressure is considerably reduced and tends to decrease rather than increase the cavity pressure. Under these circumstances it is possible to postulate an equilibrium condition in which gas neither diffuses into or out of the gas trapped in the crevice, and it is these microscopic gas volumes that are currently believed to be the nuclei needed for cavitation inception.

Knapp [11] attributed the tendency of a contaminated liquid to cavitate as soon as the local pressure drops below the vapor pressure to "weak spots" which are not present in a pure liquid. The findings of Knapp agreed with those of Harvey et. al. [6] in that weak spots which initiate cavitation usually occur on solid surfaces in contact with liquids. Knapp observed that normal cleaning methods were inadequate to remove weak spots from metal surfaces. This is probably due to the presence of innumerable cracks in the metal surface.

In summary, there are three distinct sources of nuclei. Each source is capable of causing the phenomena of cavitation. These are:

1. The free undissolved gas bubble, usually macroscopic in size.
2. The nuclei that exist in the crevices of foreign particles.
3. The nuclei that exist in the boundary material. Kermeen, McGraw, and Parkin [12] were able to take pictures of this source of nuclei during a cavitation study.

The interpretation of cavitation tests in which cavitation is actually produced in the test facility is affected by the nuclei present. To properly extrapolate such test results to predict when cavitation will occur on the prototype, the relevant scaling factors must be considered.

Cavitation Scale Effects

If the occurrence of cavitation were uncluttered by the appearance of scale effects, the experimental study of cavitation would be fairly easy. The test of a given shape over a range of K_o values would give the desired information. An indication of such an idealized cavitation behavior is presented with the aid of Figure 3.

The streamlines and pressure coefficient for potential flow past a simple shape are shown in Figure 3 (a) and 3 (b), respectively. At some point on the body, the minimum pressure occurs. The absolute value of this pressure is dependent only on the relative flow velocity, V_o; the reference pressure, p_o; and the exact shape of the body. This minimum pressure value for the given body is thus uniquely characterized by $C_{p_{min}}$, the minimum value of the conventional pressure coefficient in which

$$C_p = \frac{p - p_o}{\frac{1}{2}\rho_o V_o^2} . \qquad (2\text{-}7)$$

In the idealized situation no cavitation test would be required, because the value of K_o at which cavitation would first appear is simply $-C_{p_{min}}$. If the pressure could be measured at the proper location, $C_{p_{min}}$ could be found by a noncavitating test with water or even air as the test medium. However, as a result of scale effects, cavitation tests are required.

The manner in which a cavitation test would verify

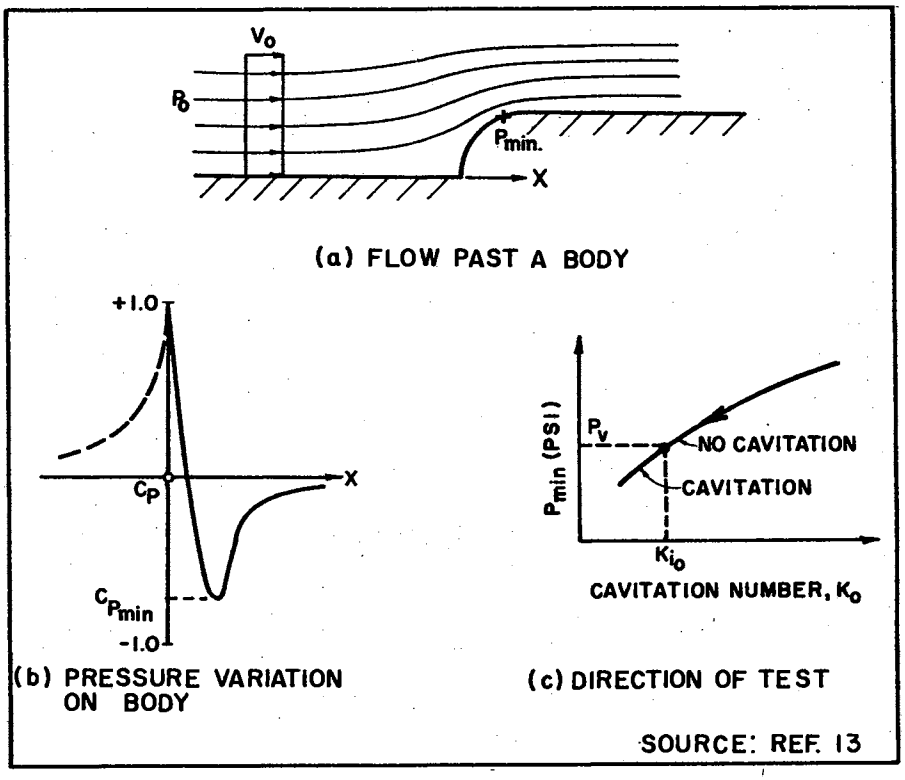

Figure 3. Body Flow Dynamics and Idealized Cavitation Test Behavior

the K_{i_o} prediction in the idealized cavitation situation is shown in Figure 3 (c). A cavitation test is normally conducted with the initial operation of the test facility at a high K_o value for which there is no possibility of cavitation. The operating K_o value is then reduced either by raising V_o or lowering p_o, with an associated decrease in the absolute pressure p_{min}, until the value $p_{min} = p_v$ is reached. The reduction of K_o below the inception value (K_{i_o}) has no further effect on p_{min}, which remains equal to p_v. However, the nature of cavitation is changed as K_o

is reduced below K_{i_o}. At the inception point the cavitation consists of small bubbles that quickly collapse with tremendous noise as they proceed into regions of higher pressure. At K_o values below K_{i_o}, larger cavities may form which change the flow and force relations for the object or conduit.

Unfortunately, little is known about how the conditions at the beginning of a cavity change with the degree of cavitation. Thus, a detailed study of this change of conditions could provide useful information.

From this discussion of the idealized cavitation occurrence situation, scale effects may be defined as any flow phenomena which will cause deviations from the idealized occurrence. Thus, if the pressure distribution over the body varies with the nature of the flow, this represents one kind of scale effect. If cavitation does not always start when p_v is reached, then another type of scale effect is represented. The pressure distribution on a body is affected by such factors as fluid viscosity, surface roughness, etc. The pressure at which cavitation occurs depends on such factors as nuclei present, surface tension, pressure distribution, etc.

Holl and Wislicenus [14] pointed out that the idealized similarity relation of cavitation ($K_o = [p_o - p_v]/\frac{1}{2} \cdot \rho_o V_o^2$) is based on certain assumptions:

1. All pressure differences in the flow are proportional to ρV^2.

2. Geometric similarity includes surface irregularities of the flow boundaries.
3. The vapor pressure in the flow field is constant and the pressure at which cavitation takes place is the equilibrium vapor pressure.
4. Cavitation takes place instantaneously whenever the vapor pressure is reached.

The correct similarity relations which are needed to describe cavitation are unknown. However, Holl and Wislicenus [14] listed several similarity relations which may help describe cavitation. These are given in Table I. The classical relation, included in Table I, must always be satisfied together with the requirement of geometric and kinematic similarity.

Investigations of the Inception of Cavitation

The following sections will be devoted to a discussion of the experimental and theoretical investigations of cavitation inception for unseparated flow past streamlined bodies, separated flow past non-streamlined bodies, and flow through venturi type nozzles, orifices, tubes, and bends.

Unseparated Flow Past Streamlined Bodies

A streamlined body is a body in which the curvatures are sufficiently mild to permit nearly ideal flow (that is,

TABLE I

CAVITATION SIMILARITY RELATIONS

	No.	Forces And Characteristics	General Similarity Requirements	Similarity Requirements For Same Fluid Properties	Probable Effects On K of Changes in V and L_1 Only
Ideal Flow	1	Inertia Forces Only (Classical Theory)	$K = \frac{p - p_v}{\frac{1}{2}\rho V^2} = \text{Const.}$	$p - p_v$ proportional to V^2	No Effects K = Const.
Hydrodynamic Scale Effects On The Fluid Pressure	2	Viscosity And Inertia Forces	Reynolds' Law of Similarity $Re = VL/\nu = \text{Const.}$	$VL_1 = \text{Const.}$	K Increases With VL_1
	3	Gravity And Inertia Forces	Froude's Law of Similarity $F_L = V/\sqrt{gL_1} = \text{Const.}$	$V/\sqrt{gL_1} = \text{Const.}$	Vertical Differences In Cavitation Decrease With Increasing $V/\sqrt{L_1}$
	4	Elastic And Inertia Forces (Compressibility)	Law of Constant Mach Number $M = V/c = \text{Const.}$	$V = \text{Const.}$	Not Predictable. Probably Effective Only With Extensive Cavitation
	5	Effects of Surface Irregularities	$h/\delta = \text{Const.}$ for $R_e = \text{Const.}$: $h/L_1 = \text{Const.}$	SAME	K Increases With h/L_1. K decreases with increasing L_1 if h increases slower than L_1.
Thermodynamic Scale Effects	6	Effects of Vapor Pressure	$p_v/p = \text{Const.}$	$p = \text{Const.}$ Therefore $V = \text{Const.}$	K increases with V
	7	Effects of Vaporization And Heat Transfer	$\frac{1}{p}\frac{\partial p_v}{\partial T}\frac{a_v}{a_\ell}\frac{v_\ell}{v_v}\frac{L_V}{C_{p_\ell}} \cdot P_e^{n_1} = \text{Const.}$ Peclet Number, $P_e = \frac{C_{p_\ell} V L_1}{v_\ell k}$	$VL_1 = \text{Const.}$	K decreases with increasing VL_1
		(6) and (7) may be neglected if p_v/p is very small (e.g. for Cold Water)			
Molecular And Other Microscopic Scale Effects	8	Surface Tension And Inertia Forces	Law of Constant Weber Number $W = \rho V^2 L_1/\sigma = \text{Const.}$	$V^2L_1 = \text{Const.}$	K increases with V^2L_1
	9	Number of Nuclei	$\sqrt[3]{N} \cdot L_1 = \text{Const.}$ (Only if nearly all nuclei form centers of cavitation)	$L_1 = \text{Const.}$	K increases with L_1 (for N = Const.)

flow without boundary layer separation). The pressure distribution on this body, as obtained from potential flow theory, would be expected to be in good agreement with experimental measurements if the boundary layer displacement thickness is small compared with the body diameter. This condition is usually met if the Reynolds number is sufficiently high to produce a fully developed turbulent boundary layer [15].

Knapp and Hollander [16] made a high-speed photographic study (20,000 pictures per second) of the formation and collapse of individual bubbles during the flow of water past a 1.5 caliber Ogive-Nosed body. The life of the bubble from the instant it was large enough to be detected until the completion of its first collapse was only about 0.003 seconds. The formation period required about three fourths of this time, leaving one fourth for the collapse period. The conditions of the water tunnel were V_o = 40 fps, p_v = 0.40 psia, and p_o = 4 psia.

In many of the pictures taken, it was obvious that the collapse of one bubble had a major effect on the collapse of its neighbor. Furthermore, as the severity of the cavitation was increased, the bubble concentration built up very rapidly, so that rarely if ever could a single bubble be seen to form and collapse without interference.

Kermeen, McGraw, and Parkin [12] investigated several geometrically similar hemispherical and 1.5-caliber Ogive-

Nosed bodies for cavitation inception at various water tunnel speeds. The results of this investigation are shown in Figure 4. Figure 4 illustrates that the measured incipient cavitation numbers were less than $\left|C_{p_{min}}\right|$ and depended on both the model size and the test velocity. However, the data indicates that the incipient cavitation number does approach $\left|C_{p_{min}}\right|$ for large size bodies and high tunnel speeds. It is suggested that the scale effects shown in Figure 4 are primarily caused by the low concentration of nuclei and the small nuclei sizes present in the test water [17]. The curves shown in Figure 4 are average curves drawn through the data.

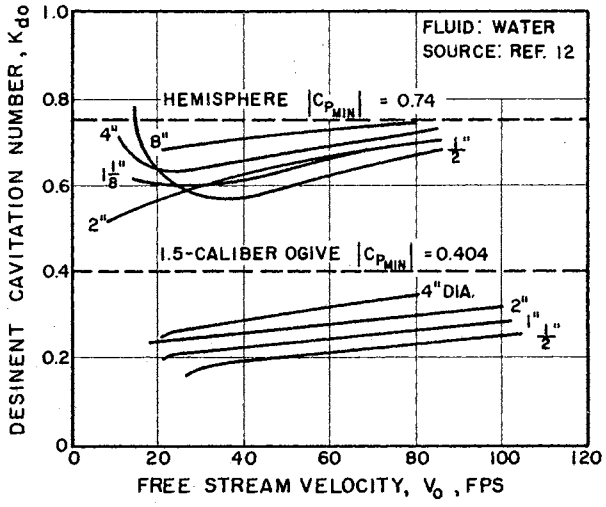

Figure 4. Incipient Cavitation Number as a Function of Free-Stream Velocity for Bodies with Hemispherical Noses and 1.5-Caliber Ogive Noses

Figure 5 shows how the desinent cavitation number varies with the Reynolds number for the flow of water past Joukowski hydrofoils. For a given size the desinent cavitation number increases with the Reynolds number. Furthermore, for a given Reynolds number the desinent cavitation number decreases with increasing size. On the other hand, the NACA 16012 hydrofoil data shown in Figure 6 differ markedly from the trend shown in Figures 4 and 5. In Figure 6 the cavitation number decreases for a given size with increasing Reynolds number (with increasing velocity) and increases for a given Reynolds number with increasing size. This unique behavior goes together with the flat pressure distribution of these profiles at 0-degree angle of attack (see Figure 7) in contrast to the peaked minimum

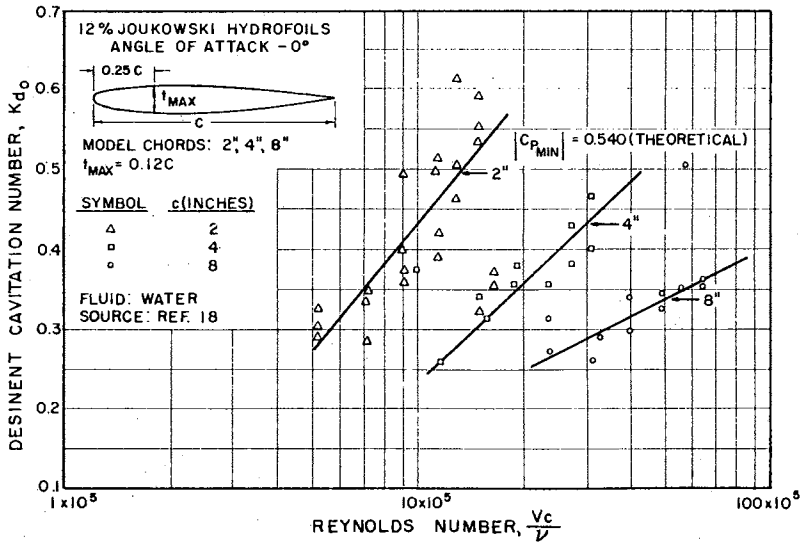

Figure 5. Desinent Cavitation Number as a Function of Reynolds Number for Water Flowing Past Joukowski Hydrofoils

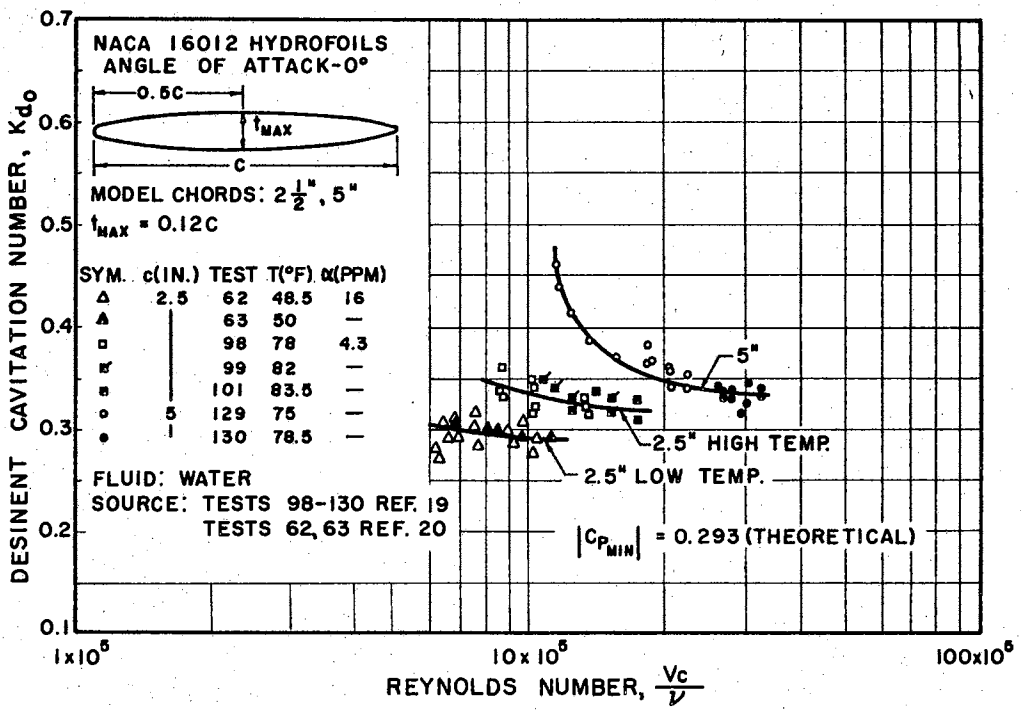

Figure 6. Desinent Cavitation Number as a Function of Reynolds Number for Water Flowing Past NACA 16012 Hydrofoils

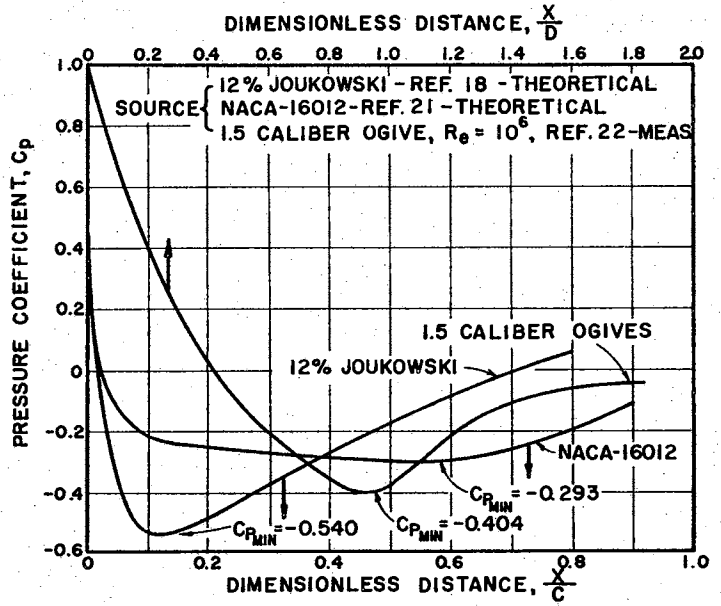

Figure 7. Pressure Distributions for Streamlined Bodies

pressure of other streamlined bodies treated. Calehuff and Wislicenus [20] reported that cavitation on the profiles with flat pressure distribution had the form of traveling bubbles; whereas, with peaked under-pressures cavitation appeared to be attached to the surface.

The scale effects can be seen by examining Figures 5 and 6. Also, the effect of pressure distribution on the inception of cavitation is shown to have an important influence.

The type of flow in the boundary-layer has an important effect on the inception of cavitation. Daily and Johnson [17] investigated the effects of a turbulent boundary-layer on the inception of cavitation for the flow of water (at a free stream velocity of 27.5 fps) through a two-dimensional nozzle. The flow in the boundary-layer was rotational and the minimum pressure did not occur on the wall (for large body curvatures) but slightly away from it in the center of the eddies that compose the boundary-layer. Thus cavitation can actually begin at values of K_o that are slightly greater than $\left|C_{p_{min}}\right|$ because of the additional pressure reduction caused by turbulence. However, Daily and Johnson pointed out that the boundary layer turbulence effect is small and can usually be neglected at the high velocities that are normally encountered in hydraulic structures where cavitation is expected.

Holl [2] investigated the effect of air content on the occurrence of cavitation for water flowing past

hydrofoils. These hydrofoils were tested at various angles of attach. Figure 8 shows the results of these tests.

Holl [2] observed that two types of desinent cavitation could be determined. As the pressure was increased, causing the cavitation to disappear, a pressure was reached at which the cavitation disappeared uniformly across the span. This was referred to as areal cavitation. However, it was observed that several cavitation bubbles still clung to the surface and continued to do so up to very high ambient pressures. These spots of cavitation were manifest on the NACA 16012 hydrofoils at angles of attack above the critical angle.

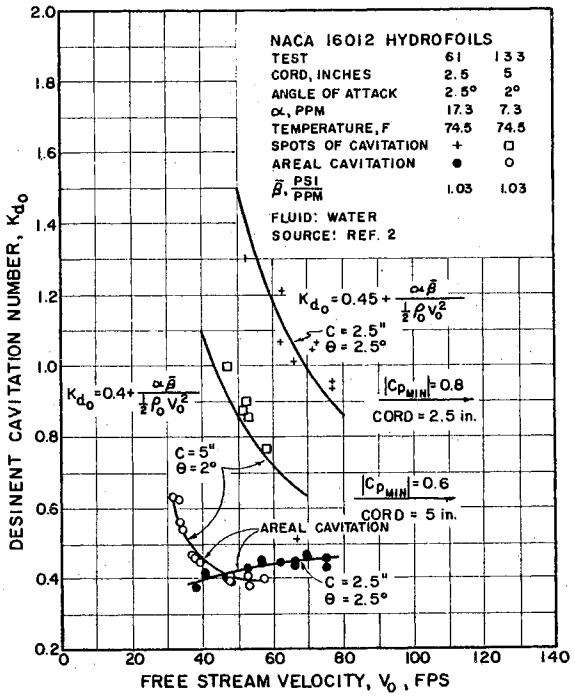

Figure 8. Two types of Cavitation on 2.5-in. and 5-in. NACA 16012 Hydrofoils

The critical angle of attack is that angle at which the change of $\left|C_{p_{min}}\right|$ with angle becomes very large. The critical angle of attack for the NACA 16012 hydrofoils is about 1.5 degrees [21].

Oshima [23] developed a relation from boundary-layer gas-nuclei interaction considerations which allows predicting the Reynolds number variation in K_{i_o} for flow past axially symmetric bodies. Calculations of the turbulent boundary-layer growth on the test bodies were combined with the suggestions of Daily and Johnson [17], concerning nuclei growth and turbulence effects to predict the scaling of cavitation inception as observed on the axisymmetric bodies as referred to previously. Oshima's formula appears to correspond closely with some selected experimental data. However, before definite conclusions can be formed about this work, additional experimental investigations (with liquids other than water) are necessary.

Knapp [24], in 1952, derived a formula which is similar to Oshima's formula. However, Oshima was able to show that Knapp's formula is a special case of his theory.

The inception of cavitation on isolated surface irregularities imbedded in a turbulent boundary layer was investigated experimentally and theoretically by Holl [25] and [19]. Holl was able to show how the effect of a small roughness element (of height, h) on a smooth surface may greatly increase the incipient cavitation number (see Figure 9). In terms of the incipient cavitation number, K_{r_o}, of the

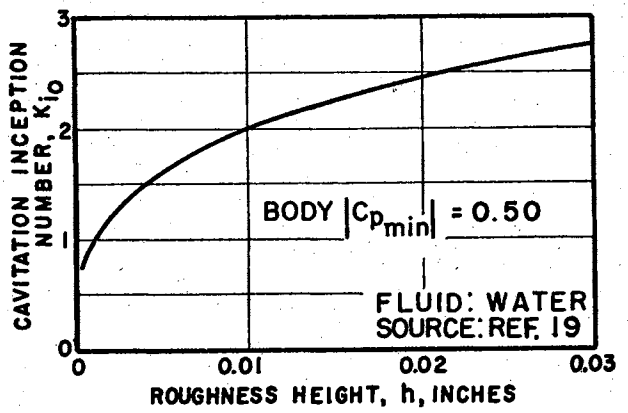

Figure 9. Calculation Effect of Relative-Roughness for a Particular Flow

roughness element and the pressure coefficient of the smooth body, the incipient cavitation number of a roughened body is

$$K_{i_o} = |C_p| + (1 + |C_p|) K_{r_o} . \qquad (2\text{-}8)$$

The roughness is most detrimental when placed at the minimum pressure-point of the parent body, that is, when $C_p = C_{p_{min}}$.

Holl [25] determined how K_{r_o} varied with the ratio of the height of a roughness element, h, to the boundary-layer thickness, δ, for different velocity-profile shapes and two different shapes of roughness elements. The velocity-profile shape was expressed by the boundary-layer shape parameter $H = \frac{\delta^*}{\theta}$, where δ^* is the displacement thickness and θ the momentum thickness. Two families of cylindrical roughness

elements having constant cross sections were studied. One family had a circular-arc cross section. The other family had a triangular cross section. The results of this study are shown in Figure 10.

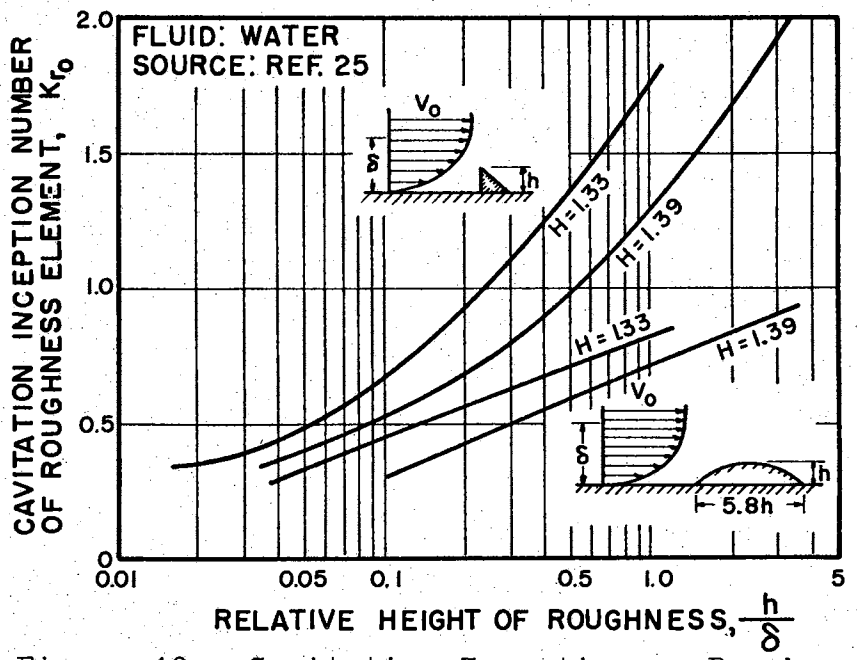

Figure 10. Cavitation Inception on Roughness Elements in Boundary-Layer Flows

The seriousness of roughness effects in producing cavitation inception scale effects is illustrated by the following example [25]. Consider a body with $C_{p_{min_s}} = -0.50$ of such proportions and tested at such a speed ($V_o = 50$ fps) that $\delta = 0.048$ in. As Figure 9 shows, the effects for the sharp roughness of Figure 10 (and a fairly-normal turbulent

boundary layer of H = 1.33) are considerable. A 102 percent increase in K_{i_o} occurs for a 0.001 in. high roughness and much larger effects are easily possible. This increase was computed by

$$\frac{K_{i_o} - C_{p_{min_s}}}{C_{p_{min_s}}} \times 100 .$$

Separated Flow Past Non-Streamlined Bodies

If the flow past a body is decelerated too rapidly, the boundary-layer separates and the pressure distribution along the boundary is no longer a true indication of the minimum pressure in the field. Unfortunately, there is no exact method of obtaining the minimum pressure coefficient in the flow field in terms of the measured boundary pressure. Nevertheless, some experimental studies of cavitation inception have been reported.

Most of the available test data pertain to sharp-edged disks (Figure 11) and zero caliber ogives, i.e., cylinders with a flat cutoff end facing the flow (Figure 12). The most striking difference, compared to the behavior of streamlined bodies, lies in the magnitude of the changes in the desinent cavitation number, which varies by a factor of two for a change in Reynolds number by a factor of ten. This appears to be at least twice the largest change observed with most of the streamlined bodies (excepting the

Joukowski hydrofoil data shown in Figure 5). Furthermore, the cavitation number of bluff bodies (i.e., separated flow) continues to increase with increasing Reynolds number. In this respect the test points of the zero-caliber ogives (Figure 12) seem to continue the sharp disk data (Figure 11) without a break or indication of leveling off.

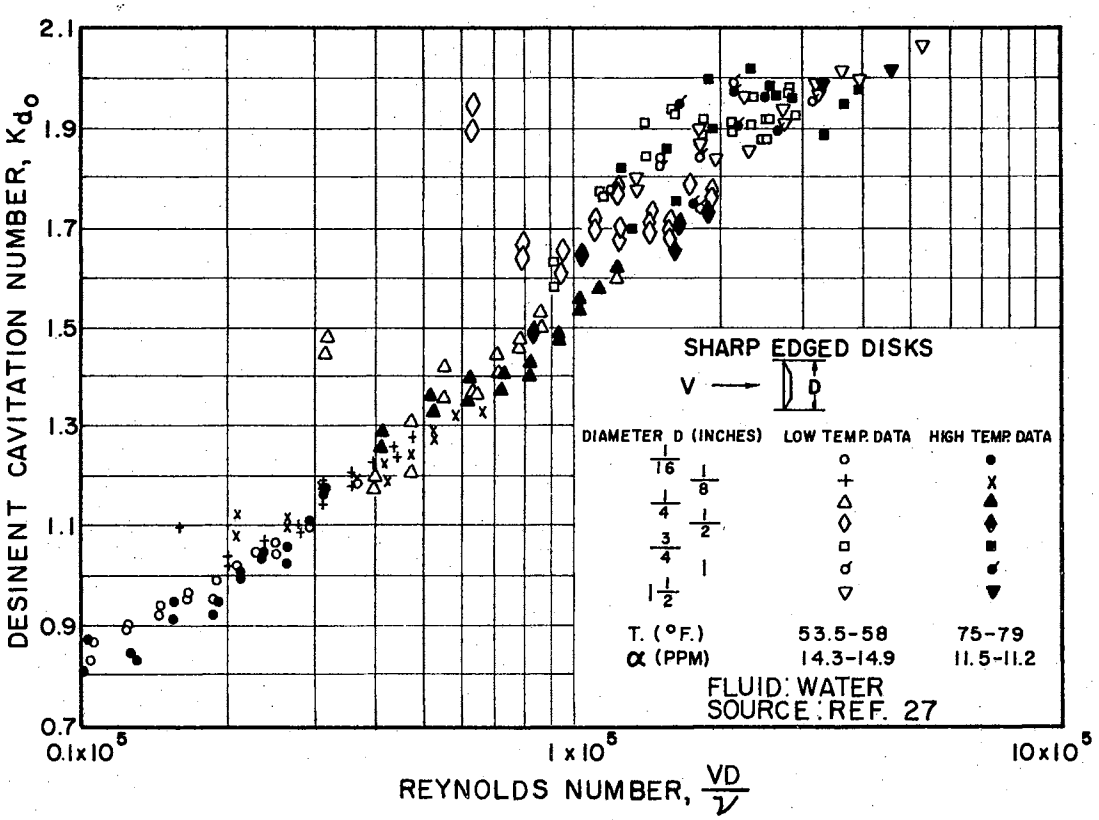

Figure 11. Desinent Cavitation Number as a Function of Reynolds Number for Water Flowing Past Sharp-Edged Disks

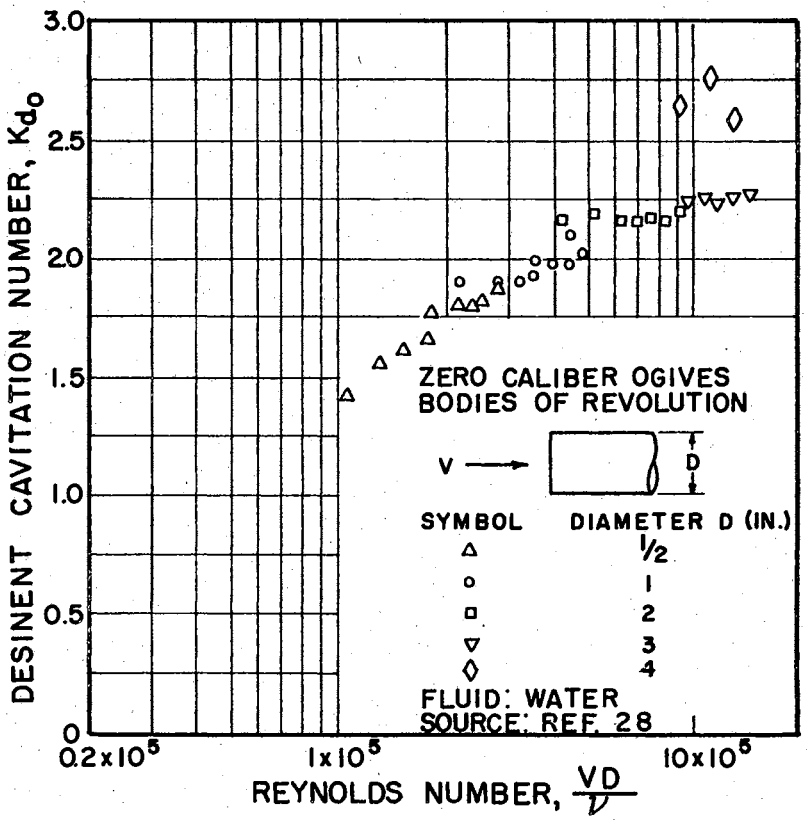

Figure 12. Desinent Cavitation Number as a Function of Reynolds Number for Water Flowing Past Zero-Caliber Ogives

Flow Through Venturi-Type Nozzles

The venturi-type nozzle has proved to be an effective shape for studying cavitation. This is due to the fact that a wide range of flow conditions are easily obtained; thus, studies can be made for various degrees of cavitation under different pressure distributions.

In the experiments cited above (Kermeen, McGraw, and Parkin [12], no consistent effect of air content, varied

between 7 and 13 ppm, could be detected. This disagrees with the observations of Numachi and Kurokawa [29], McCormick [26], Crump [30], [31], and others. Crump [30] found a significant dependence of inception on total air content in experiments with a venturi nozzle having a diffuser angle of 5°. He reports that in fully aerated fresh water cavitation first appeared at the boundary in the form of a small vapor cavity. Crump found that in deaerated fresh water cavitation first appeared in the form of individual bubbles which did not necessarily form at the boundary. Under these conditions, bubbles formed and disappeared downstream under ambient tensions $(p_{\infty} - p_{v})$ as high as four atmospheres. Furthermore, he found that higher tensions were required as the velocity was increased.

Figure 13 shows that in the liquid undersaturated with air it was possible to obtain tensions as the relative air content α/α_{s} was reduced. Results in a nozzle with an abrupt expansion show opposite trends in the pressures required for inception [31]; although here, too, tensions were obtained. Comparable results for sea water are shown in Figure 14; in this case, bursts of cavitation were observed at pressures well above vapor pressure. While the trends in these experiments were fairly definitive, the very large scatter of results is indicative of the need for understanding the behavior and distribution of nuclei, i.e., the mechanisms by which nuclei are stabilized

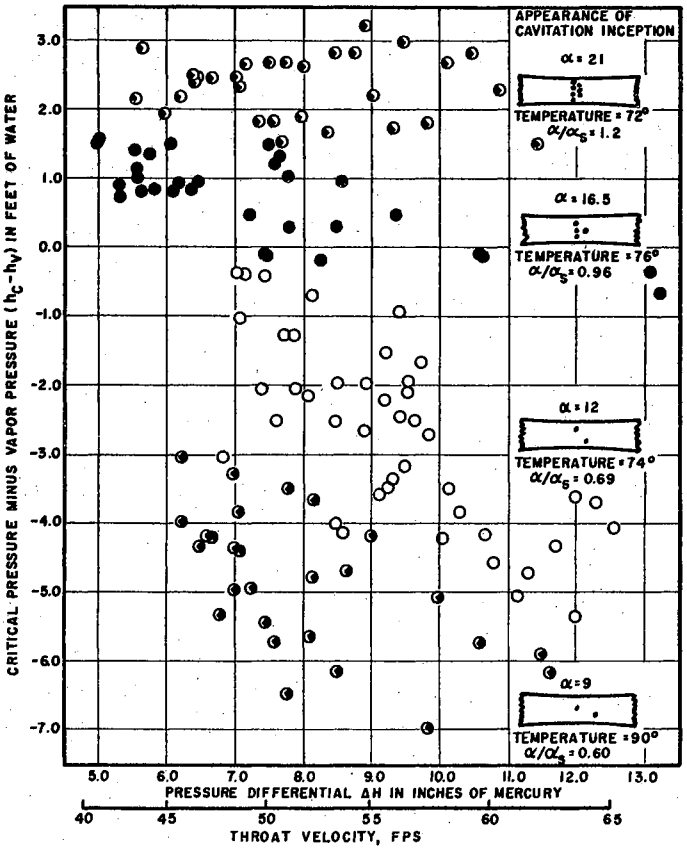

Figure 13. Critical Pressures for the Inception of Cavitation in Fresh Water of Varying Air Content (Ref. 30)

and the characterization of nuclei content, e.g., a "spectrum," or description of number and distribution in size [43].

Williams and McNutly [32] investigated the effect of an additive (sodium nitrate dissolved in distilled water) on cavitation inception. The incipient cavitation number was found to increase (cavitation to become easier) with an increase in the percentage (from 0 to 0.4% by weight) of dissolved sodium nitrate.

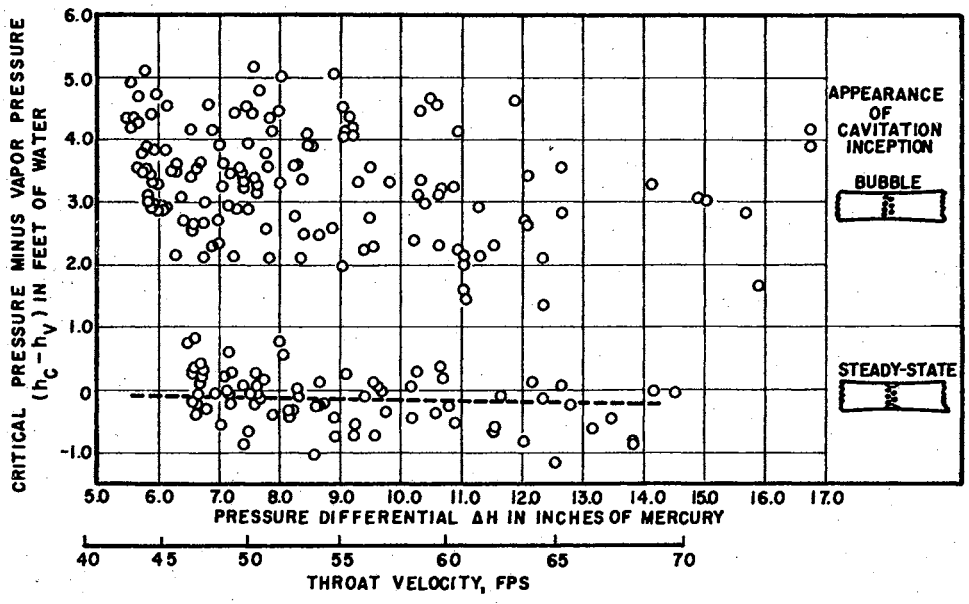

Figure 14. Critical Pressures for the Inception of Cavitation in Sea Water (Ref. 30)

The flow of liquid nitrogen through a venturi test section has been investigated by Ruggeri and Gelder [34]. Just prior to incipient cavitation, the minimum local wall pressure was significantly less than the vapor pressure corresponding to the stream liquid temperature. This pressure difference was called effective liquid tension. The temperatures and pressures measured within regions of well-developed cavitation were in thermodynamic equilibrium but were less than the temperature and the saturation vapor pressure of the approaching stream. These differences increased with both stream velocity and extent of cavitation.

Figures 15 and 16 show comparisons of cavitation tests of nitrogen, water, Freon-114, and ethylene glycol (References

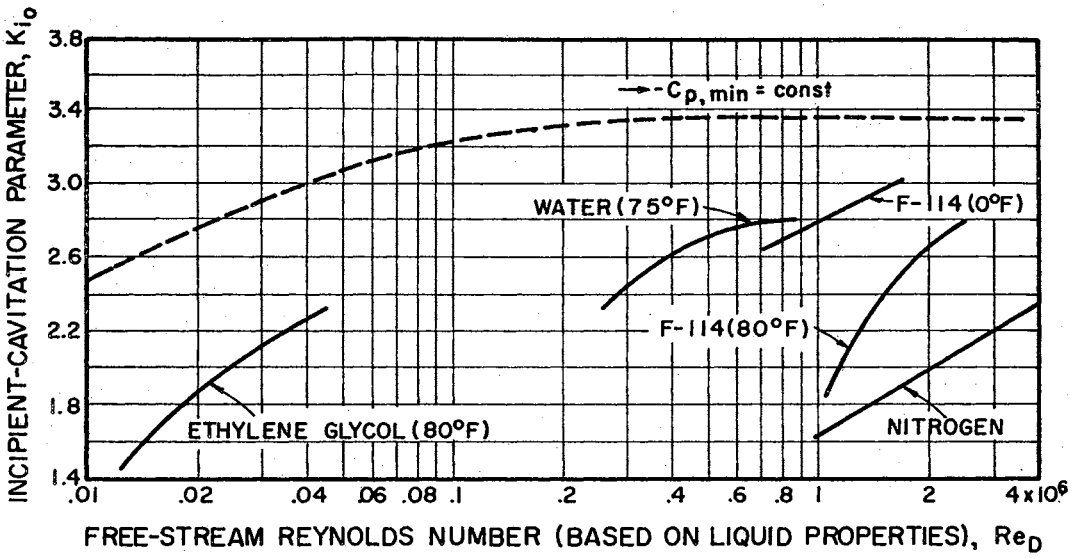

Figure 15. Comparison of Incipient Cavitation Number for Nitrogen, Water, Freon-114, and Ethylene Glycol Flowing Through Same Venturi Model (Ref. 33, 34, 35, and 36)

[34], [33], [35], and [36]) in the same venturi test section. Nitrogen sustained more effective tension than the other liquids tested. This indicates a possibility that temperature influences the nuclei within the liquid and test section.

The effective tensions for all liquids studied increased with increasing flow velocity. The effective tensions for ethylene glycol were practically independent of the temperature level for the range studied. For water in the 40° to 80°F range, effective liquid tension was practically independent of temperature but increased appreciably as the temperature was increased to 120°F. This increase in liquid tension is not shown in Figure 16.

Lehman and Young [3] investigated the pressures and

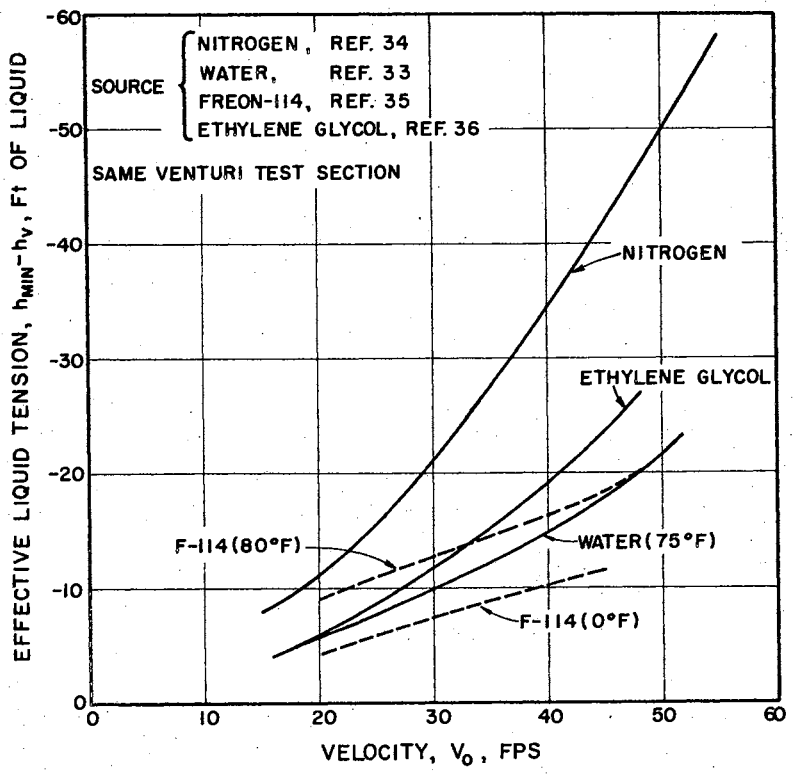

Figure 16. Comparison of Effective Liquid Tension Based on Visible Incipient Cavitation for Nitrogen, Water, Freon-114, and Ethylene Glycol Flowing Through Same Venturi Model

cavitation numbers near the location where incipient and desinent cavitation occurred for water flowing through different convergent-divergent test sections. The results of this investigation are shown in Figures 17 and 18. The cavitation pressures measured near the plane of incipient and desinent cavitation were generally higher for the tests made using an abrupt contour test section. The curves shown in Figure 17 disagree with what might be expected.

Hammitt [37] made an investigation similar to the

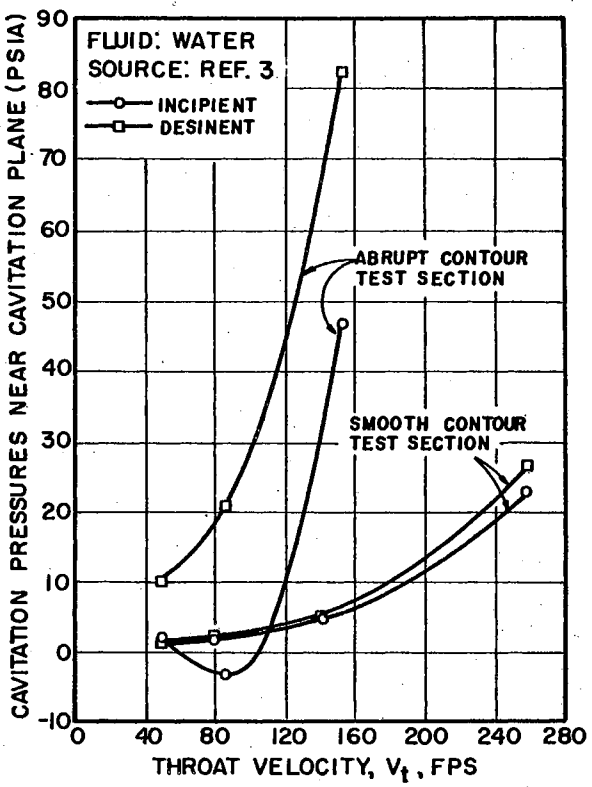

Figure 17. Cavitation Pressures Near Planes of Incipient Cavitation as a Function of Throat Velocity in Venturi-Type Test Sections

investigation made by Lehman and Young [3]. Hammitt observed no difference between the incipient and desinent cavitation numbers while studying the flow of water through a smoothly changing internal contour nozzle. This corresponds closely with the investigation made by Lehman and Young on a similar shape nozzle. However, the abrupt contour tested by Lehman and Young indicates that the conditions at the plane of cavitation are a function of the pressure distribution prior to cavitation.

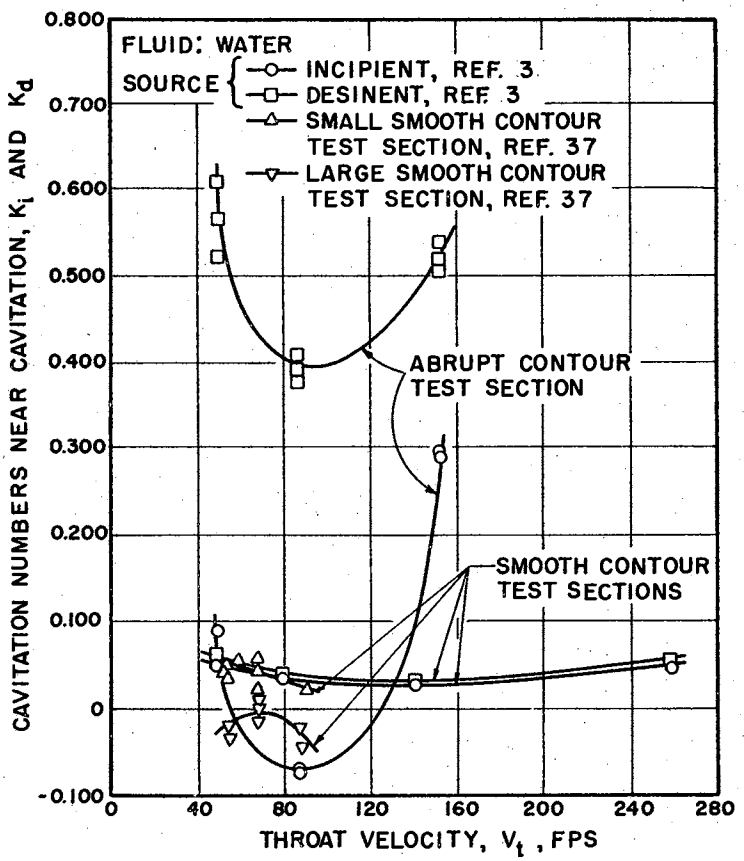

Figure 18. Comparison of Cavitation Numbers for Water Flowing Through Abrubt- and Smooth-Contour, Venturi-Type Test Sections

Flow through Orifices

The jets flowing from orifices into filled conduits (sudden enlargements) represent cases of extreme separation where in addition to expansion and diffusion of the main jet there is the generation of secondary flow and countless small eddies and vortices. The pressures within the eddies will be appreciably below that of the surrounding fluid,

particularly when the velocity of orifice efflux is high. These low pressures can quite easily reach the vapor pressure of the fluid and there exists the possibility of cavitation.

The effect of cavitation on the discharge coefficient of orifices has received some attention [39] and [40]. However, only the investigation of the flow of pure fluids through orifices will be reported at this time.

Jacobs and Martin [38] investigated the flow of water, liquid hydrogen, and liquid nitrogen through sharp-edged orifices. They were unable to produce cavitation as long as pure liquid entered the orifices. With liquid nitrogen the pressures at the venae contractae were as much as 170 inches of liquid below the vapor pressure, while with liquid hydrogen the pressures at the venae contractae were as much as 192 inches of liquid below the vapor pressure. These were the lowest pressures attainable with their apparatus.

Jacobs and Martin observed that the only way cavitation could be produced, with their apparatus, was to have two-phase flow entering the orifices. Cavitation symptoms were not evident in many tests even when two-phase flow entered the orifices.

Flow through Conduits

Mikol and Dudley [41] investigated the conditions at which cavitation inception occurs for the flow of Freon-12 through small bore copper and glass tubes. The point of

inception of cavitation was observed to move by discrete jumps rather than in a continuous manner as operating conditions were changed. This was probably due to the gradual and uniform pressure gradient in the tube and/or the location of "weak spots" in the walls of the tube. In venturi tests the inception site is fixed within rather close limits by the nonuniform and sharper pressure gradients imposed by the geometry. No such shift has been reported in any venturi test.

Mikol and Dudley observed that the tube material had the most important influence on the incipient cavitation number. The incipient cavitation number for the glass tube was nearly twice that for the copper tube. This result is in agreement with the nucleation theory expectation that a metal surface should provice many more nucleation sites than a glass surface.

Fauske and Min [42] investigated the flow of slightly sub-cooled Freon-11 through apertures and short tubes. They used a modified cavitation number to establish a criterion for determining single-phase or two-phase flow regimes in short tubes. The modified cavitation number is:

$$\overline{K}_o = \frac{2g\Delta P}{\rho_o V_o^2} \left[\frac{L_1}{D}\right] , \qquad (2\text{-}9)$$

where ΔP is the pressure difference, $p_o - p_e$ for two-phase flow or $p_o - p_b$ for single-phase flow. Figure 19 indicates that for modified cavitation number below 10 the fluid

exhibits completely metastable single-phase flow. When the modified cavitation number exceeds 14, two-phase flow exists. In the range of $\overline{K}_o$ between 10 and 14, unstable transitional flow occurs.

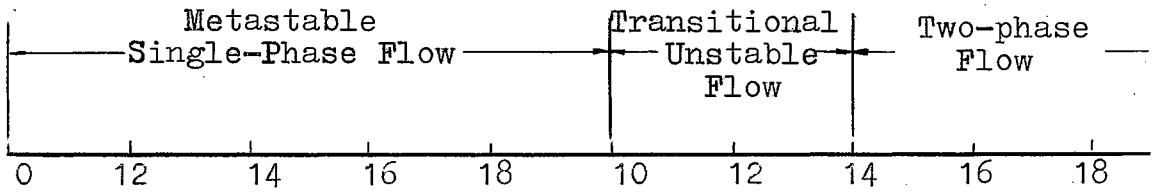

Figure 19. Correlation Number Determining the Occurrence of Single- and Two-Phase Flow Regimes for the Flow of Freon-11 in Short Tubes

Flow through Bends

As a fluid flows through a bend, a pressure gradient occurs across the bend to balance the centrifugal forces acting upon the fluid. The pressure on the outside of the bend becomes larger than the initial stream pressure, attaining some maximum value part way through the bend. The pressure on the inside, nearer the bend origin, becomes smaller than the initial value until some minimum value is reached. Thus, as the flow undergoes the transition from rectilinear to curvilinear motion, a positive pressure gradient in the direction of flow is initially imposed on

the outer wall of the elbow; and then a negative gradient is generated as the static pressure readjusts to a uniform value when the flow leaves the bend. Conversely, on the inner wall a negative axial pressure gradient is initially present as the pressure decreases to some minimum value at approximately midway through the bend and then a positive gradient is formed as the pressure increases back to a uniform value across the pipe downstream of the turn (see Figure 20).

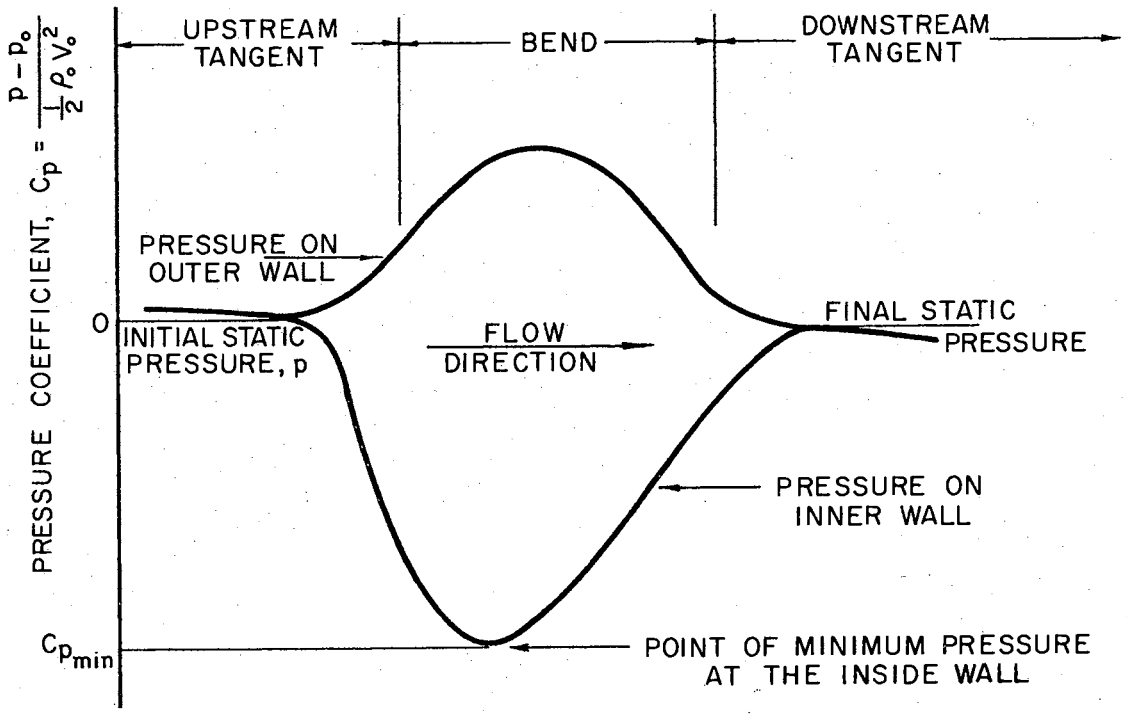

Figure 20. Schematic of the Pressure Distribution on the Inner and Outer Walls in the Plane of Curvature of an Elbow

If the fluid is a liquid of sufficiently high vapor pressure, the static pressure near the inner wall of the duct may decrease to a value equal to or below the vapor pressure and thus cause cavitation within the elbow, which is an entirely different phenomenon from separation, although both may occur simultaneously.

Stonemetz [48] experimentally investigated incipient cavitation for water flowing through circular pipe bends of 60°, 90°, and 120° in one plane. Pipe diameters ($\overline{d}$) of 1.5, 2.0, and 4.0 inches and bend radius ratios ($\overline{R}/\overline{d}$) of 0.7, 1.0, and 1.5 were investigated.

For all configurations investigated, the incipient cavitation number decreased with increasing values of Reynolds number. The incipient cavitation number was greater for smaller ratios of bend radius to pipe diameter. The variations in bend angles investigated, 60° — 120°, had insignificant effect.

Stonemetz obtained an empirical relationship for the determination of the incipient cavitation number. This relationship takes into account the effects of bend radius and pipe diameter. The empirical equation is

$$\overline{K}_{i_o} = \frac{p_{i_o} - p_v}{\frac{1}{2}\rho_o V_{i_o}^2} - 0.67\,(\overline{R}/\overline{d})^{-\overline{d}}. \qquad (2\text{-}10)$$

The results of this investigation are shown in Figure 21.

The preceding discussions in this chapter are primarily an attempt to point out some of the knowns and unknowns

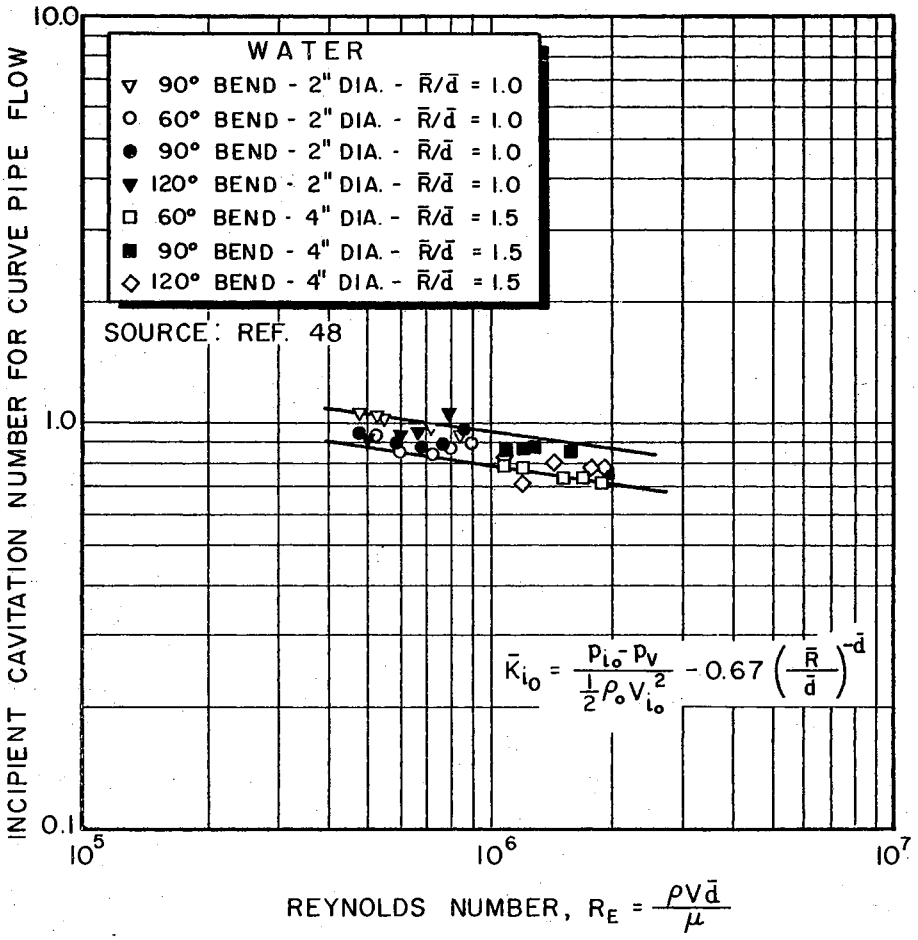

Figure 21. Curved Pipe Incipient Cavitation Number as Computed vs Reynolds Number

about cavitation. For a constant cavitation number, both the time of exposure to the region of pressure below the vapor pressure (underpressure) and the amount of this underpressure are functions of velocity. It may not be unreasonable to assume that the gross cavitation pattern is largely controlled by the nucleation process. It is conceivable that the nucleation process may depend upon time of exposure to underpressure and absolute value of this underpressure

in such a way that the effects are not cancelled for constant cavitation number. With systematic experimental studies of different liquids flowing through various pressure distributions, it may be possible to obtain a reasonably correct K_{i_o} value or trend for an arbitrary body and liquid by means of some relations between underpressure and relaxation time (time fluid remains at pressures below the vapor pressure before cavitation occurs). Also, a method is needed to accurately predict the conditions at the position where cavitation starts for limited and profuse cavitation.

CHAPTER III

THEORETICAL INVESTIGATION OF INCIPIENT CAVITATION

It is the purpose of this chapter to investigate the conditions for incipient cavitation by analytical means so that more precise ideas can be obtained about the influence of various properties upon the conditions at the inception of cavitation. This is accomplished by investigating the equition which describes the growth of small bubbles. These small bubbles are assumed to serve as nucleation sites for cavitation.

The spherical bubbles which serve as nucleation sites for cavitation may have an initial stable radius of approximately 10 microns. This radius will depend upon the particular liquid and the pressures within the liquid and the bubble. When the pressure within the liquid is decreased, these small bubbles will grow. The rate of growth depends upon the rate at which the liquid pressure is decreased and upon the magnitude of this pressure. The mass of inert gas within the bubble will also have an influence upon its behavior and stable radius.

The stable radius is necessary as an initial condition for obtaining solutions to the equation of motion for a bubble. Some knowledge of the stable radius can be

gained by investigating the conditions for static equilibrium of a spherical bubble.

Static Analysis of a Spherical Bubble

Examining the conditions for static stability of a spherical gas-vapor bubble that is surrounded by a liquid is very helpful in understanding the inception of cavitation. Although cavitation is a dynamic phenomenon, the basic principles of inception will be revealed by such a static analysis.

The first part of this section will be devoted to the development of the general equation for the static equilibrium of a spherical bubble. The last part will be devoted to showing the effects of various parameters upon the stable bubble radius.

Development of Static Equilibrium Equation for a Spherical Bubble

The forces acting on the inside of a bubble are those due to the partial pressure, p_g, of an inert gas and the partial pressure, p_v, of the liquid vapor (see Figure 22). At the interface (boundary between the liquid and the gas-vapor mixture) is a force which is called the surface tension force. The force acting on the outside of a bubble is due to the pressure, p_∞, within the liquid. Applying Newton's second law to the composite forces as shown on the free body diagram in Figure 22, yields the following

equation:

$$P = p_{\infty} + \frac{2\sigma}{R} \quad , \tag{3-1}$$

where P is the total pressure within the bubble.

If the bubble contains a fixed mass, m_g, of ideal gas, then the pressure p_g can be represented by

$$p_g = \frac{3m_g R_g T}{4\pi R^3} \quad . \tag{3-2}$$

The quasistatic expansion of the inert gas during growth can be represented by

$$p_g (\underline{V})^n = \text{Constant},$$

or

$$p_g (R)^{3n} = \text{Constant}, \tag{3-3}$$

where n is the polytropic constant. Equation (3-3) can be written in terms of the initial conditions within the bubble. This equation is

$$p_g = p_{g_o} \left[\frac{R_o}{R}\right]^{3n} \quad . \tag{3-4}$$

The initial gas pressure, p_{g_o}, can be represented by equation (3-2). Thus, equation (3-2) becomes

$$p_{g_o} = G_o \frac{2\sigma}{(R_o)^3} \quad , \tag{3-5}$$

where

$$G_o \equiv \frac{3m_g R_g T_o}{8\pi\sigma} \quad . \tag{3-6}$$

Equation (3-1) can be expressed in a general form with the use of equations (3-4) and (3-5). Thus, the general equation which describes the quasistatic behavior of a spherical bubble is

$$\frac{p_\infty - p_v}{2\sigma} = G_o \frac{(R_o)^{3(n-1)}}{(R)^{3n}} - \frac{1}{R} \quad . \tag{3-7}$$

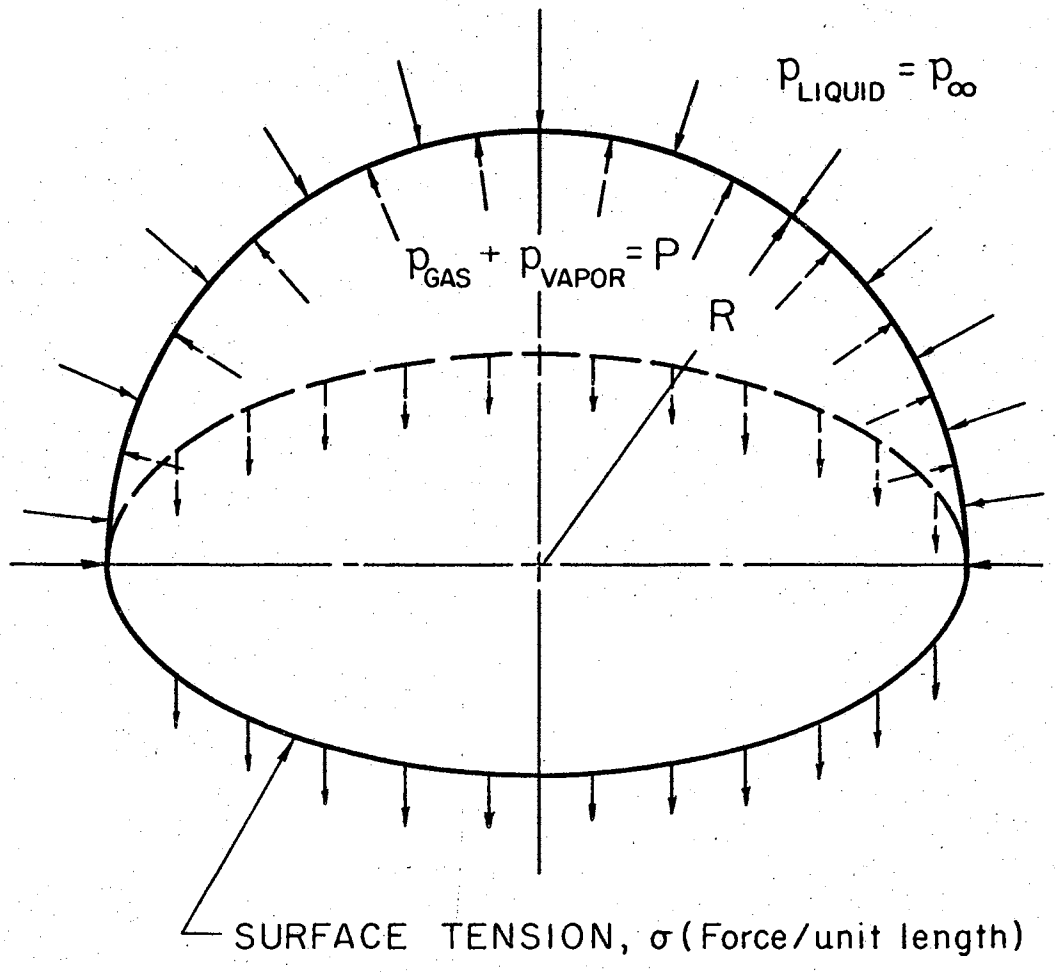

Figure 22. Free Body Diagram of a Spherical Bubble

Results of the Static Analysis of a Spherical Bubble

The results of this investigation are shown in Figures 23, 24, and 25 for two values of the parameter G_o/R_o^2. Two values of the polytropic constant were selected to illustrate the effect of the assumed process within the bubble. A polytropic constant of 1 corresponds to isothermal bubble behavior while the polytropic constant of 4/3 approximately represents adiabatic behavior within the bubble. Two values of the parameter G_o/R_o^2 were assumed in order to show a comparison between the polytropic processes. The liquid pressure, at which the bubble becomes unstable, decreases as the polytropic constant is increased. Daily and Johnson [17] obtained a family of similar curves for the isothermal behavior of a bubble in water at 68°F. The curves shown in Figures 23, 24, and 25 are not restricted to any particular fluid. Also, the process which occurs within a bubble is not restricted to isothermal changes.

Lienhard [44] reported that the thermodynamic criterion for mechanical stability specifies that a system is stable if for all possible variations of its state

$$\left[\frac{\partial p}{\partial v}\right]_T < 0 . \qquad (3\text{-}8)$$

Thus, the descending lines of constant G_o/R_o^2 in Figures 23 and 24 represent stable states and the ascending lines represent unstable conditions. The maximum stable radius,

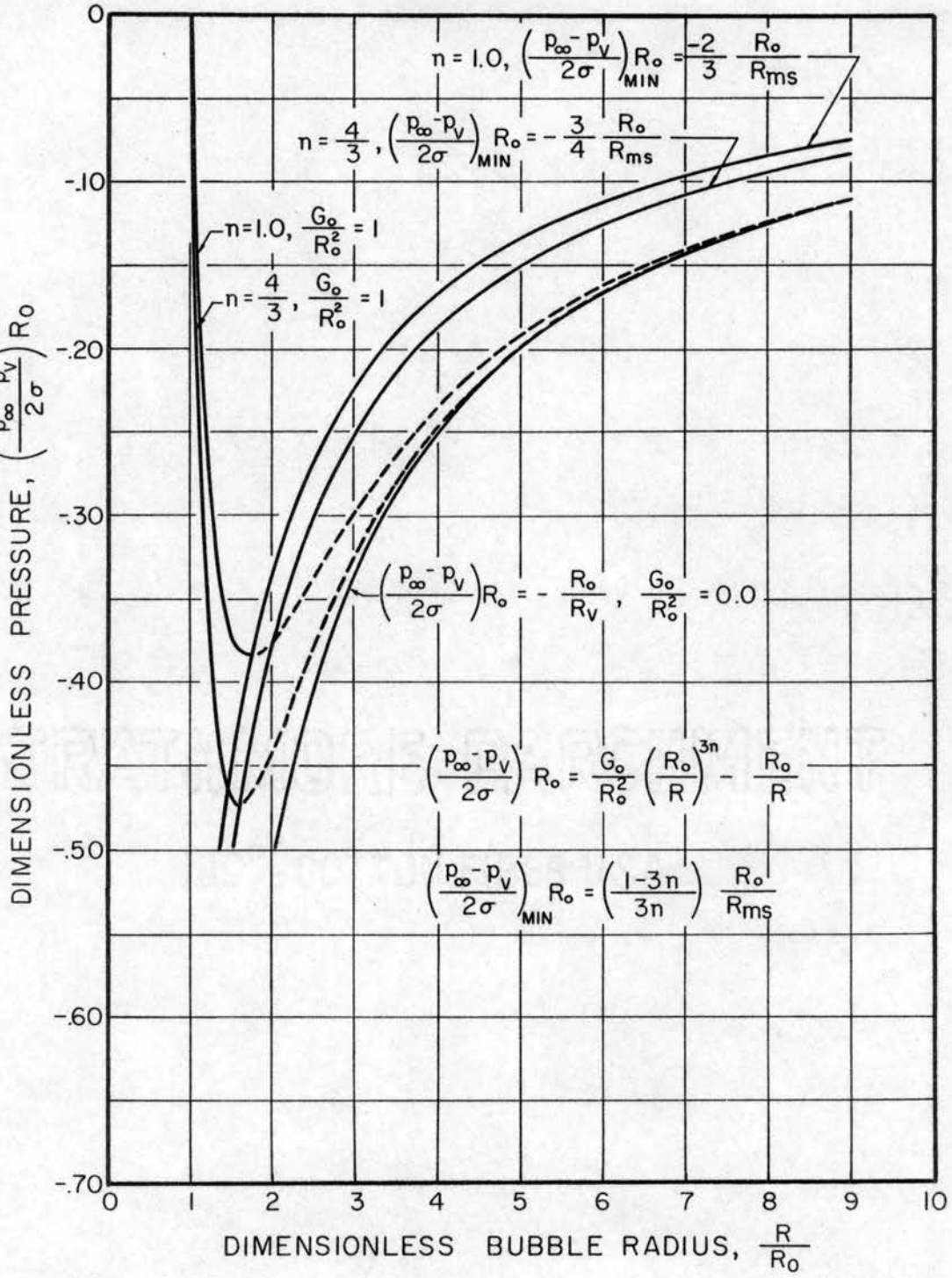

Figure 23. Generalized Dependence of $R_o(p_\infty - p_v)/2\sigma$ on Dimensionless Equilibrium Gas-Vapor Bubble Radius, for Two Values of the Polytropic Constant and a Value of 1 for the Parameter G_o/R_o^2

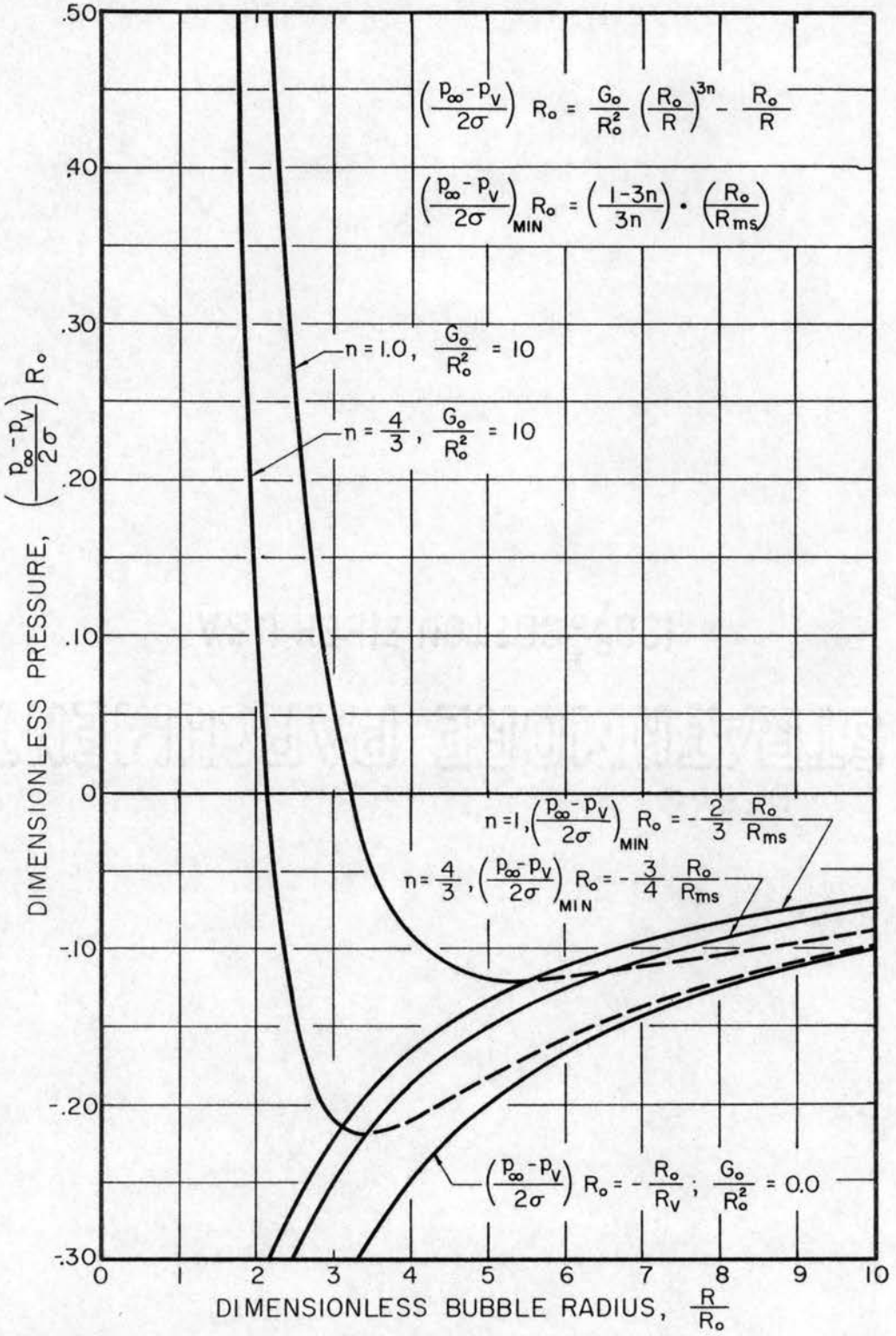

Figure 24. Generalized Dependence of $R_o(p_\infty - p_v)/2\sigma$ on Dimensionless Equilibrium Gas-Vapor Bubble Radius, for Two Values of the Polytropic Constant and a Value of 10 for the Parameter G_o/R_o^2

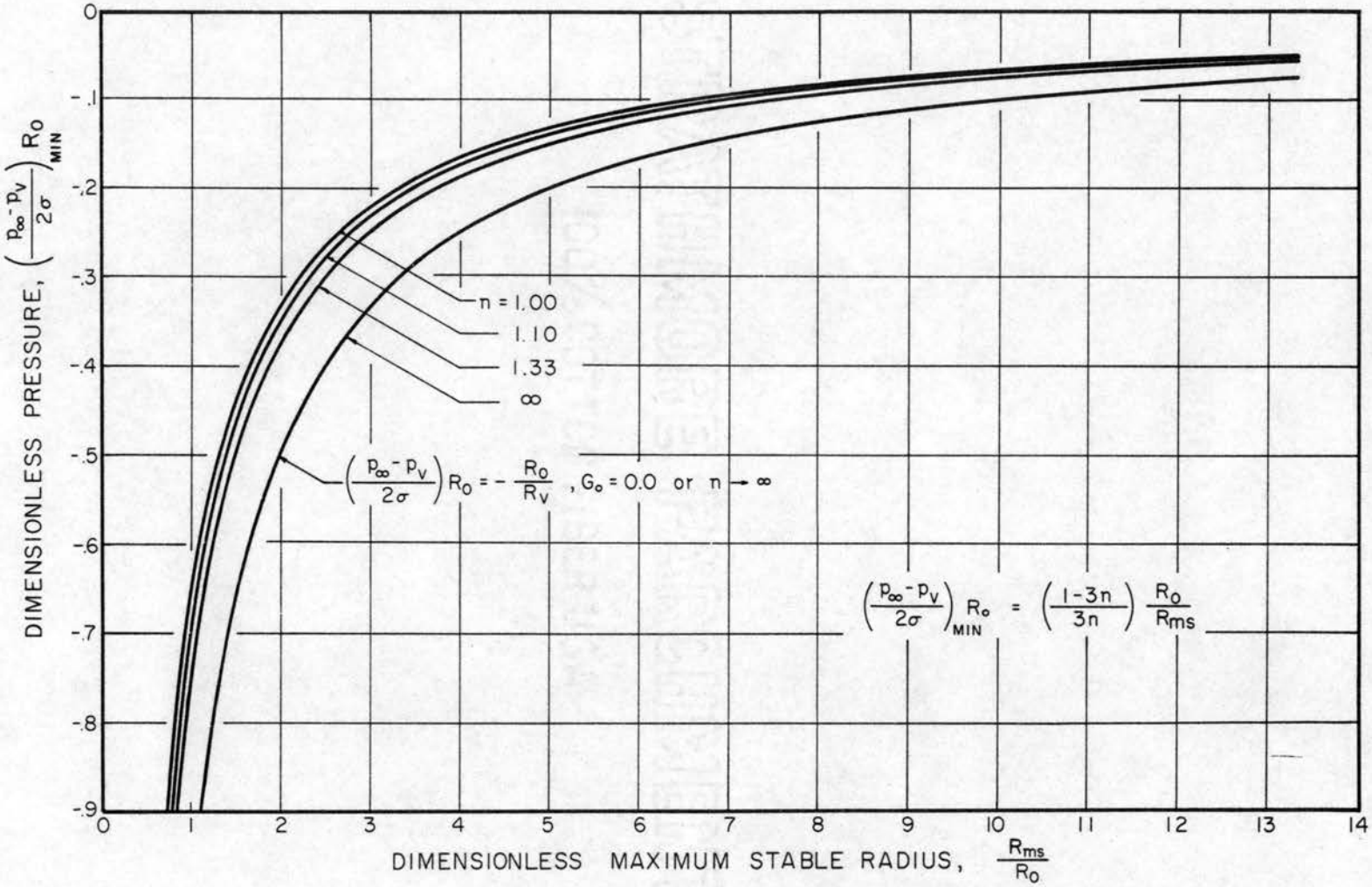

Figure 25. Variation of $R_o(p_\infty - p_v)_{min}/2\sigma$ with Dimensionless Maximum Stable Bubble Radius for Various Values of the Polytropic Constant

R_{ms}, for a given G_o is obtained by maximizing R in equation (3-7). The resulting general expression is

$$R_{ms} = \left[\frac{1 - 3n}{3n}\right] \left[\frac{2\sigma}{p_\infty - p_v}\right] . \qquad (3\text{-}9)$$

The radius, R_v, of a pure vapor bubble at the same pressure is obtained by setting $G_o = 0$ in equation (3-7):

$$R_v = \frac{2\sigma}{p_v - p_\infty} . \qquad (3\text{-}10)$$

Equations (3-9) and (3-10) are also plotted in Figures 23, 24, and 25.

An expression for R_{ms} as a function of R_v for the same $(p_\infty - p_v)/2\sigma$ can be obtained through the use of equations (3-9) and (3-10). This expression is

$$R_{ms} = \left[\frac{3n - 1}{3n}\right] R_v . \qquad (3\text{-}11)$$

Equation (3-11) is shown in Figure 26 (a) for various values of the parameter n. As G_o/R_o^2 is diminished at constant n, all possible unstable equilibrium radii will occur between R_{ms} and R_v (see Figure 26 (b)). The value of R_{ms} decreases as the value of $(p_\infty - p_v)/2\sigma$ is decreased.

Quasistatic Growth of a Small Bubble

Equation (3-7) may be used to describe the quasistatic growth of a small bubble provided conditions are such that the maximum stable radius is not exceeded. This is illus-

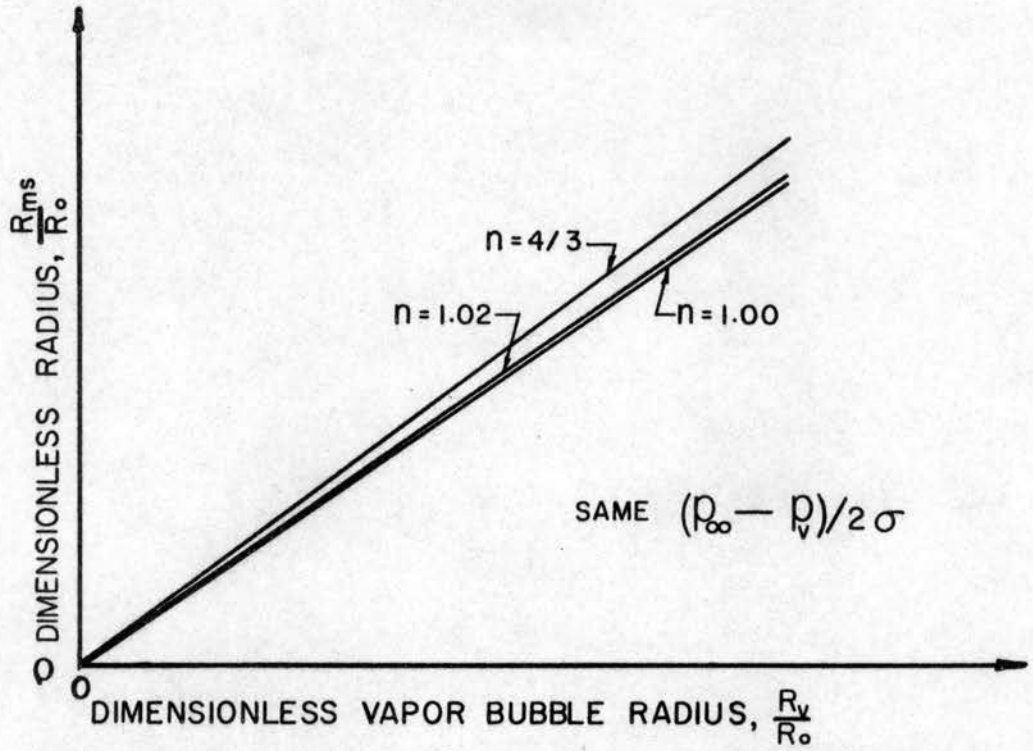

(a) Variation of R_{ms} with R_v for Various Values of n

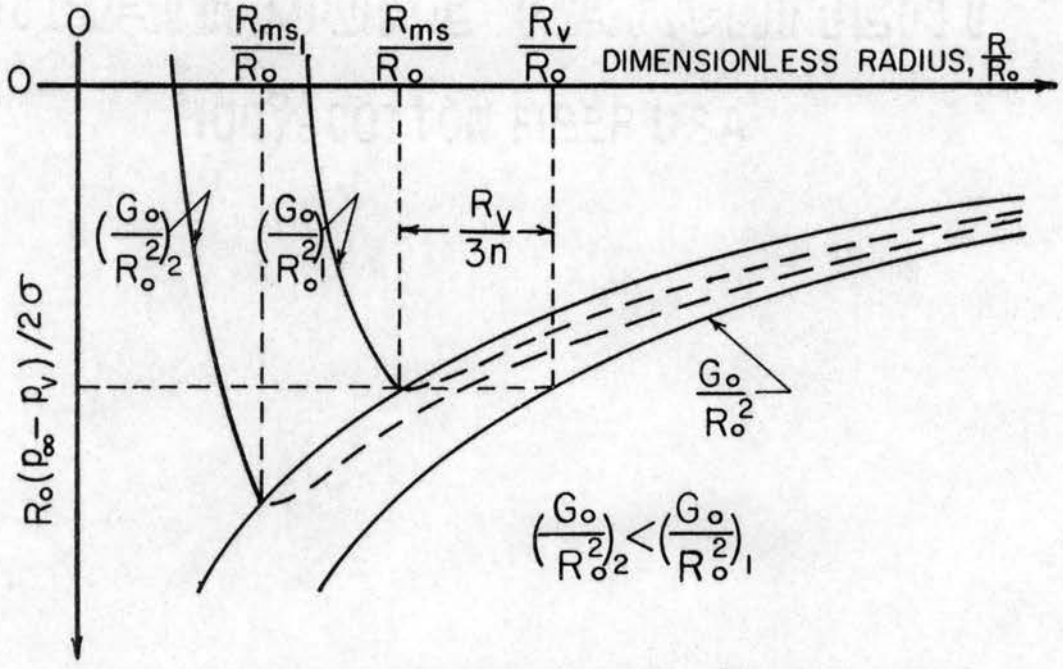

(b) Effect of Gas Content upon Bubble Growth

Figure 26. Effect of Polytropic Constant Upon Bubble Equilibrium

trated by the following example.

The pressure distribution experienced by a liquid flowing through a venturi type test section may be approximated by

$$p_\infty (t) = p_A + p_o \text{ Cos } (\omega t) .$$

Equation (3-7) was used to obtain an estimate of how the bubble radius varies as a function of time for the pressure distribution shown above. When the maximum radius is greater than R_{ms} the solution does not exist. Figure 27 illustrates the growth and collapse for various values of the polytropic constant.

Discussion of Polytropic Constant

Several investigators ([8], [17], etc.) of incipient cavitation have assumed that the process which takes place within a small bubble during growth is isothermal. In the preceding part of this chapter, the previous investigations of static bubble behavior were extended to cover various polytropic processes within a bubble. However, the actual process which takes place in small bubbles during growth is neither isothermal nor adiabatic. The actual process is at some intermediate position between these two limiting processes. Various arguments can be used to show that the temperature within a growing bubble does not remain constant. This is probably expressed most clearly by the experimental investigation of Hord, Jacobs, Robinson, and Sparks [45].

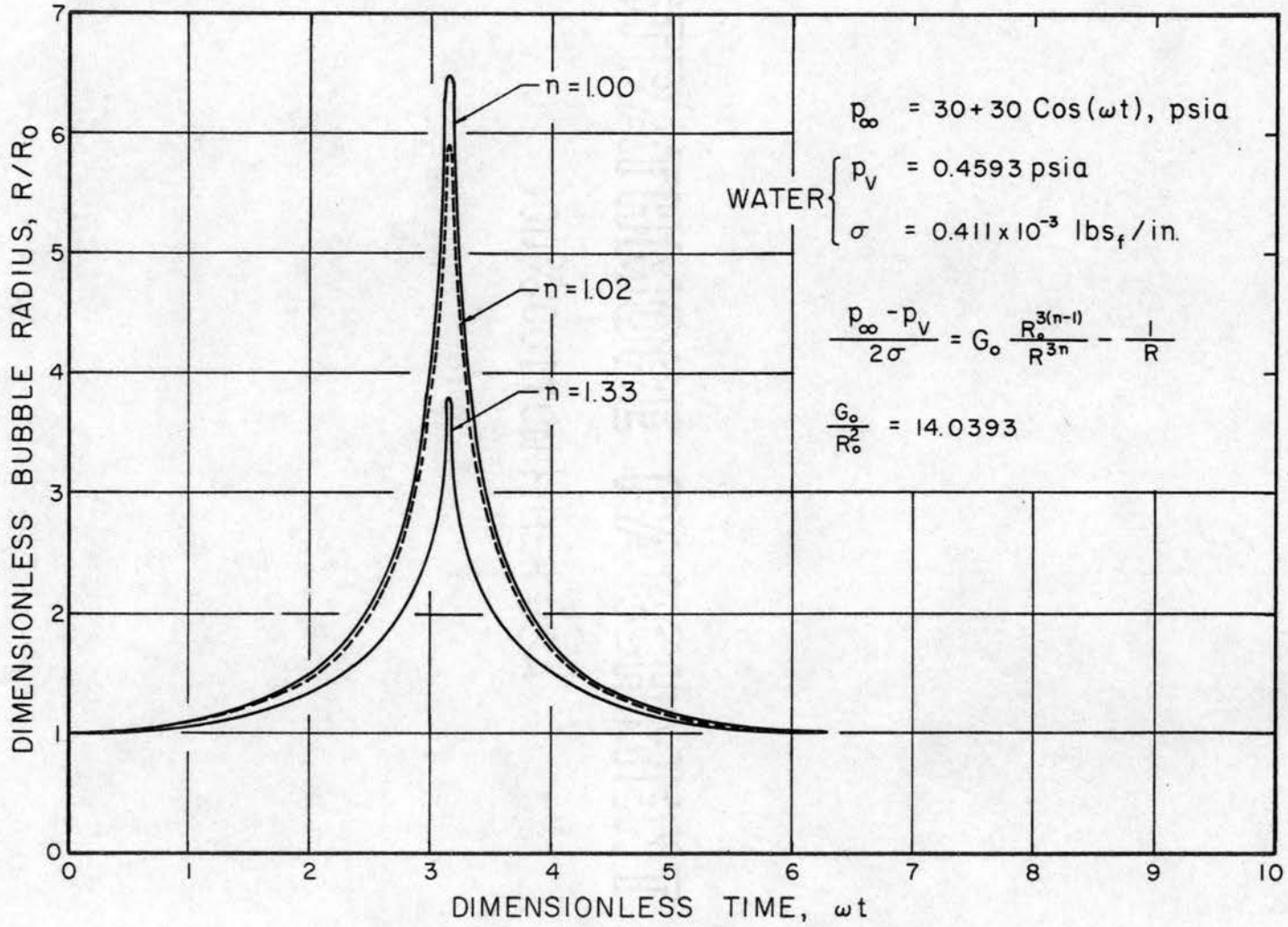

Figure 27. Quasistatic Growth of a Small Bubble for Various Polytropic Constants

The temperature in a bubble was expressed as a function of the initial conditions, polytropic constant, and bubble radius. The desired equation is

$$T = T_o \left[\frac{R}{R_o}\right]^{3(1-n)} . \qquad (3\text{-}12)$$

This equation was obtained by assuming that the inert gas pressure can be represented by a polytropic process and that the inert gas obeys the ideal gas equation of state. Equation (3-12) may not describe the actual process occurring in the bubble; however, it does furnish an equation which accounts for the temperature change, and this equation is simple enough to handle mathematically.

The correct selection of a value for the polytropic constant is important. This is illustrated by the following examples. If the bubble contains air and the process in the bubble is reversible and adiabatic, then n = k. For air, k has a value of 1.40. If the radius at incipient cavitation is 10 times the initial bubble radius and the initial temperature is 540°F, then a final temperature of 34.2°R is obtained by applying equation (3-16). This assumption of n = k is unrealistic because the final temperature is too low. A value of 1.01 for the polytropic constant results in a final temperature of 503°R. The correct value for the polytropic constant is difficult to estimate. However, the author feels that the following range of values for the polytropic constant should be considered when investigating

the growth of small bubbles:

$$1.00 \leq n \leq 1.02.$$

The above discussion explains the reason why many investigators have selected n to be 1.00. This assumption of 1.00 for n appears to be good when compared to the range of values given above. In the latter part of this chapter, the effect of small changes in n upon the maximum bubble radius will be demonstrated.

Analysis of Spherical Bubble Growth

The conditions for the static stability of a spherical gas-vapor bubble were examined in a preceding section. This is important in investigating the growth of small spherical bubbles because the stable bubble radius is necessary, as an initial condition, before a solution to the equation of motion of a spherical bubble can be obtained. This section is devoted to an investigation of the effects of viscosity, surface tension, stream pressure, stream velocity, polytropic changes within the bubble, and initial bubble radius upon bubble growth and hence, upon incipient cavitation.

Assumptions and Discussion of Model

The mathematical model is formulated so that it will simulate the actual conditions that occur when a liquid flows through a venturi type test section. Several assumptions are necessary in order to be able to mathe-

matically determine when incipient cavitation will occur.

The interaction between the flow around an expanding bubble and the flow of the liquid through a convergent-divergent test section is not considered. Thus, the motion of the expanding bubble will be treated as though the liquid is infinite in all directions. The effect of the flow through the test section is related to the bubble growth through the $p_\infty(t)$ term in the equation of motion for a spherical bubble.

The bubble is assumed to move with the liquid. For the very small bubbles considered here, buoyant forces are small and the viscous drag will be high so that any relative motion between the bubble and the liquid will be very small.

In this investigation it is assumed that cavitation is initiated from small nuclei (small spherical bubbles) which contain air or vapor, or both. These small bubbles are assumed to remain spherical during the growth period. In the noncavitating flow regime it is assumed that the nuclei do not have an opportunity to grow into bubbles of macroscopic or visible size. The difference, then, between the noncavitating and the cavitating flow regimes is that in the latter the nuclei are exposed to a pressure environment favorable to bubble growth for a period sufficient to allow the appearance of macroscopic bubbles (see Figure 28). Consequently, two distinct problems must be considered in dealing with the matter of incipient cavitation. The first problem is the effect of free stream velocity, free stream

static pressure, and test section size and shape in establishing a pressure environment favorable to bubble growth. The second problem is the response of the nuclei to the transient low pressure created by the flow of the liquid through the test section. If the pressure distribution through the test section is given, the first problem is trivial. In addition to difficulties of a purely mathematical nature, the second problem poses some questions about the physical properties of the nuclei for which no definite information is available.

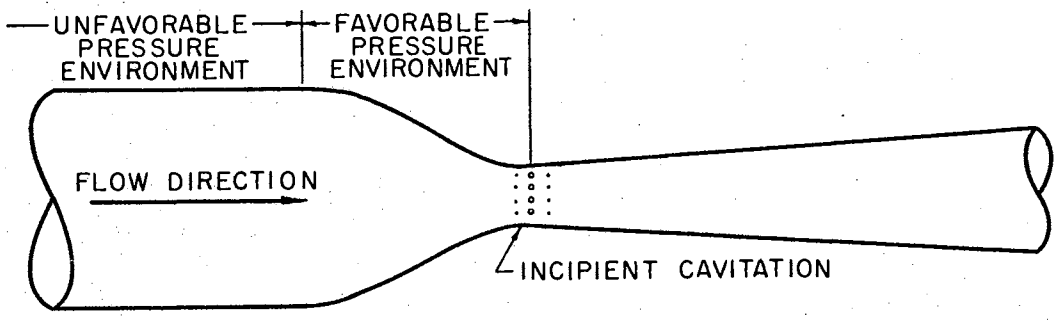

Figure 28. Physical Description of Model

Although it seems quite probable that the nuclei in a liquid have a range of sizes, it will be assumed here that all nuclei are of equal radius R_o. Incipient cavitation will be said to exist if a nucleus grows from its initial radius R_o to a radius of 254 microns (10^{-2} inches) during the time it is exposed to the pressure which favors growth. This definition is arbitrary, but it does have the virtue of being simple enough to work with. This definition, although certainly not an absolute measure of a physical event, provides a framework within which the properties that influence the inception of cavitation may be investigated. If this definition is used, the problem of finding the conditions for incipient cavitation is: Given a fixed time for growth, determined by the free stream velocity and test section size and shape, what must the free stream static pressure be, p_{ref} (and hence K_{i_t}), such that the required bubble growth will just take place?

Equation of Motion for a Spherical Bubble

The equation which describes the growth of a small spherical bubble containing a fixed mass of inert gas is (see Appendix A for derivation)

$$\rho_L \left[R \ddot{R} + \frac{3}{2} (\dot{R})^2\right] + \frac{2\sigma}{R} + \frac{4\mu_L \dot{R}}{R} = p_g + p_v - p_\infty . \quad (3\text{-}13)$$

The density and viscosity of the liquid are assumed to remain constant during bubble growth. The vapor pressure and surface tension can be represented as functions of the

temperature within the bubble. During growth the temperature can be represented as a function of the bubble radius (equation (3-12)). The inert gas pressure may be expressed as a function of the bubble radius and the polytropic constant n. Thus, the inert gas pressure is given by

$$p_g = \left[p_\infty(0) - p_v(T_o) + \frac{2\sigma(T_o)}{R_o}\right]\left[\frac{R_o}{R}\right]^{3n} . \qquad (3\text{-}14)$$

By substituting equation (3-14) into equation (3-15), we obtain

$$\rho_L\left[R\ddot{R} + \frac{3}{2}(\dot{R})^2\right] + \frac{2\sigma}{R} + \frac{4\mu_L\dot{R}}{R} = \left[p_\infty(0) - p_v(T_o) + \frac{2\sigma(T_o)}{R_o}\right]\left[\frac{R_o}{R}\right]^{3n} + p_v - p_\infty . \qquad (3\text{-}15)$$

The pressure, p_∞, within the liquid can be represented as a function of time.

The necessary boundary conditions are

$$R(0) = R_o, \quad \text{and} \quad \dot{R}(0) = \ddot{R}(0) = 0. \qquad (3\text{-}16)$$

Equation (3-15) is a nonlinear ordinary differential equation. There are no known exact solutions to this equation; therefore, it will be necessary to resort to numerical techniques in order to obtain an approximate solution.

Numerical Technique

Several numerical methods were investigated in an

attempt to obtain a solution to equation (3-15). Only a brief discussion of the unsuccessful attempts will be presented. The major part of this section will be devoted to the numerical technique used to obtain solutions to equation (3-15).

The functional representation of equation (3-15 is

$$\ddot{R} = f(R, \dot{R}, t). \tag{3-17}$$

Several of the numerical methods (Milne [46], Adams-Stormer [47], etc.) investigated were not self-starting. That is, in these methods each step of the integration requires the knowledge of past values of the solution which are not available at the start of the integration. There exist analytic methods for computing the starting values. The most common of the analytic methods is to expand R in a Taylor series about t_o,

$$R(t) = R_o + t\,\dot{R}_o + \frac{t^2\,\ddot{R}_o}{2!} + \cdots \tag{3-18}$$

This series provides an equation for computing the necessary starting points if the Taylor series converges. The Taylor series which describes R for equation (3-15) did not appear to converge.

One of the most common ways of starting the solution is to use the self-starting Runge-Kutta method. This method requires only the initial conditions to start the solution. In contrast to the formal Taylor series solution, equation (3-18), the Runge-Kutta method does not require explicit

definitions or evaluations of derivatives beyond the second. Approximations are obtained at the expense of several evaluations of the second derivatives.

The Runge-Kutta fourth-order integration procedure is shown in Table II. This is the numerical technique followed in obtaining solutions to equation (3-15).

The accuracy of a step-by-step solution of a differential equation is often difficult to determine. The Runge-Kutta method has no check; therefore, the error cannot be determined. However, it is near the order of $(\Delta t)^5$. Improvement on the accuracy can be achieved by taking smaller intervals. However, a decrease of interval size adds to the labor and increases the possible round-off error.

Solutions to equation (3-15) were obtained with the aid of the IBM 7040 digital computer (See Appendices B and C for listings of programs). All computations were performed using double precision. Double precision provides extra storage (16 digits) for the data and calculations. This was necessary in order to help eliminate the round-off error.

Solutions to Equation of Motion for Isothermal Bubble Growth

Equation (3-15) was solved using the Runge-Kutta fourth-order procedure outlined in Table II. A value of 1.00 was selected for the polytropic constant, n. Thus, the temperature within the bubble remains constant during the growth period.

Before a solution to equation (3-15) can be obtained the

TABLE II

RUNGE-KUTTA METHOD

$$\ddot{R} = f(R, \dot{R}, t)$$

Initial Conditions: R_o, $\dot{R}_o$, t_o			
t	R	$\dot{R}$	$\ddot{R}$
$t_{11} = t_o$	$R_{11} = R_o$	$\dot{R}_{11} = \dot{R}_o$	$\ddot{R}_{11} = f(R_o, \dot{R}_o, t_o)$
$t_{12} = t_{11} + \frac{\Delta t}{2}$	$R_{12} = R_{11} + \dot{R}_{11} \frac{\Delta t}{2}$	$\dot{R}_{12} = \dot{R}_{11} + \ddot{R}_{11} \frac{\Delta t}{2}$	$\ddot{R}_{12} = f(R_{12}, \dot{R}_{12}, t_{12})$
$t_{13} = t_{11} + \frac{\Delta t}{2}$	$R_{13} = R_{11} + \dot{R}_{12} \frac{\Delta t}{2}$	$\dot{R}_{13} = \dot{R}_{11} + \ddot{R}_{12} \frac{\Delta t}{2}$	$\ddot{R}_{13} = f(R_{13}, \dot{R}_{13}, t_{13})$
$t_{14} = t_{11} + \Delta t$	$R_{14} = R_{11} + \dot{R}_{13} \Delta t$	$\dot{R}_{14} = \dot{R}_{11} + \ddot{R}_{13} \Delta t$	$\ddot{R}_{14} = f(R_{14}, \dot{R}_{14}, t_{14})$
		$\Delta\dot{R}_1 = \frac{\Delta t}{6}[\dot{R}_{11} + 2\dot{R}_{12} + 2\dot{R}_{13} + \dot{R}_{14}]$	$\Delta\ddot{R}_1 = \frac{\Delta t}{6}[\ddot{R}_{11} + 2\ddot{R}_{12} + 2\ddot{R}_{13} + \ddot{R}_{14}]$
$t_{21} = t_{11} + \Delta t$	$R_{21} = R_{11} + \Delta R_1$	$\dot{R}_{21} = \dot{R}_{11} + \Delta\dot{R}_1$	$\ddot{R}_{21} = f(R_{21}, \dot{R}_{21}, t_{21})$
$t_{22} = t_{21} + \frac{\Delta t}{2}$	$R_{22} = R_{21} + \dot{R}_{21} \frac{\Delta t}{2}$	$\dot{R}_{22} = \dot{R}_{21} + \ddot{R}_{21} \frac{\Delta t}{2}$	$\ddot{R}_{22} = f(R_{22}, \dot{R}_{22}, t_{22})$
$t_{23} = t_{21} + \frac{\Delta t}{2}$	$R_{23} = R_{21} + \dot{R}_{22} \frac{\Delta t}{2}$	$\dot{R}_{23} = \dot{R}_{21} + \ddot{R}_{22} \frac{\Delta t}{2}$	$\ddot{R}_{23} = f(R_{23}, \dot{R}_{23}, t_{23})$
$t_{24} = t_{21} + \Delta t$	$R_{24} = R_{21} + \dot{R}_{23} \Delta t$	$\dot{R}_{24} = \dot{R}_{21} + \ddot{R}_{23} \Delta t$	$\ddot{R}_{24} = f(R_{24}, \dot{R}_{24}, t_{24})$
		$\Delta\dot{R}_2 = \frac{\Delta t}{6}[\dot{R}_{21} + 2\dot{R}_{22} + 2\dot{R}_{23} + \dot{R}_{24}]$	$\Delta\ddot{R}_2 = \frac{\Delta t}{6}[\ddot{R}_{21} + 2\ddot{R}_{22} + 2\ddot{R}_{23} + \ddot{R}_{24}]$
$t_{31} = t_{21} + \Delta t$	$R_{31} = R_{21} + \Delta R_2$	$\dot{R}_{31} = \dot{R}_{21} + \Delta R_2$	$\ddot{R}_{31} = f(R_{31}, \dot{R}_{31}, t_{31})$

pressure-time history within the liquid must be specified. In this investigation, two different functions were used to represent the liquid pressure, $p_\infty(t)$. The first function selected to represent the liquid pressure is

$$p_\infty(t) = p_A - p_o \operatorname{Sin}(\omega t). \qquad (3\text{-}19)$$

This function was selected to represent the pressure within the liquid so that a comparison between this investigation and the investigation reported by Noltingk and Neppiras [8] could be made. Noltingk and Neppiras obtained solutions to equation (3-15) by using a differential analyzer. They neglected the effect of viscosity and vapor pressure. They obtained solutions for a range of values of the parameters p_o, p_A, ω and R_o for a water medium with a density of 1 gram-mass/cm^3 and a surface tension of 80 dynes/cm. The parameter ω was selected so that equation (3-19) described the pressure experienced by a liquid in ultrasonically ($\omega \geq 10^5$ rad/sec) induced cavitation.

If equation (3-19) is substituted into equation (3-15) and if the viscosity and vapor pressure terms are neglected, the bubble growth equation becomes

$$\rho_L \left[R\ddot{R} + \frac{3}{2}(\dot{R})^2\right] + \frac{2\sigma}{R} = \left[p_A + \frac{2\sigma}{R_o}\right]\left[\frac{R_o}{R}\right]^3 - p_A + p_o \operatorname{Sin}(\omega t). \qquad (3\text{-}20)$$

Equation (3-20) was solved for various values of the parameters p_A, p_o, R_o, and ω. Figure 29 shows one of these

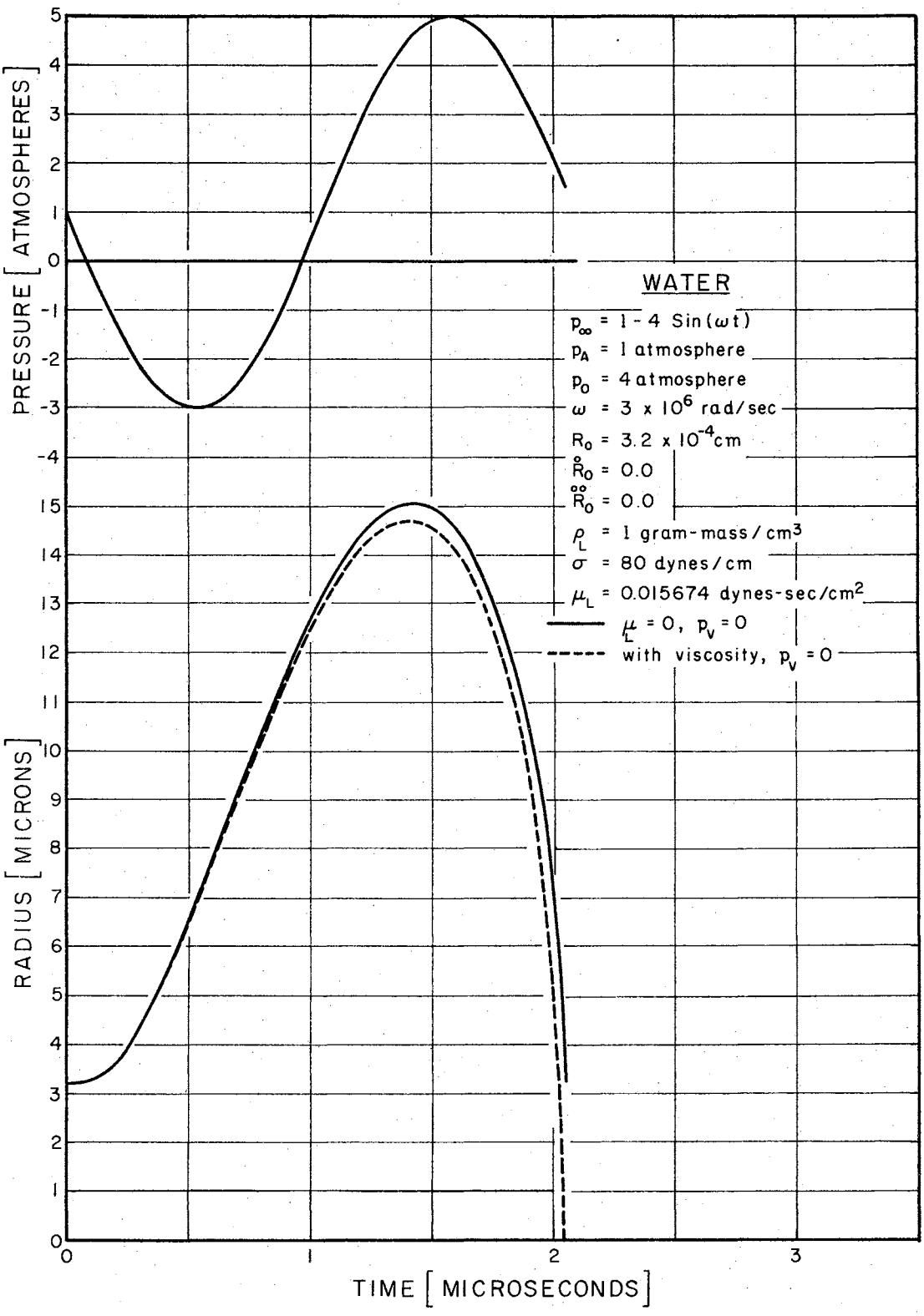

Figure 29. Growth of a Small Gas-Vapor Bubble for an ω of 3×10^6 rad/sec

solutions. A maximum bubble radius of 15.05 microns occurred at 1.42 microseconds. This agrees with the maximum radius of 15 microns at 1.40 microseconds obtained by Noltingk and Neppiras.

In order to illustrate the effect of viscosity upon the growth of small bubbles, the viscosity term, $4\mu_L\dot{R}/R$, was added to the left side of equation (3-20). The effect of considering the viscosity term can be seen in Figure 29. A maximum radius of 14.7 microns occurred at 1.41 microseconds. Thus, the viscosity term caused a 2.3 per cent decrease in the maximum bubble radius. Several other solutions, for lower values of ω, did not show this much change. Thus, as the velocity of the bubble wall increases the viscous term becomes more important; however, the effect on the maximum bubble radius is small.

The second function selected to represent the pressure within the liquid is

$$p_\infty(t) = p_A + p_o\text{Cos}(\omega t). \qquad (3\text{-}21)$$

This function was selected to approximate the pressure experienced by a liquid while flowing through a venturi type test section. Thus, when equation (3-21) is substituted into equation (3-15) the equation of motion for isothermal bubble growth becomes

$$\rho_L\left[R\ddot{R} + \frac{3}{2}(\dot{R})^2\right] + \frac{2\sigma}{R} + \frac{4\mu_L\dot{R}}{R} = \left[p_A + p_o - p_v + \frac{2\sigma}{R_o}\right]\left[\frac{R_o}{R}\right]^3 + p_v - p_A - p_o\,\text{Cos}(\omega t). \qquad (3\text{-}22)$$

Several solutions to equation (3-22) are shown in Figures 30, 31, 32, 33, 34, and 35. These figures illustrate the effect of the parameter ω.

Figures 33, 34, and 35 show variations of the bubble radius with time for various values of the parameter R_o. The maximum bubble radius increases as R_o is increased.

Figure 34 illustrates the effect of viscosity, vapor pressure, and surface tension upon the growth of a small bubble. Three different values of the initial bubble radius were selected. Viscosity was found to have little effect upon the maximum bubble radius. This is due to a much smaller growth rate than is illustrated in Figure 29. When the surface tension term was neglected the maximum bubble radius increased by a factor of 1.25 times the value of R_M obtained by considering surface tension. Thus, the surface tension term should not be neglected when studying the growth of bubbles of this size.

A vapor pressure of 0.8268×10^{-2} atmospheres was used to show the effect of vapor pressure upon maximum bubble radius. This effect can be seen in Figure 34. The result of considering the vapor pressure term is, in effect, a change in the forcing function term, $p_\infty(t)$. Nevertheless, Figure 34 does point out that a small decrease in the stream pressure once it is near the vapor pressure will cause a considerable change in the maximum bubble radius.

The effect of liquid properties upon bubble growth can be seen by examining Figures 34 and 35. The liquid

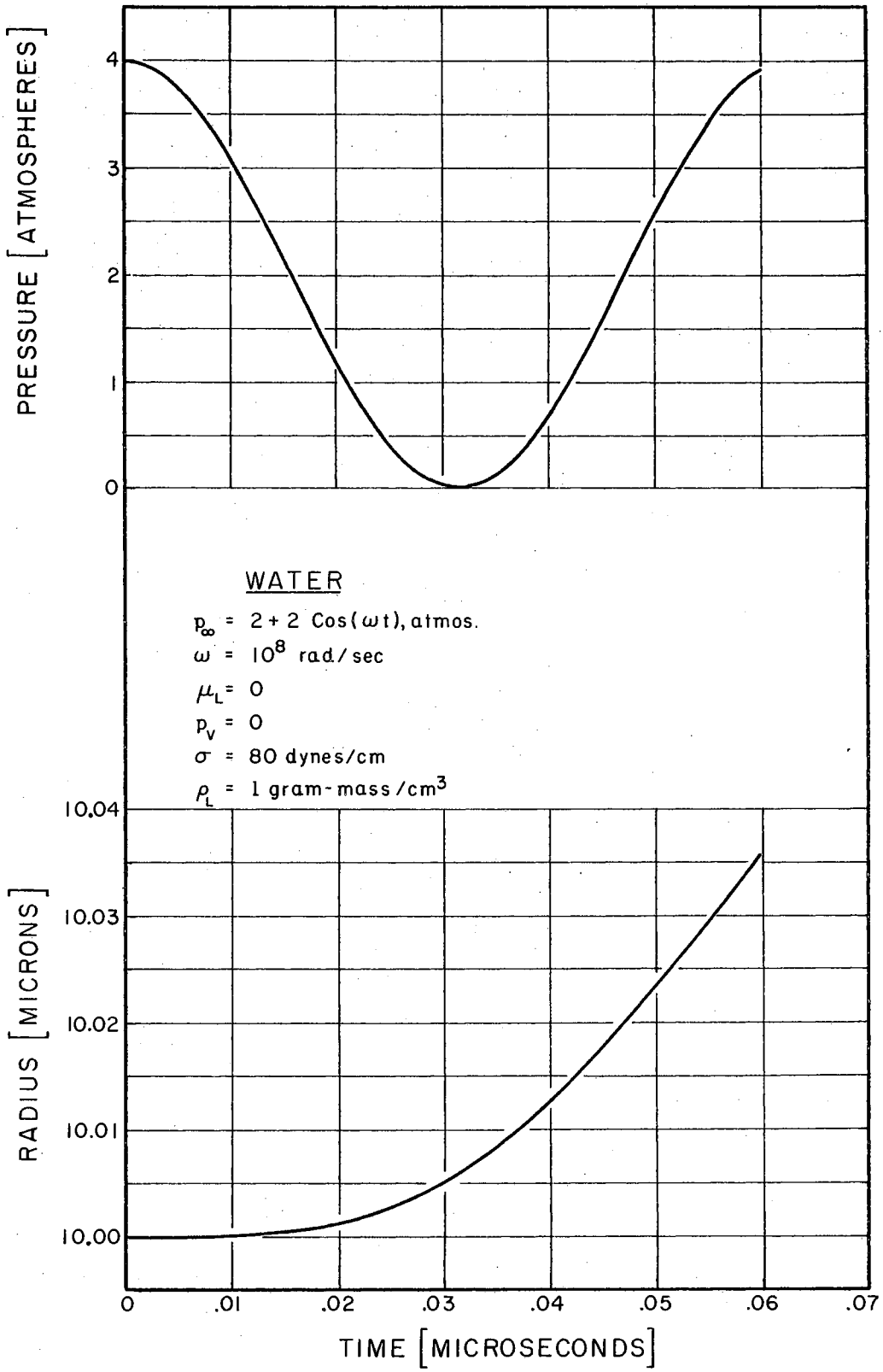

Figure 30. Growth of a Small Gas-Vapor Bubble for an ω of 10^8 rad/sec

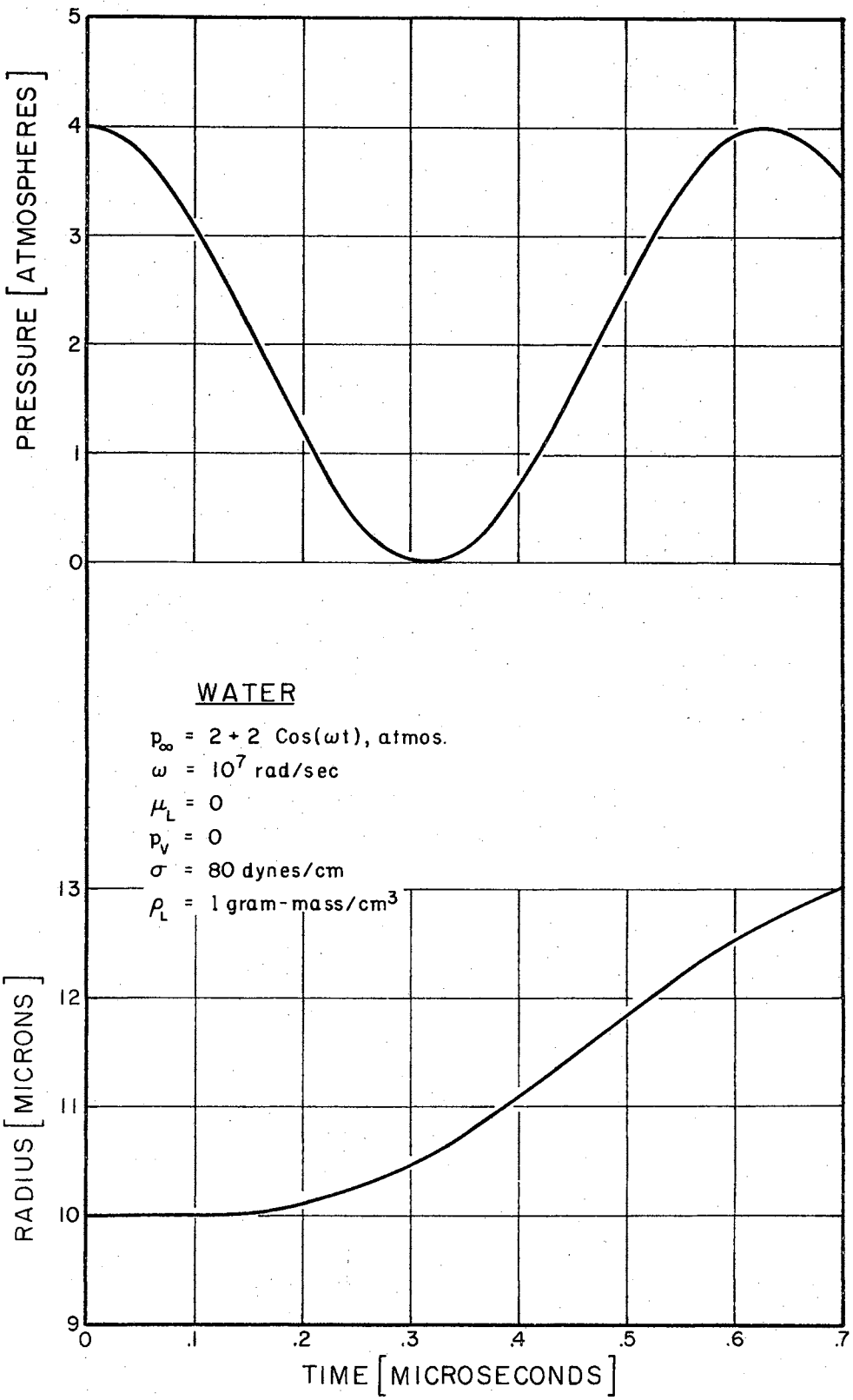

Figure 31. Growth of a Small Gas-Vapor Bubble for an ω of 10^7 rad/sec

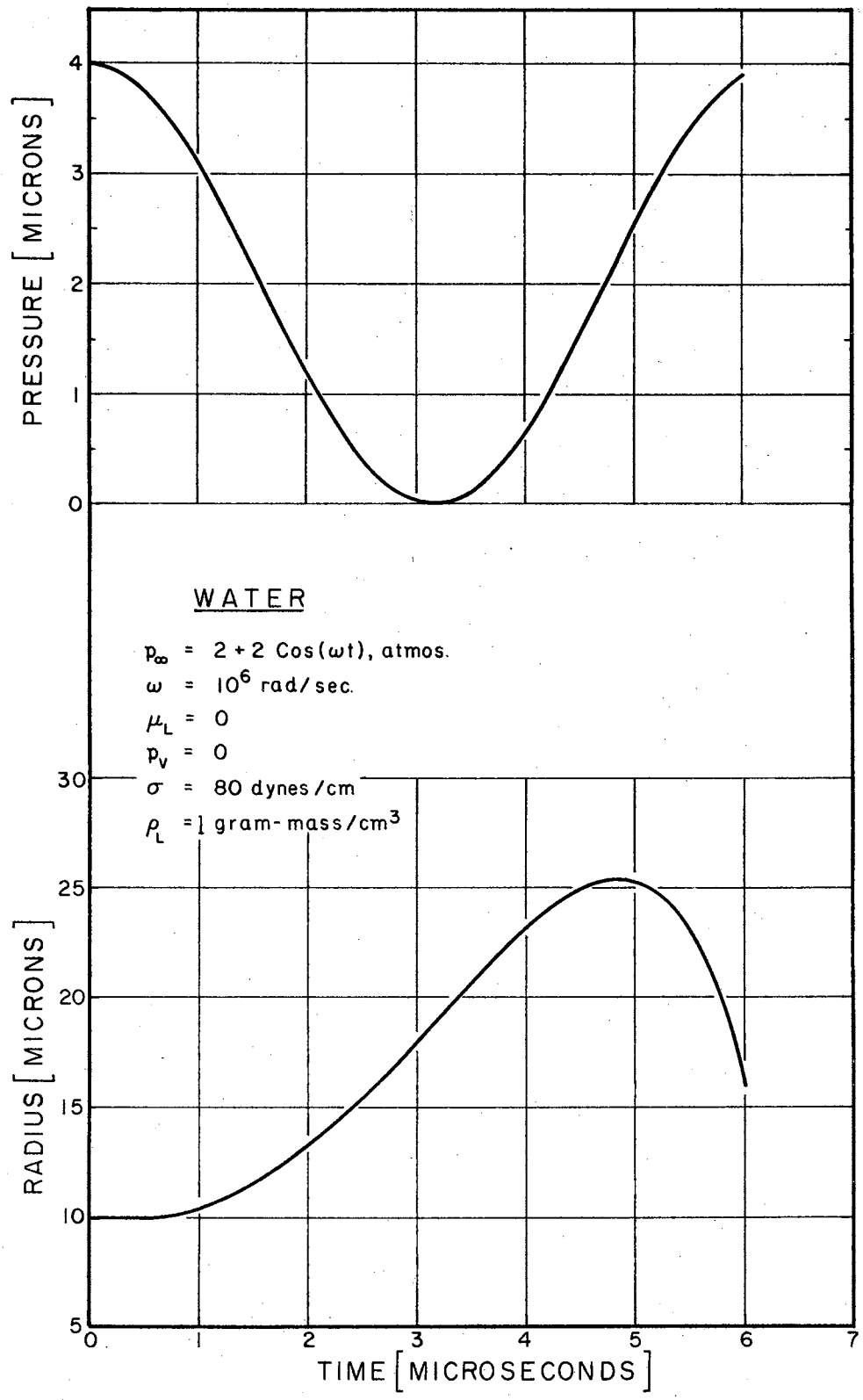

Figure 32. Growth of a Small Gas-Vapor Bubble for an ω of 10^6 rad/sec

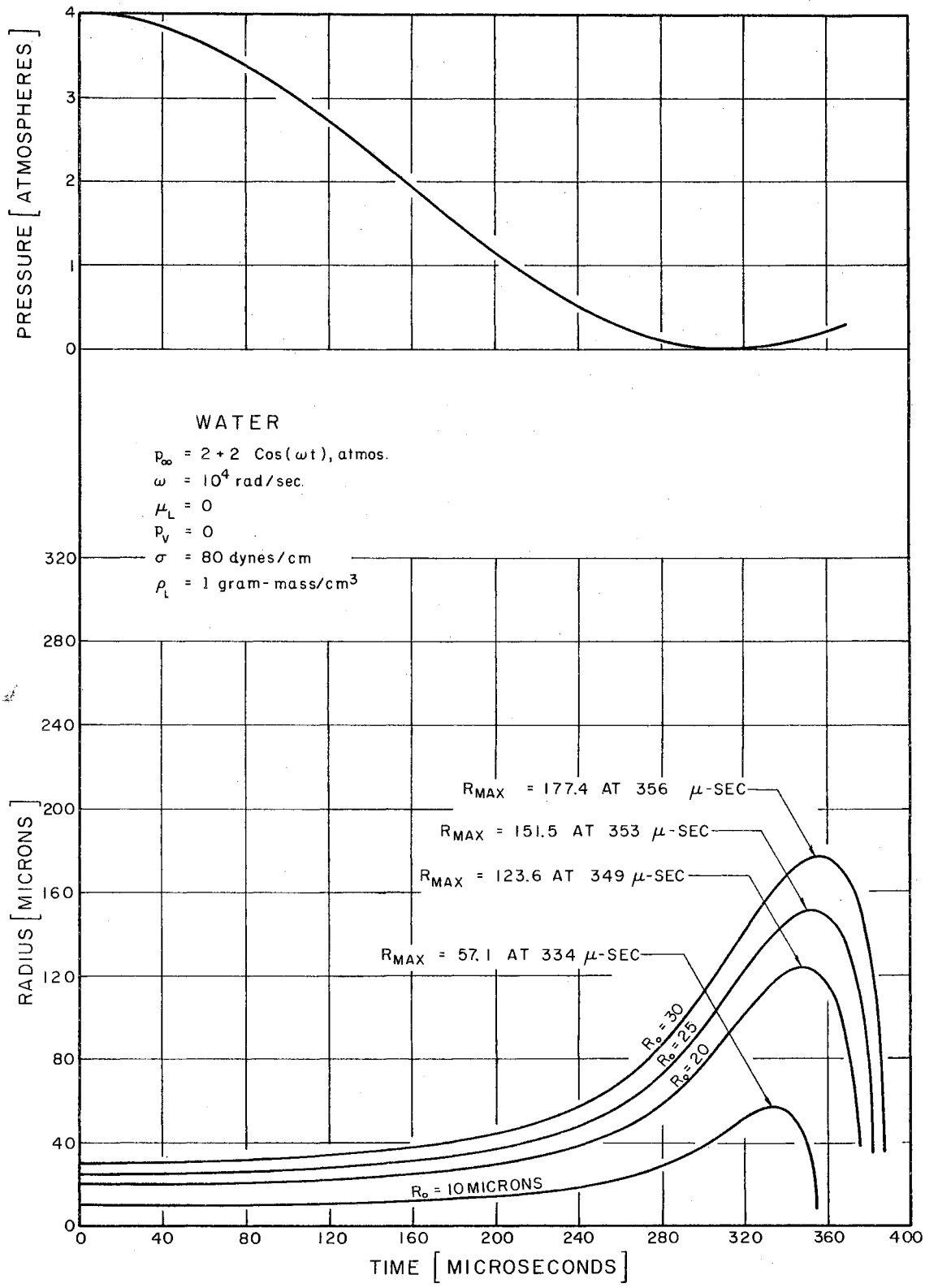

Figure 33. Growth of a Small Gas-Vapor Bubble for an ω of 10^4 rad/sec

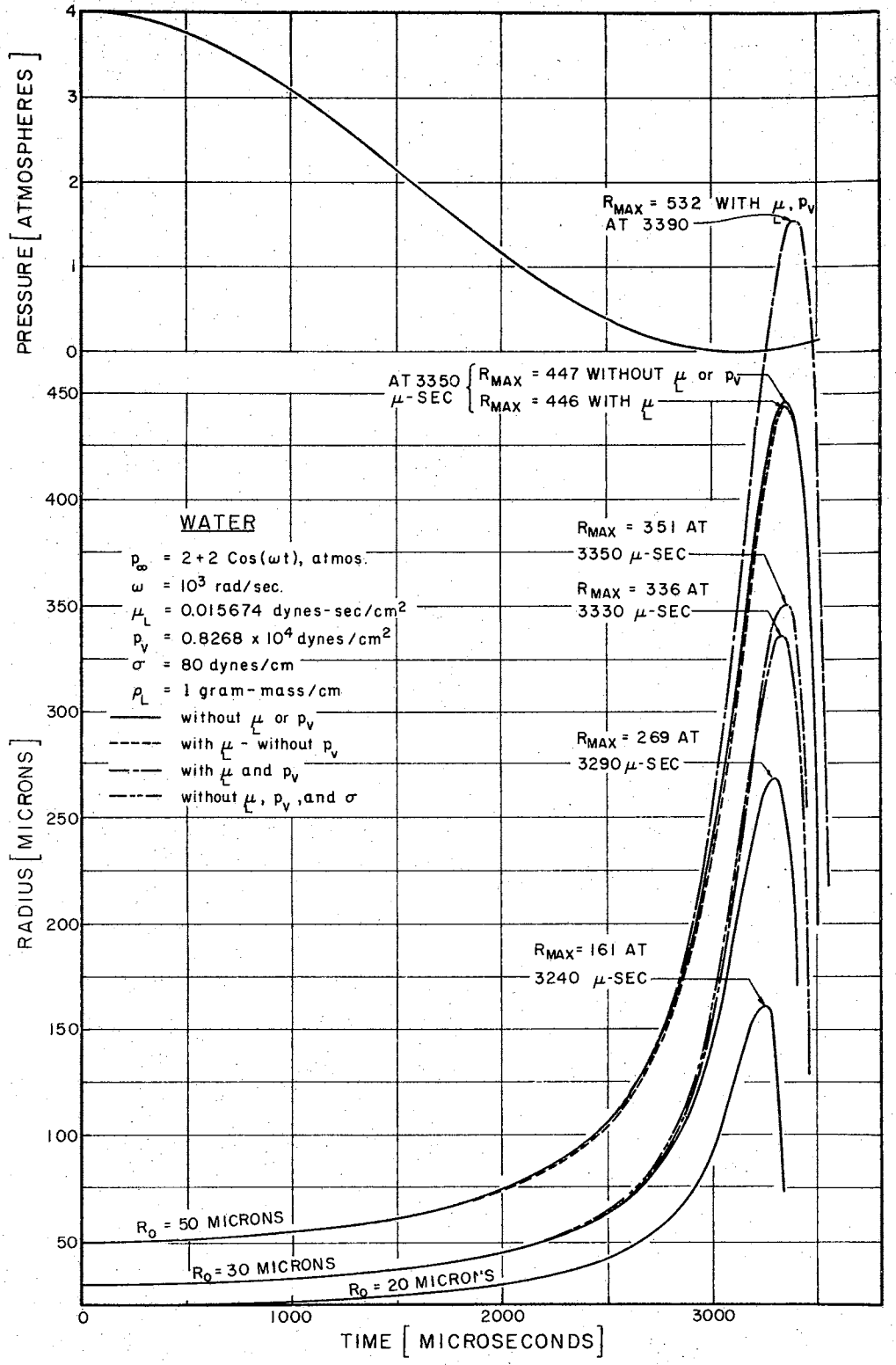

Figure 34. Effect of Viscosity, Vapor Pressure, and Surface Tension Upon the Growth of a Small Gas-Vapor Bubble

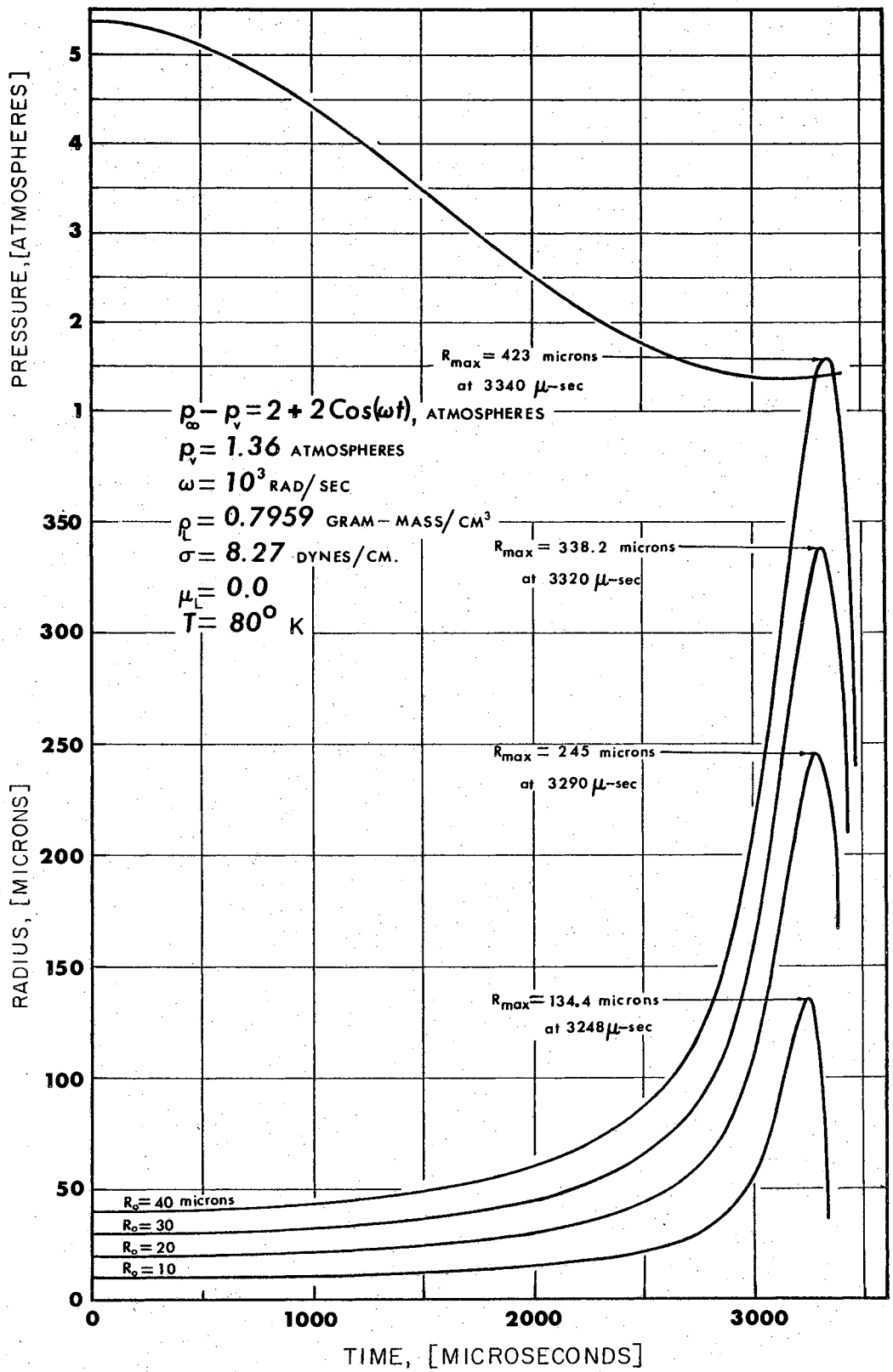

Figure 35. Growth of a Small Bubble in Liquid Nitrogen

properties used in obtaining Figure 35 are those of liquid nitrogen at 80°K. The magnitude of the surface tension was taken to be 8.27 dynes/cm. This is approximately an order of magnitude lower than was used in obtaining Figure 34. These figures help to illustrate the importance of the magnitude of surface tension when investigating the growth of small bubbles. As the magnitude of the surface tension decreases (for different liquids), it becomes easier for small nuclei to grow.

Summary of Solutions to Equation of Motion for Isothermal Bubble Growth

The theoretical investigation of the growth of small bubbles, using equation (3-22), is summarized and presented in Figures 36, 37, 38, 39, and 40. Two different values of the parameter ω were selected. The parameter ω simulates the effect of liquid velocity upon bubble growth.

The variation of maximum bubble radius with initial bubble radius for various amplitudes of the forcing function is shown in Figures 36 and 37. The maximum bubble radius increases as the initial bubble radius increases for a given amplitude of the forcing function. This increase is greater as ω is decreased.

Figure 38 shows the variation of time (at which the maximum bubble radius occurs) with initial bubble radius for various amplitudes of the forcing function. The time at which R_M occurs will increase as the initial bubble

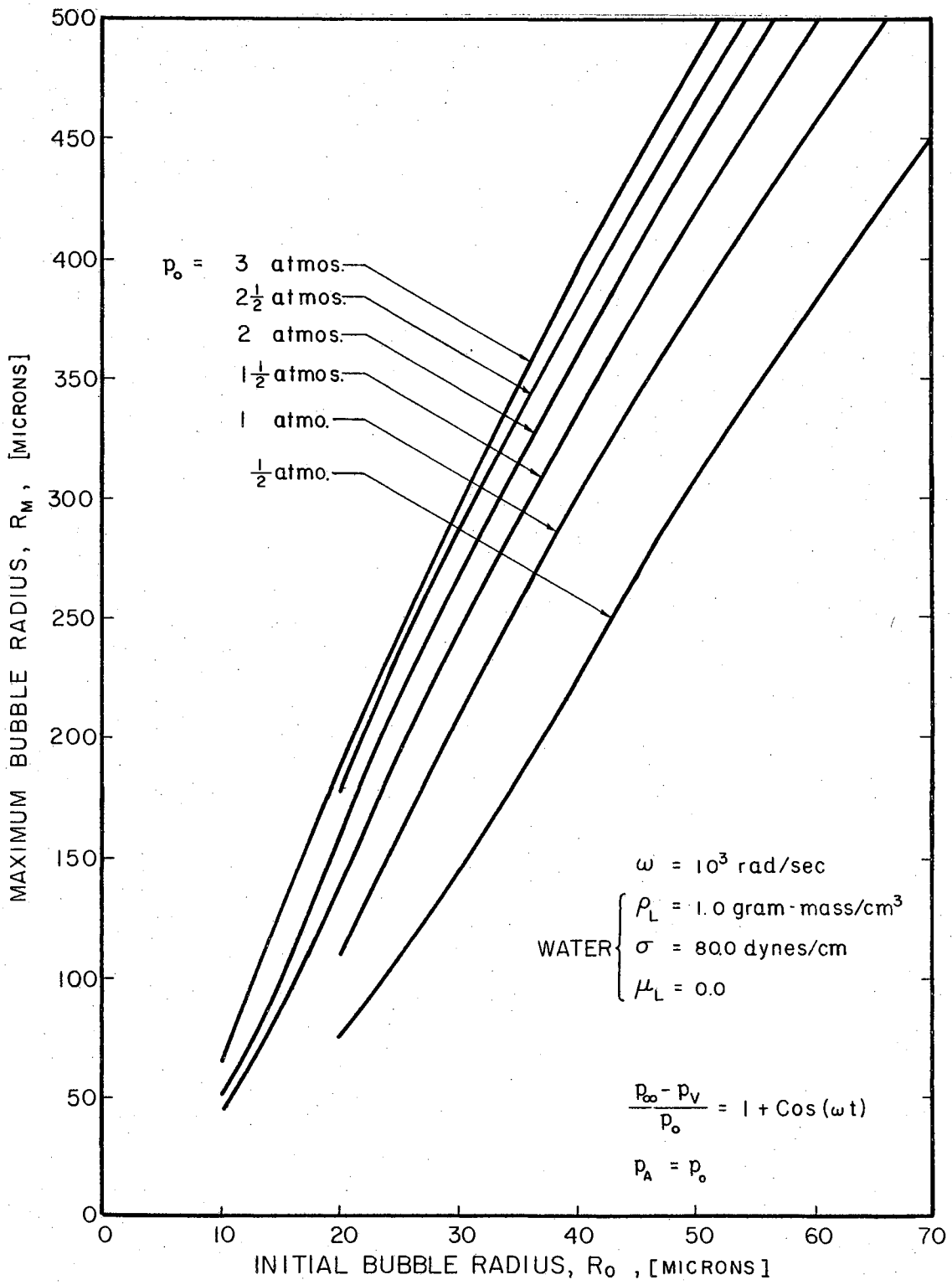

Figure 36. Effect of Changing Amplitude of Forcing Function on Maximum Bubble Radius for an ω of 10^3 rad/sec

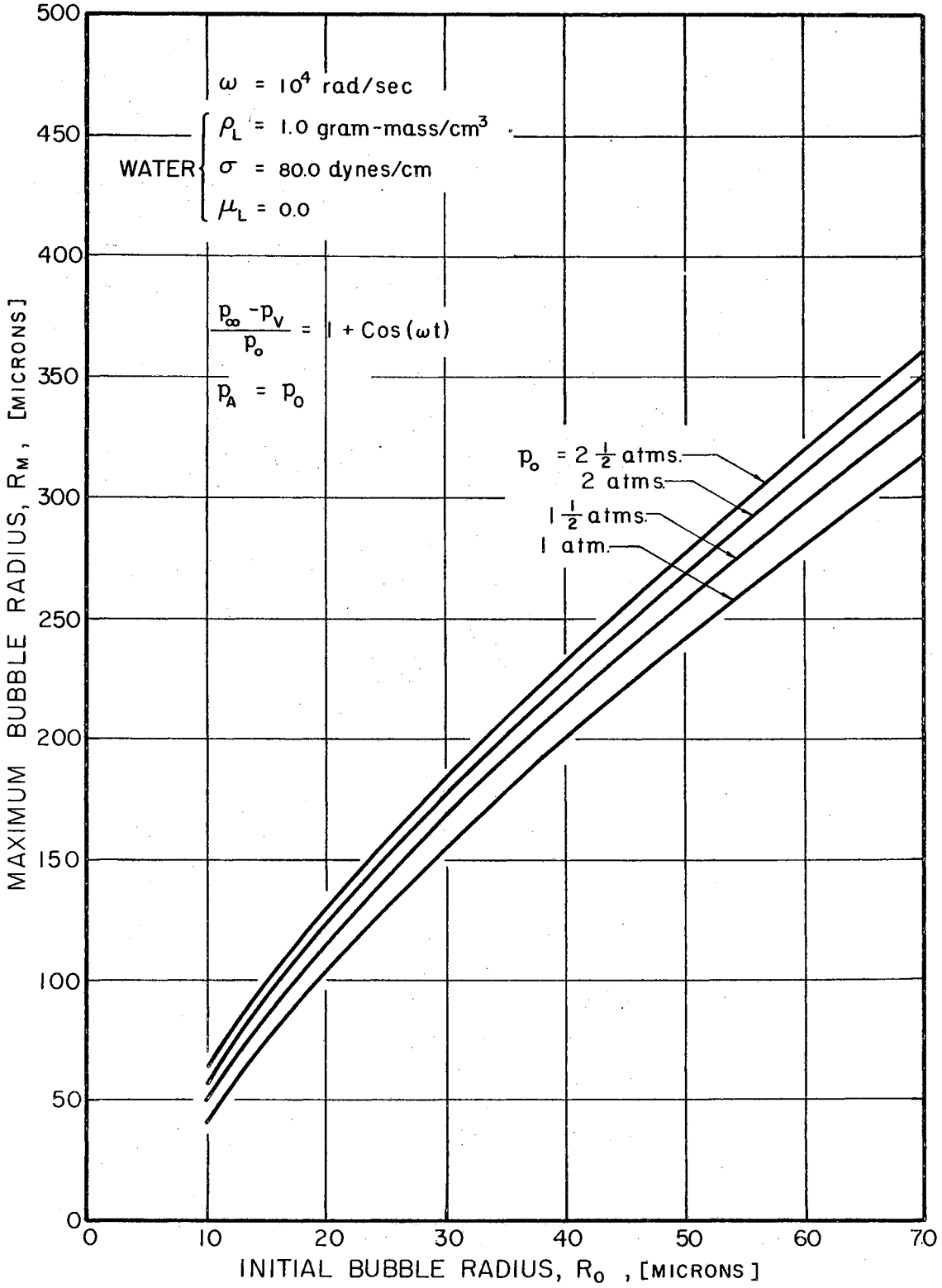

Figure 37. Effect of Changing Amplitude of Forcing Function on Maximum Bubble Radius for an ω of 10^4 rad/sec

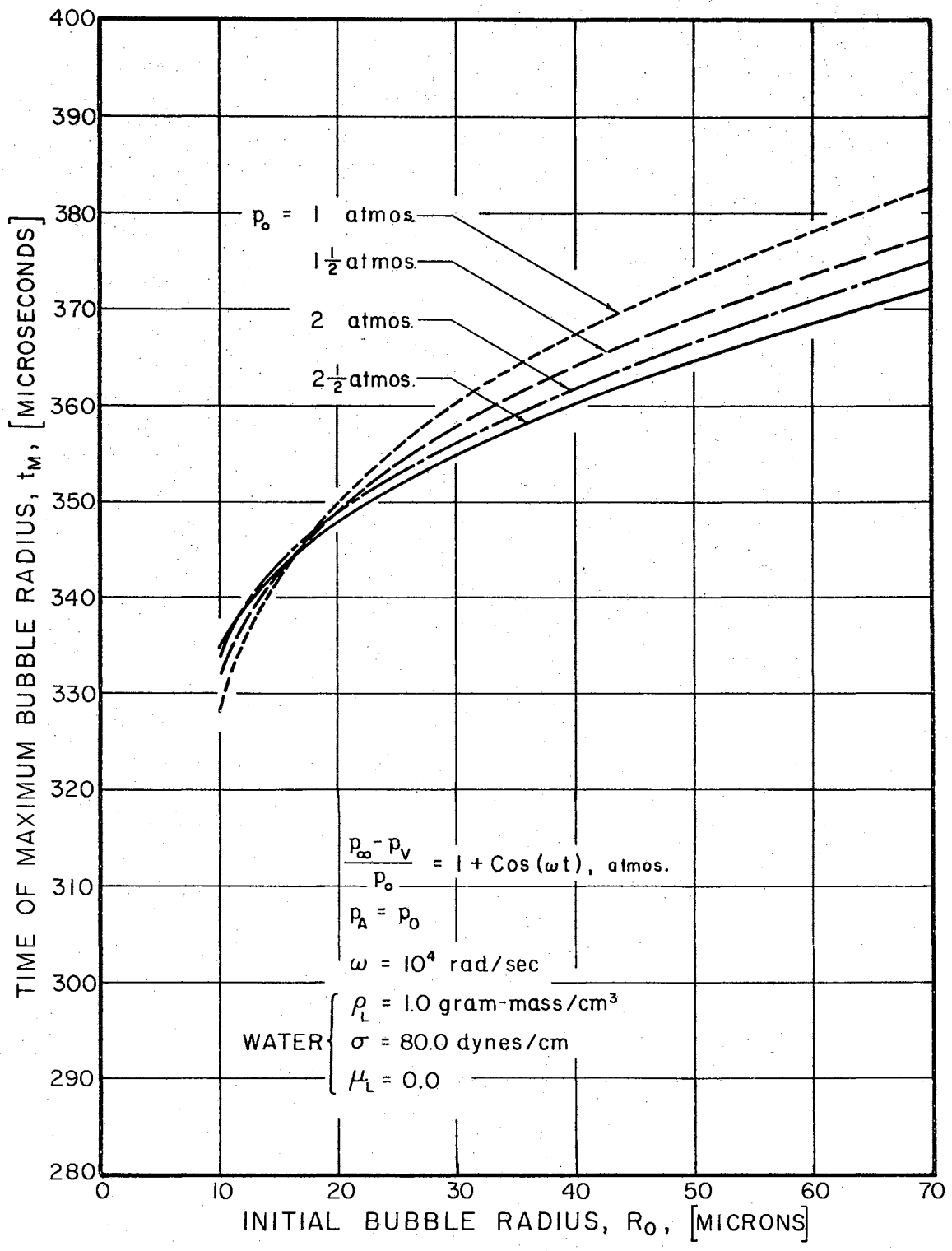

Figure 38. Effect of Changing Amplitude of Forcing Function on the Time at which R_M Occurs for an ω of 10^4 rad/sec

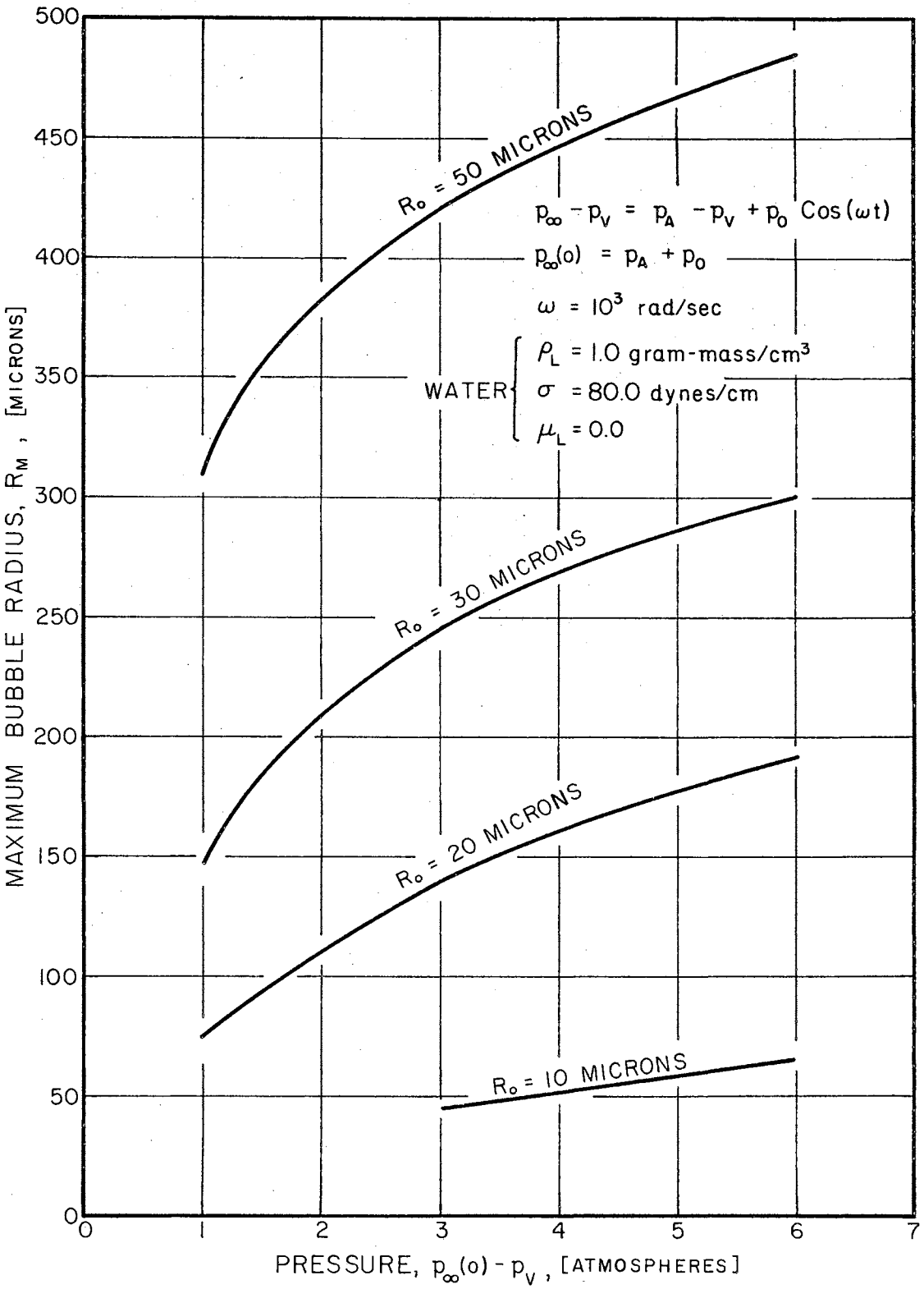

Figure 39. Effect of Maximum Pressure on R_M

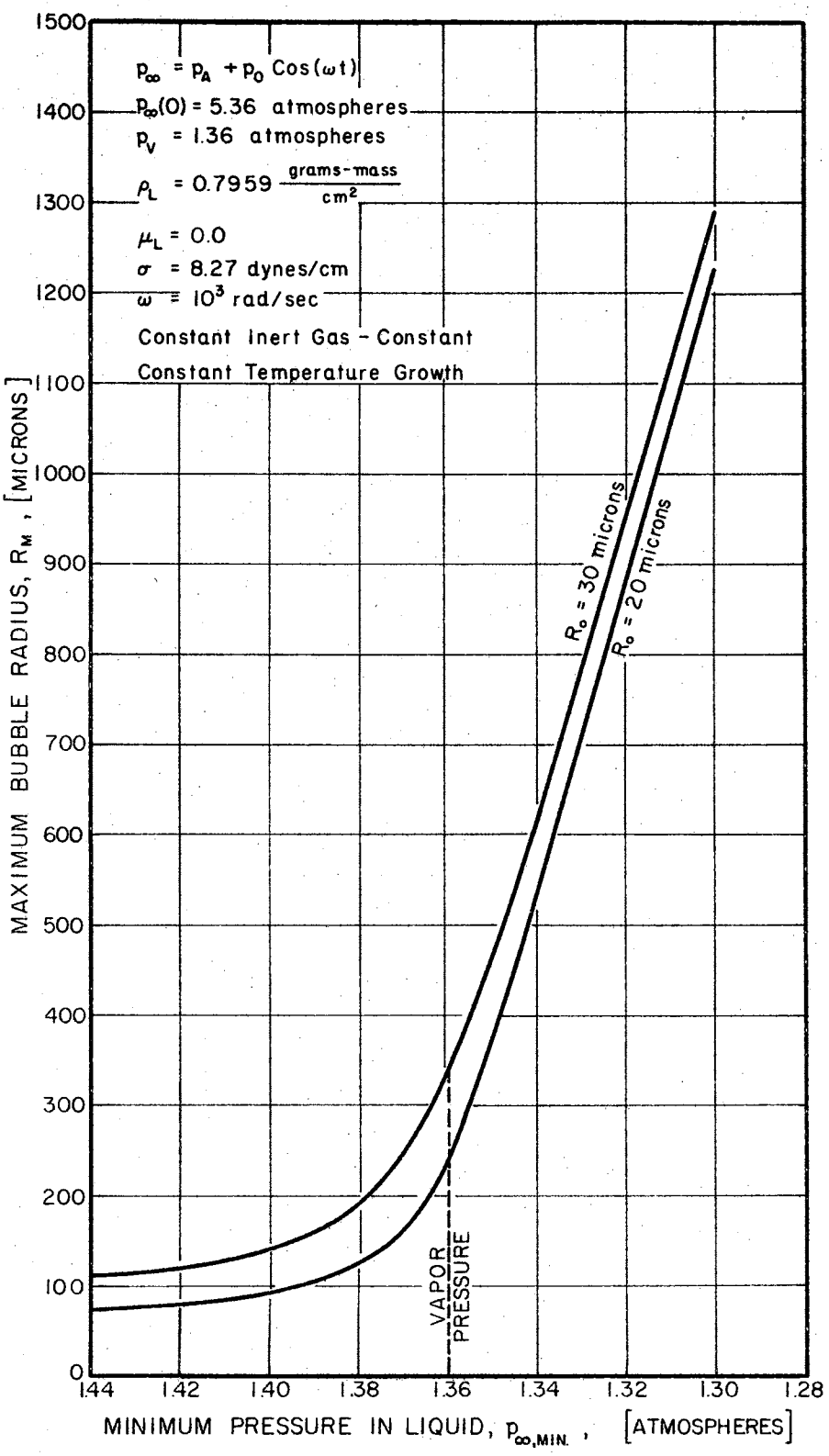

Figure 40. The Effect of Minimum Pressure Upon Maximum Bubble Radius

radius increases. This is due to an increase in the inertia of the liquid.

The variation of maximum bubble radius with the maximum value of the forcing function is shown in Figure 39. For small initial bubble radii the functional relation between R_M and $p_\infty(0) - p_v$ appears to be linear.

An investigation was made to determine whether the maximum bubble radius experiences a large change whenever the minimum pressure within the liquid is equal to the vapor pressure. The maximum pressure within the liquid was held constant. This, in effect, holds the inert gas content of the bubble constant. A change in the minimum liquid pressure was produced by changing the magnitudes of p_A and p_o in equation (3-21). The results of this investigation are shown in Figure 40 for two values of the parameter R_o. The maximum bubble radius increases at a much faster rate as the minimum pressure is reduced to values below the vapor pressure.

Effect of Neglecting Inertia and Viscous Terms in Equation of Motion for Isothermal Bubble Growth

The following equation is obtained when the inertia and viscous terms in equation (3-22) are neglected:

$$\frac{p_\infty - p_v}{2\sigma} = \frac{G_o}{R^3} - \frac{1}{R} . \qquad (3\text{-}23)$$

Thus, equation (3-23) is the static equation for isothermal

bubble behavior. The gas content parameter, G_o, can be determined by using the initial values of R and p_∞. The parameter G_o was assumed to remain constant during bubble growth.

The maximum bubble radius occurs when $p_\infty - p_v$ reaches a minimum value. This minimum value has a lower limit. In this analysis this minimum value was taken equal to zero in order to show a comparison with the results shown in Figures 36 and 37. Therefore, the maximum radius is

$$R_M = \sqrt{G_o} \quad . \tag{3-24}$$

Figure 41 shows the variation of R_M with R_o for various values of $p_\infty(0) - p_v$. The inertia terms do affect the maximum radius. This effect can be seen by comparing Figure 41 with Figures 36 and 37.

As the magnitude of $p_\infty - p_v$ is decreased to values below zero, the maximum stable radius is reached. Equation (3-23) cannot be used to obtain an estimate of the maximum bubble radius when this radius is greater than R_{ms}.

Solutions to Equation of Motion for Nonisothermal Bubble Growth

Several solutions to equation (3-15) have been reported in preceding sections of this chapter for a polytropic constant of 1.00. The temperature within a bubble will usually decrease when growth is produced by reducing the pressure within the liquid. This decrease in temperature

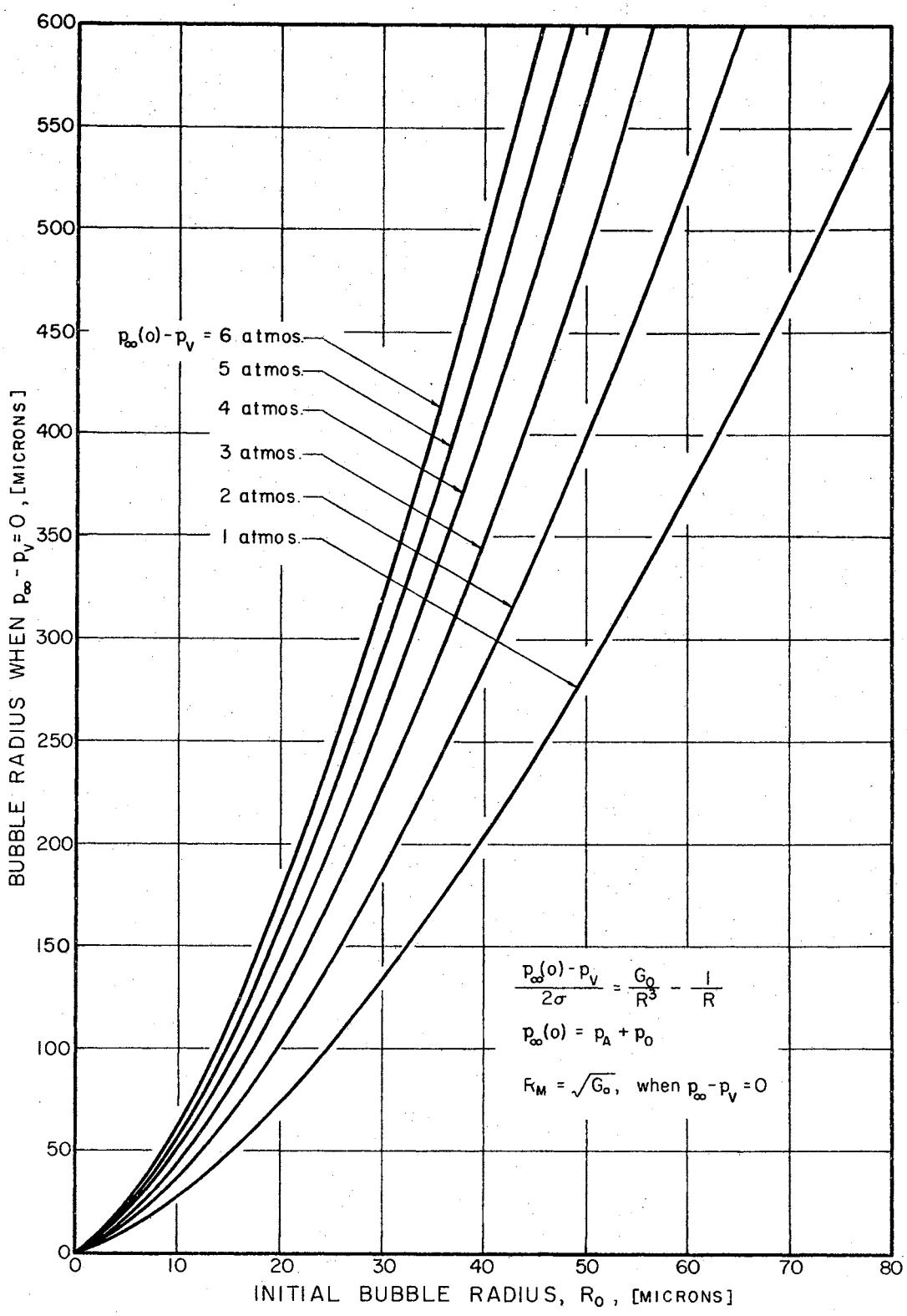

Figure 41. Variations of R_M with R_0 for Quasistatic Growth

can be taken into account by selecting the correct value for the polytropic constant. The exact magnitude of the polytropic constant is difficult to determine. This section will be devoted to showing how small changes in n affect the maximum bubble radius.

The first case investigated was for a polytropic constant of 1.02. The vapor pressure and surface tension were assumed to remain constant during bubble growth. Thus, the temperature changes within the bubble affected only the inert gas pressure, thereby causing a reduction in the maximum bubble radius. The results of this investigation are shown in Figure 42.

Since the temperature within a bubble decreases as the radius increases, it appears that changes in the vapor pressure and surface tension should be considered. Figures 43 and 44 show the effects of considering changes in vapor pressure and surface tension upon the maximum bubble radius. The particular example is for water at 104^{o}F. The method of least squares was used to obtain an equation for the vapor pressure as a function of temperature. A linear relation was used to describe the variation of surface tension with temperature. Changes in surface tension had little effect upon the maximum bubble radius. This was as expected, since the magnitude of the surface tension does not change noticeably with temperature. Also, the surface tension force remains almost constant during the early stages of growth. Changes in the vapor pressure have a

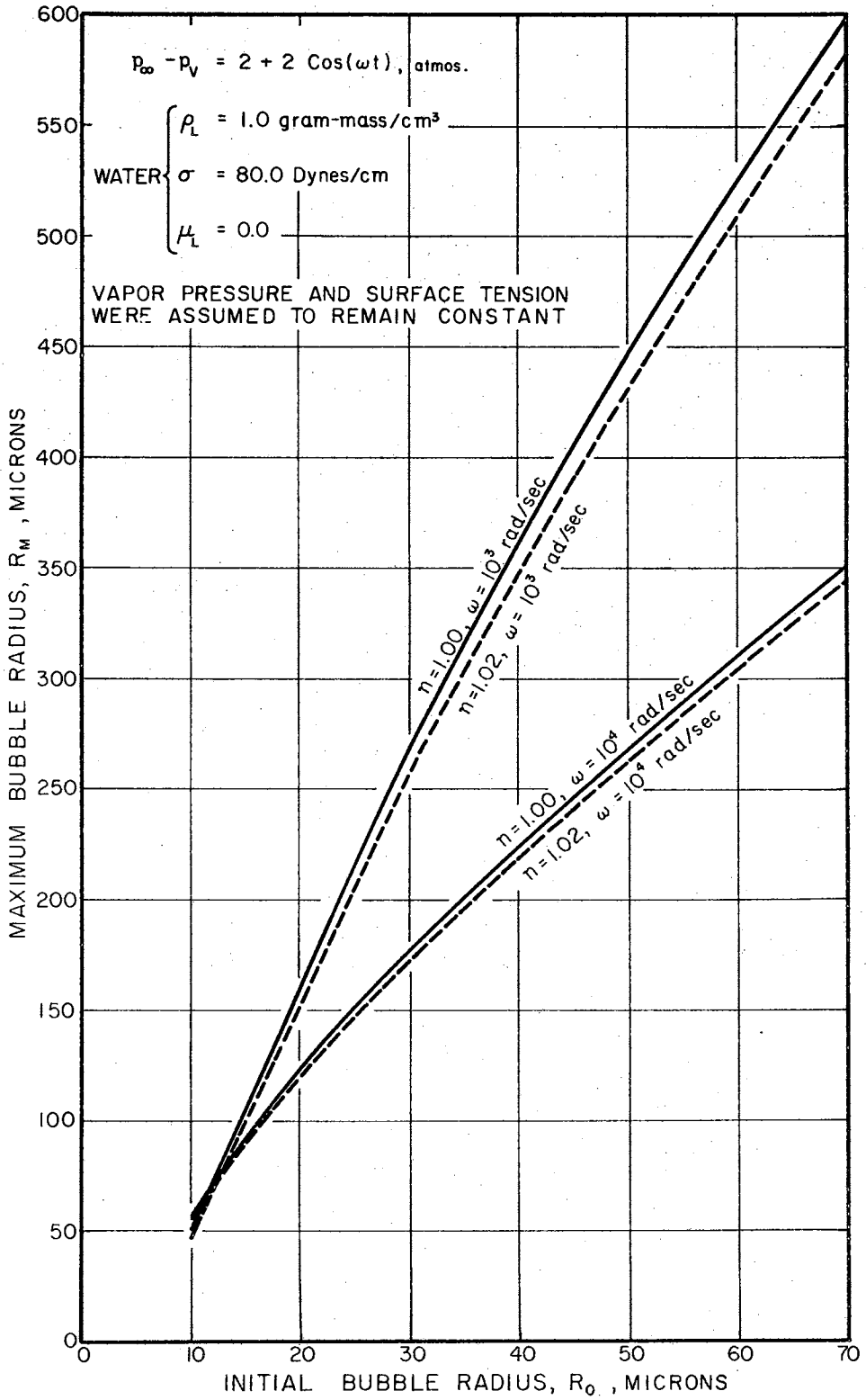

Figure 42. Effect of the Polytropic Constant Upon Maximum Bubble Radius

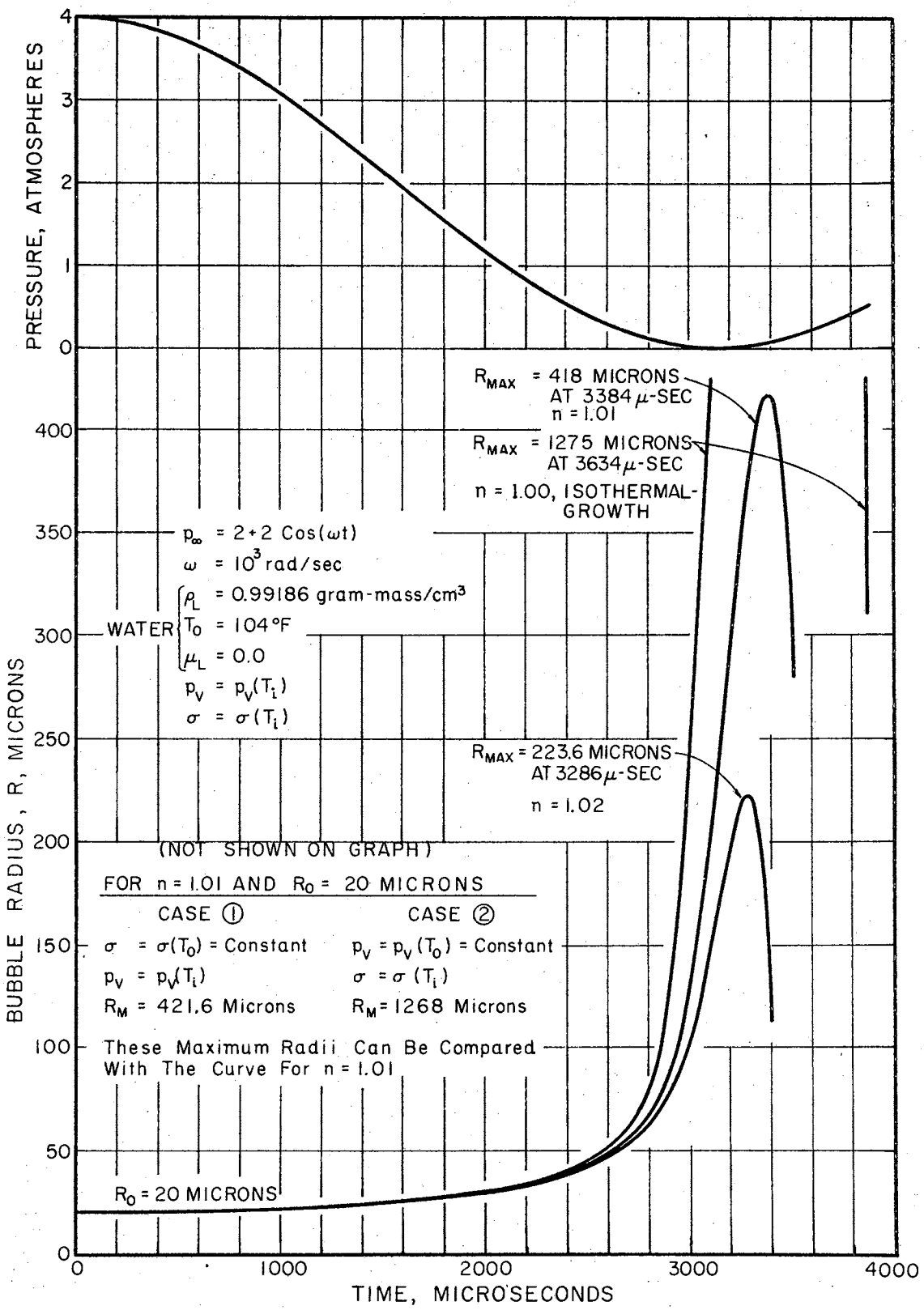

Figure 43. Growth of a Small Gas-Vapor Bubble Under Various Polytropic Processes

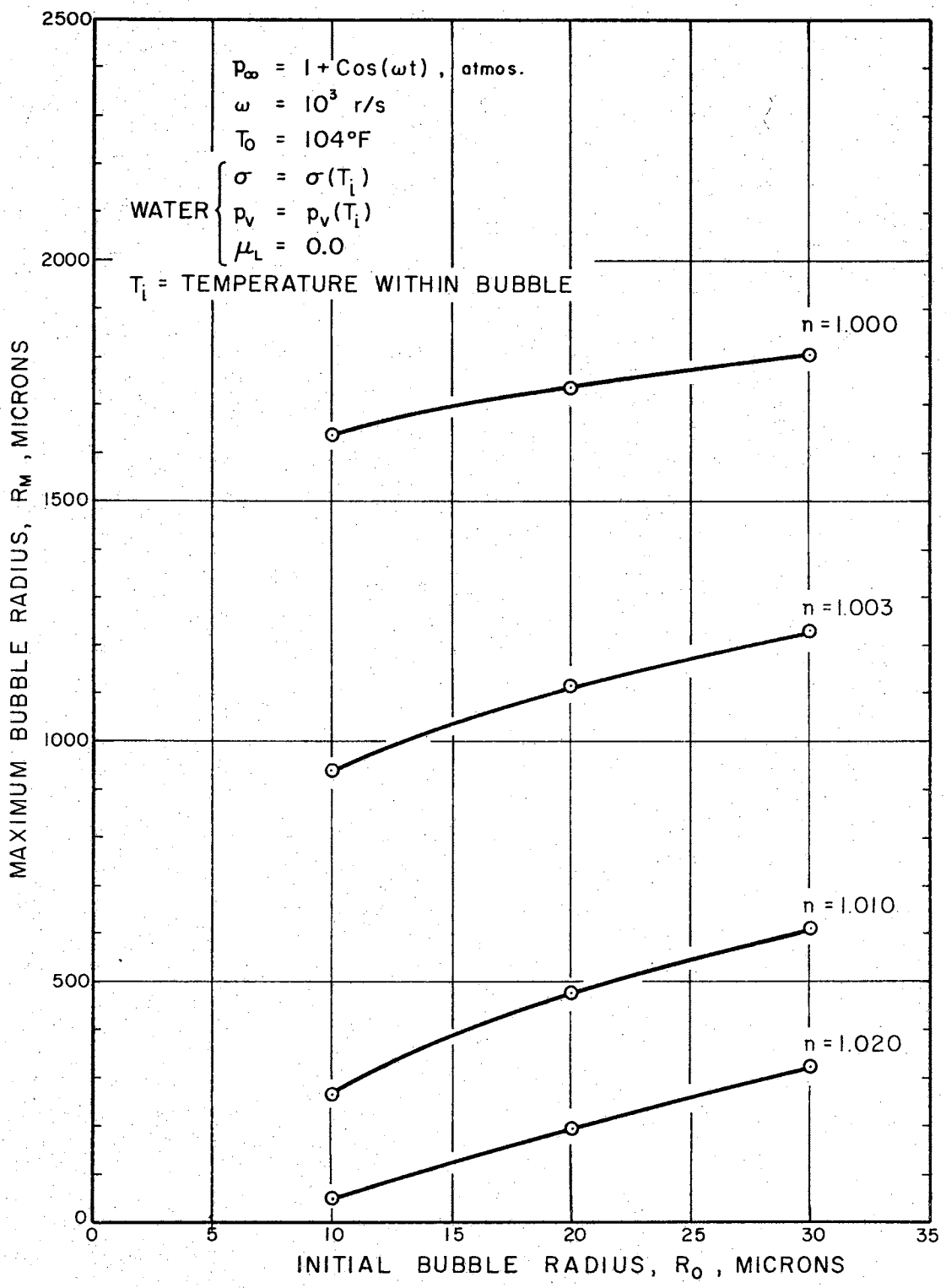

Figure 44. Variation of Maximum Bubble Radius With Initial Bubble Radius for Various Polytropic Processes and an ω of 10^3 rad/sec

pronounced effect upon the maximum bubble radius. This effect is due to the decrease in the vapor pressure, which in effect reduces the effective forcing function term.

The investigation reported in this chapter points out the influence that various properties have upon nuclei growth. The following variables must be known in order to describe the phenomenon which occurs during cavitation:

1. Exact pressure distribution
2. Initial nuclei size and content
3. Process which occurs within nuclei during growth
4. Fluid properties

The first three items are very difficult to predict. This chapter has been devoted to enumerating some of the effects of each of these items. All of these variables play an important role in the growth of small nuclei. At the present state of the art, one might think that it is impossible to describe the phenomenon which occurs during cavitation by mathematical means; however, a particular problem can be satisifed by changing the conditions listed in 2 or 3. A complete analysis would require an extensive experimental program. The author feels that this is beyond the scope of this work.

CHAPTER IV

HYDRODYNAMIC TUNNEL

A small hydrodynamic tunnel was designed and constructed in order to investigate experimentally the limited cavitation characteristics of various fluids. A discussion of the tunnel, test sections, and instrumentation is given below.

Description of Tunnel

The facility used in this investigation was a small closed-return liquid tunnel. A schematic drawing and photograph are shown in Figures 45 and 46, respectively. The tunnel was designed so that flow through the test section would be vertically downward. All tunnel components, except the heat exchanger and pump, were made of stainless steel. Two interchangeable tubes (one of stainless steel and the other of copper) were made for the heat exchanger. Flat ring gaskets of 1/16-inch thick Buna N compound were used as seals between all flanges. Straightening vanes of 3/8-inch diameter stainless steel tubing were installed upstream of the metering venturi to favor the attainment of uniform, steady, irrotational flow at the metering venturi. The liquid capacity including the pump and settling chamber but excluding the expansion and pressurizing chambers was about

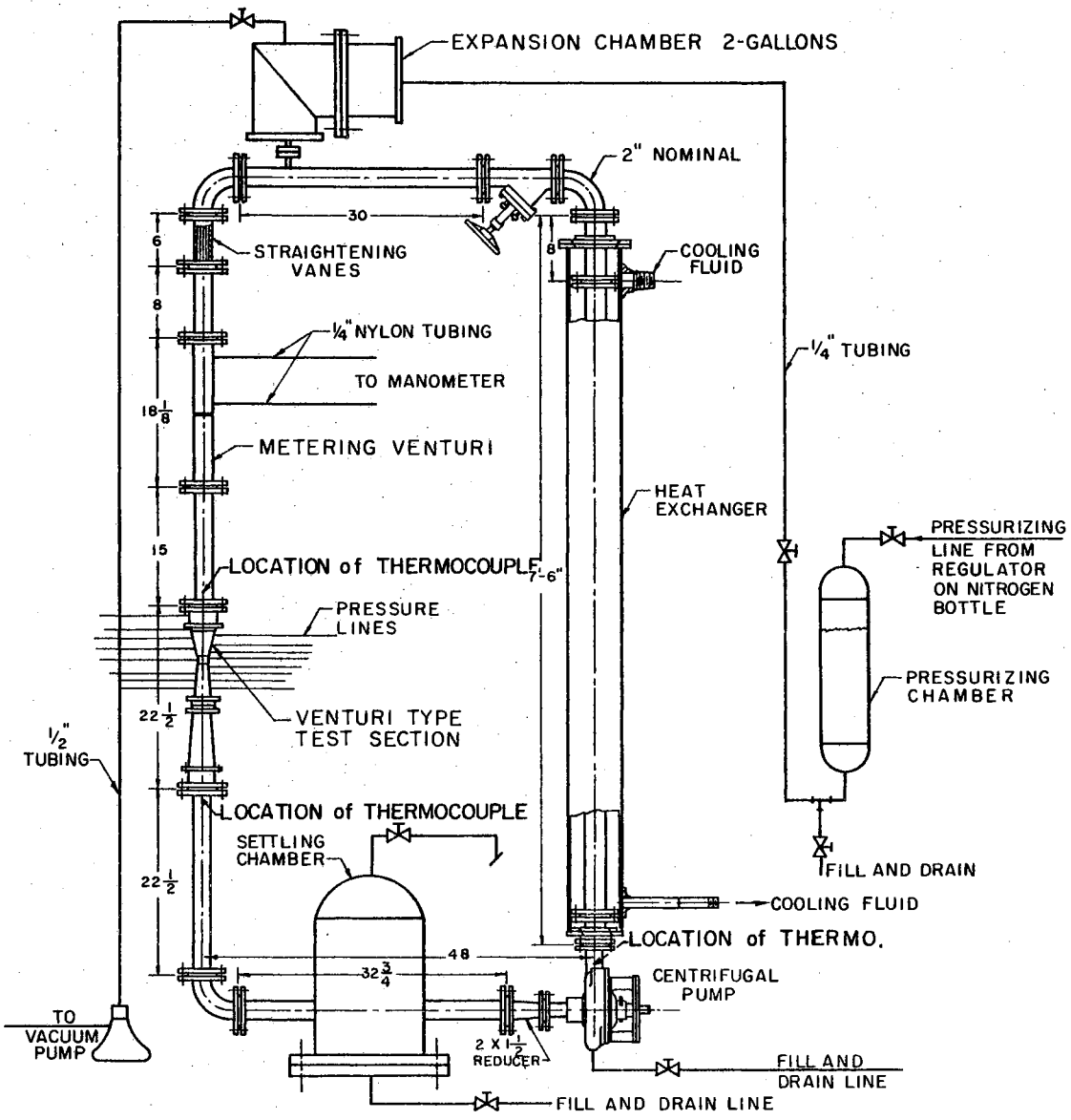

Figure 45. Schematic of Hydrodynamic Tunnel

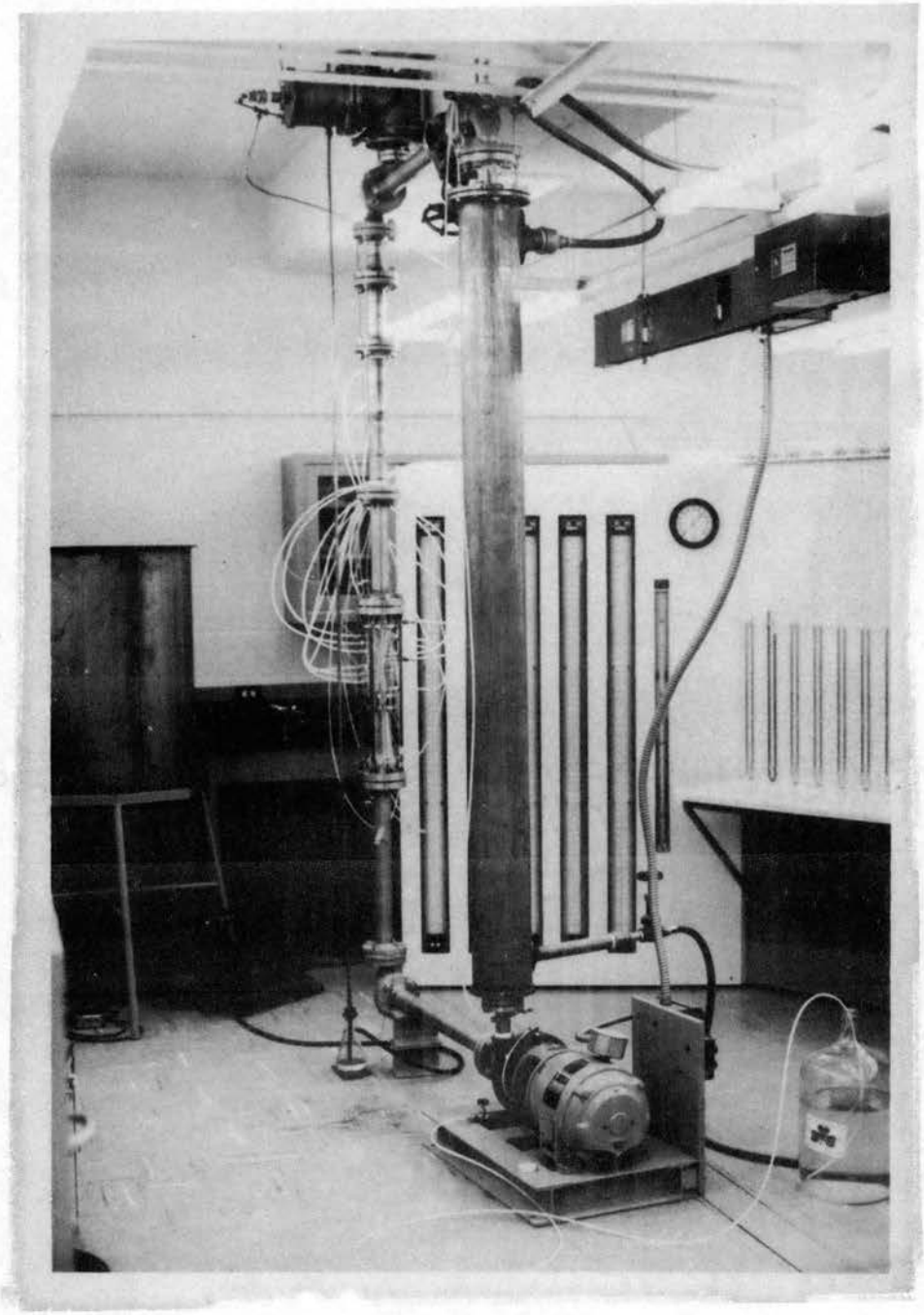

Figure 46. Photograph of Test Facility

10 U.S. gallons.

The pump-drive system consisted of a 5-horsepower, 220-volt, three-phase motor coupled directly to a centrifugal pump. The pump was made of aluminum and contained a 6-inch diameter three-vaned brass impeller. The motor was operated at a constant speed of 3500 rpm.

The tunnel components were thoroughly cleaned before final assembly. All components were cleaned by a liquid honing process, which removed foreign particles from the inner surfaces of the tunnel. Following "preliminary cleaning," a final scale removing and whitening operation was performed by placing the stainless steel components in a solution containing 12 per cent by volume of 40° Bé nitric acid and 1 1/2 per cent by volume of 52 per cent hydrofluoric acid for about 30 minutes. The acid solution was kept at room temperature. The operation was followed by thoroughly rinsing each component in hot water.

The aluminum part of the pump was heavily anodized to help prevent particles from entering the system. Following anodizing, the pump was thoroughly rinsed in hot water.

The tunnel facility was designed to operate over a pressure range from 0 to 200 pounds per square inch absolute. High pressure nitrogen gas was used as the pressurizing medium. The high pressure nitrogen gas was placed above the liquid in the pressurizing chamber. The pressurizing chamber was located approximately 10 feet from the expansion chamber. A 1/4-inch copper line was used to connect the pressurizing

chamber to the expansion chamber. This eliminated the possibility of any nitrogen entering the expansion chamber. Tunnel pressures less than atmospheric were obtained by means of a vacuum system which could be connected to either the expansion or pressurizing chambers.

Flanges were installed on all tunnel components. This was done to increase the flexibility of the tunnel. Various test sections may be installed without any major change in the tunnel.

Description of Test Sections

Three different hydrodynamic-tunnel test sections were used in the experimental investigation. The test sections were designed to provide a wall-pressure profile with a deep but relatively narrow valley. This was accomplished by controlling the test section shape between the converging-diverging sections. The cross-sectional area at the throat of each test section was about 0.197 square inches. The throat is followed by a diffuser of 7° total angle. Test sections 1 and 2 were designed to provide axisymmetric flow while test section 3 was designed to provide two-dimensional flow at the throat.

The test sections were fabricated from transparent acrylic plastic. Test sections 1 and 2 were machined from solid round stock. The converging-diverging walls of test section 3 were machined and polished together. This was necessary to insure a symmetrical test section. The top

and bottom pieces of 3 were flat stock. The 4 pieces were fastened together with plastic solvent.

Instrumentation of the test sections consisted of static pressure taps, located as shown in Figures 47, 48, and 49. The taps were carefully and accurately machined perpendicular to the local contour of the previously polished inner wall. Tap openings were then carefully hand polished to remove all evidence of imperfections. Tap openings on the inner wall were 0.040-inch in diameter. The taps on test sections 1 and 3 were installed along two lines parallel to the axis. These lines were located 180° apart. The taps on test section 2 were installed at various circumferential positions to minimize possible downstream interference effects of aligned taps.

Instrumentation

In order to assemble the instrumentation needed for the experimental investigation an instrument panel was constructed (see Figure 50). This panel contained the manometers, the pressure gages, and a thermocouple selector switch. The panel was designed so that pressures and temperatures could be read with minimum effort.

Pressure

The pressures within the test sections were measured by mercury manometers. Four 60-inch one tube "Meriam" manometers were connected in series to measure pressures

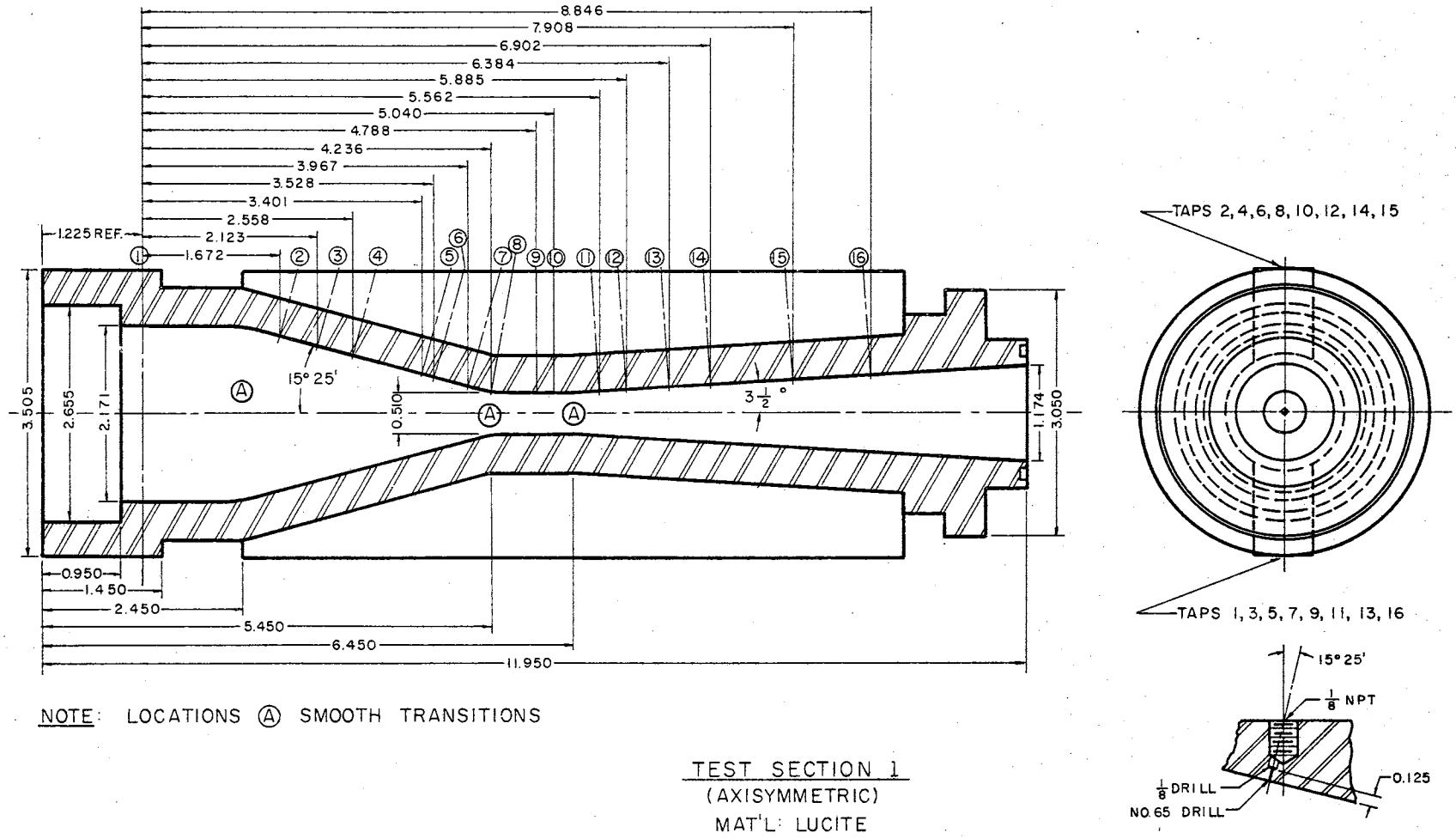

NOTE: LOCATIONS Ⓐ SMOOTH TRANSITIONS

TEST SECTION 1
(AXISYMMETRIC)
MAT'L: LUCITE

TAP NO. 4 - TYPICAL

(a) Schematic of Test Section 1 Showing Dimensions and Instrumentation

Figure 47. Test Section 1

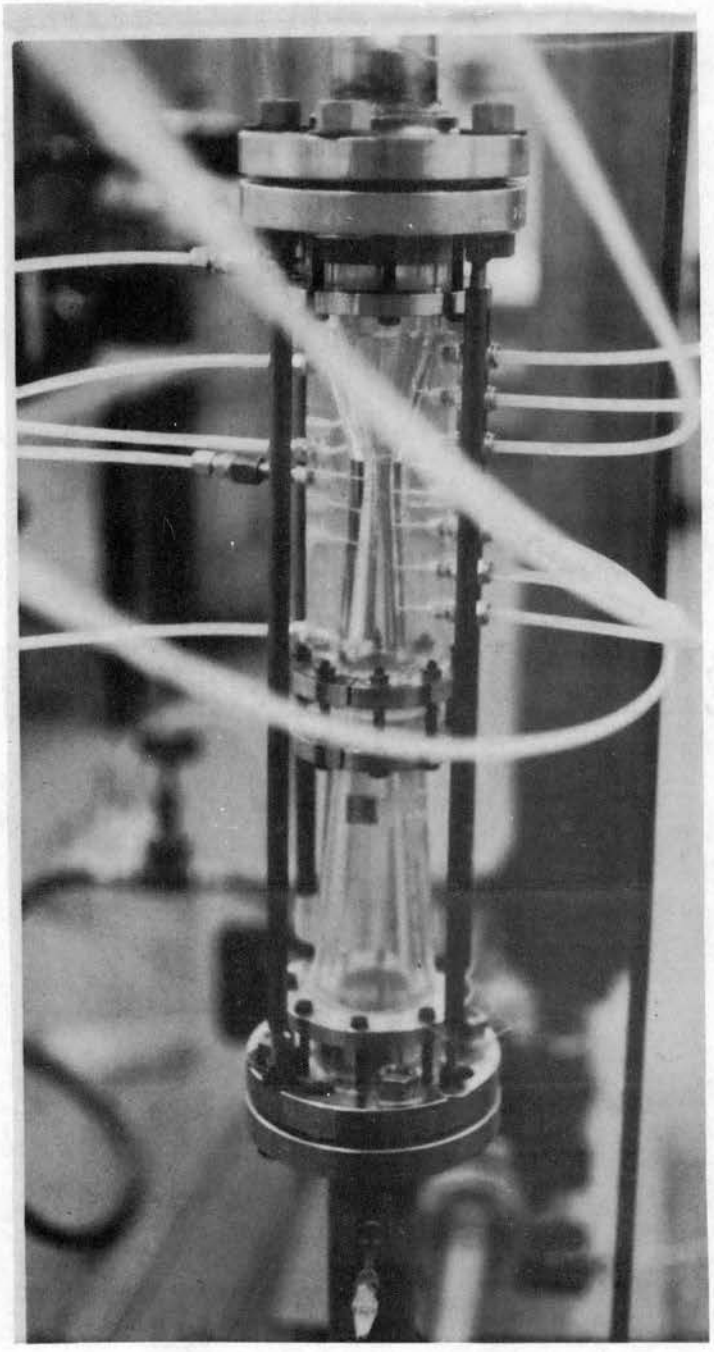

(b) Photograph of Test Section 1 Located in Tunnel

Figure 47. — Concluded. Test Section 1

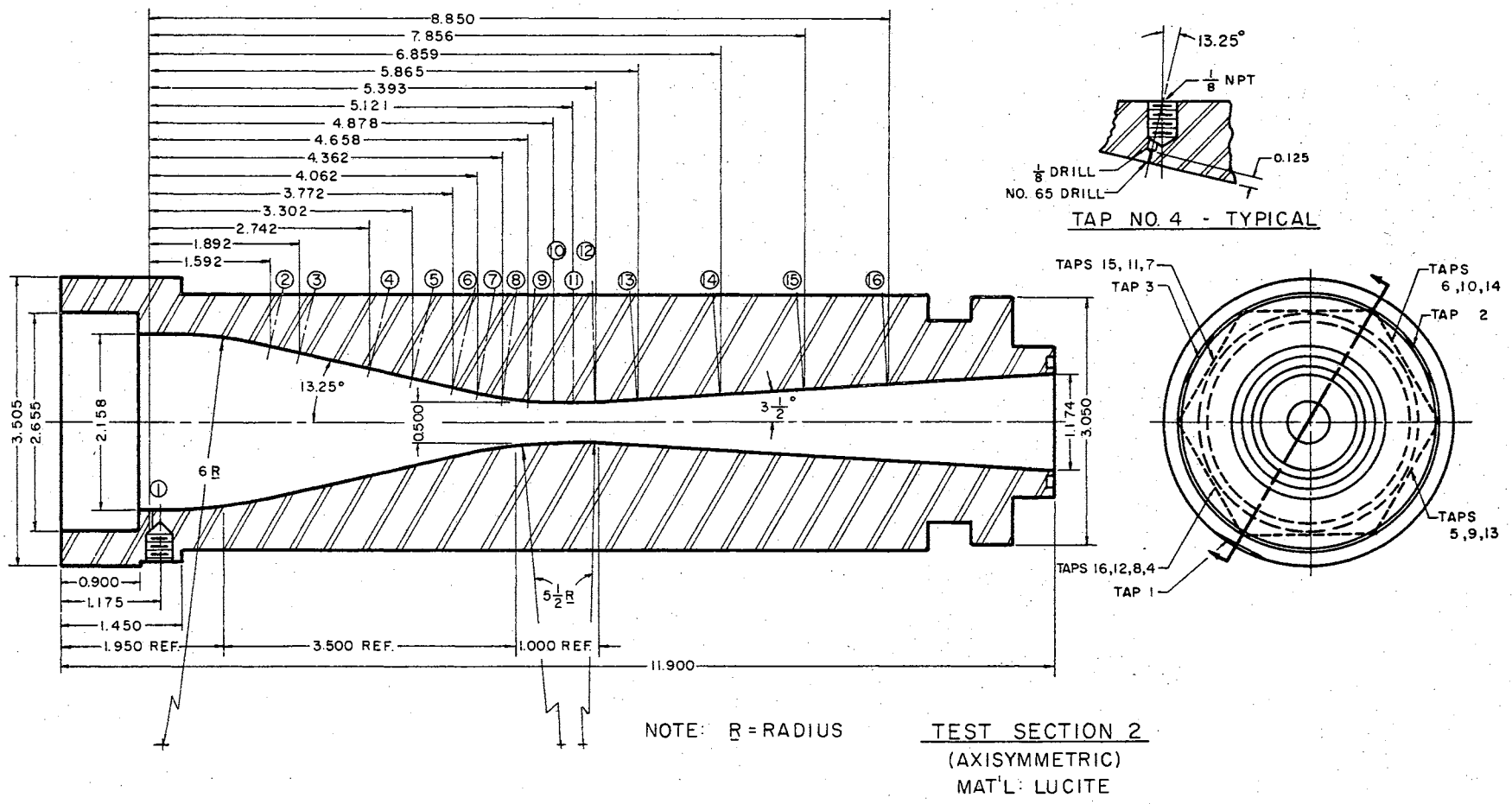

Figure 48. Schematic of Test Section 2 Showing Dimensions and Instrumentation

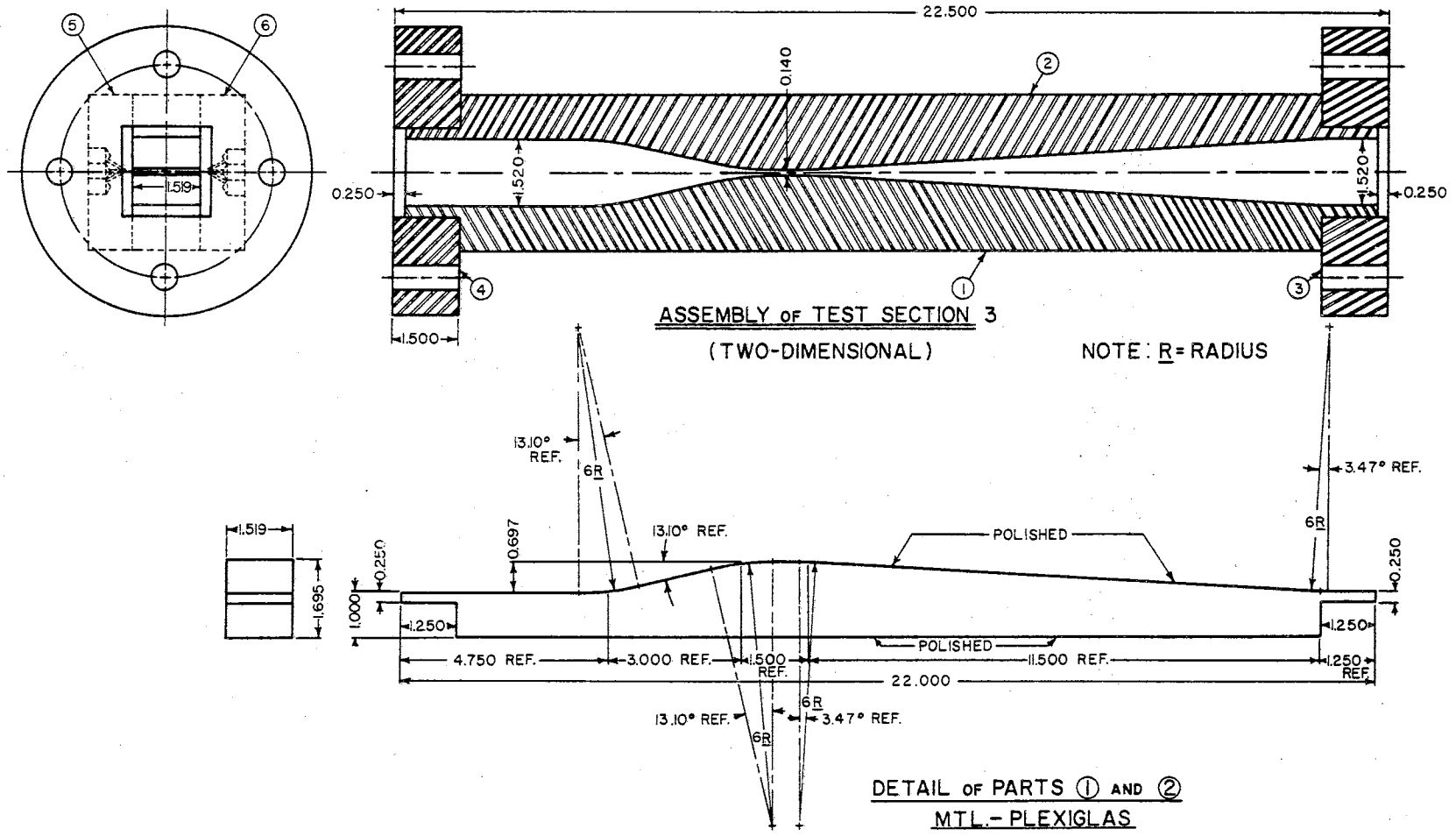

(a) Details of Test Section 3

Figure 49. Schematic of Test Section 3 Showing Dimensions and Instrumentation

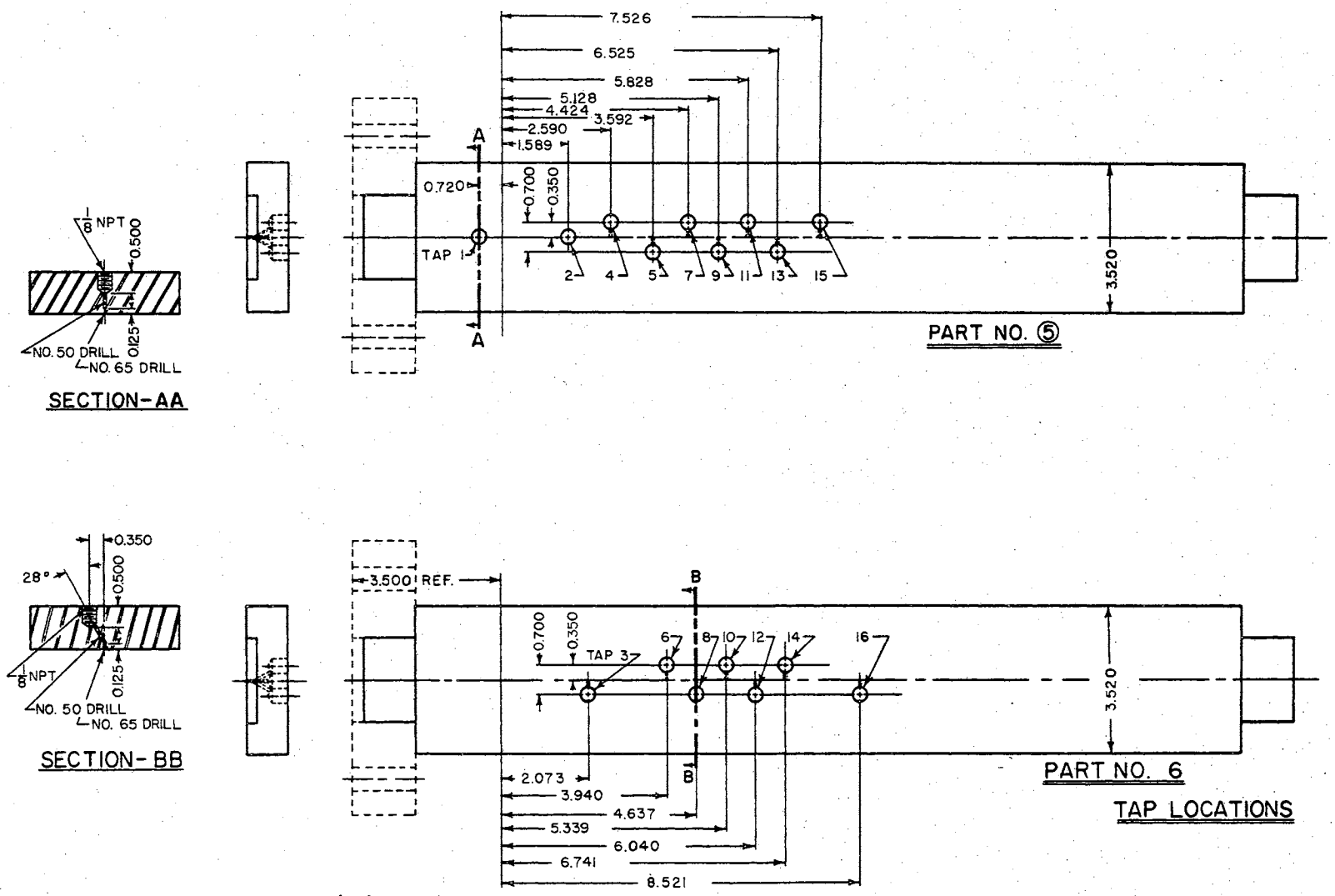

(b) Location of Pressure Taps

Figure 49.—Concluded. Schematic of Test Section 3 Showing Dimensions and Instrumentation

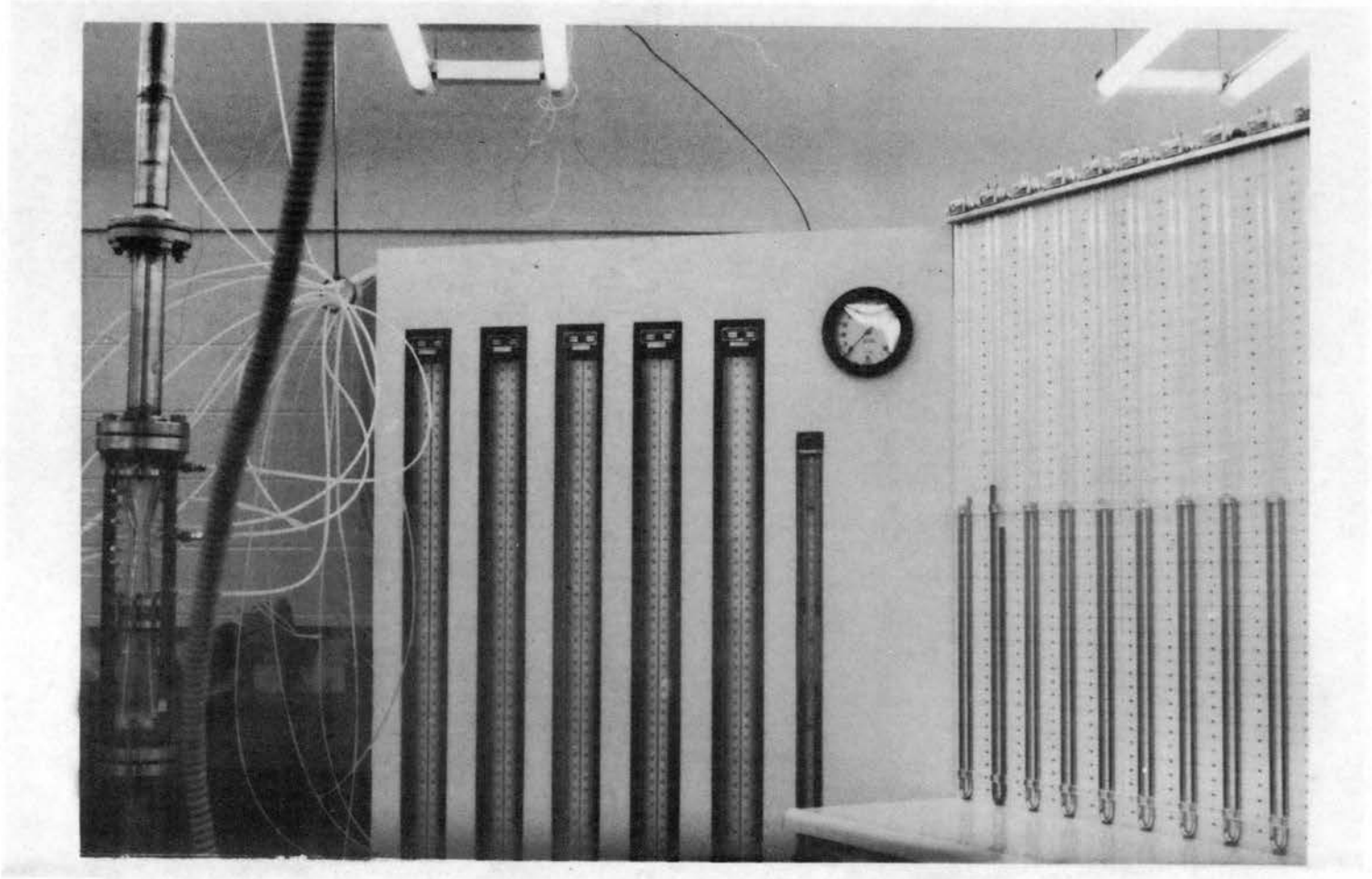

Figure 50. Instrument Panel with Test Section 1 Shown at Left of Photograph

up to 100 pounds per square inch absolute (see Figure 51). The manometers were connected so that the number in series could be increased as needed. The pressures at tap locations 1, 2, 3, 4, 5, 6, 15, and 16 were calculated by

$$p_{\text{tap opening}} = p_{\text{atm.}} + (H_1 + H_2 + H_3 + H_4)_{\text{in.-}H_g} - (H_{\text{tap}} + H_1 + H_2 + H_3)_{\text{in.-}H_2O}(0.073718).$$

Pressures less than atmospheric were measured by the short U-tube manometer shown in Figure 51. The pressures in the minimum area section of each test section were measured with 40-inch U-tube mercury manometers. All pressures were measured relative to atmospheric pressure. Pressure lines were of transparent nylon tubing and contained a bleed valve at the manometer end. Monometers were read to within about $\pm$ 0.025 inch.

Temperature

Temperatures were recorded at three locations in the tunnel with copper-constantan thermocouples. The design of a typical thermocouple is shown in Figure 52. Thermocouples were located at the entrance and exit of the test section and at the pump discharge. An ice bath was used as the thermocouple cold junction. The emf generated by a thermocouple was read to within $\pm$ 0.001 millivolt with a digital voltmeter.

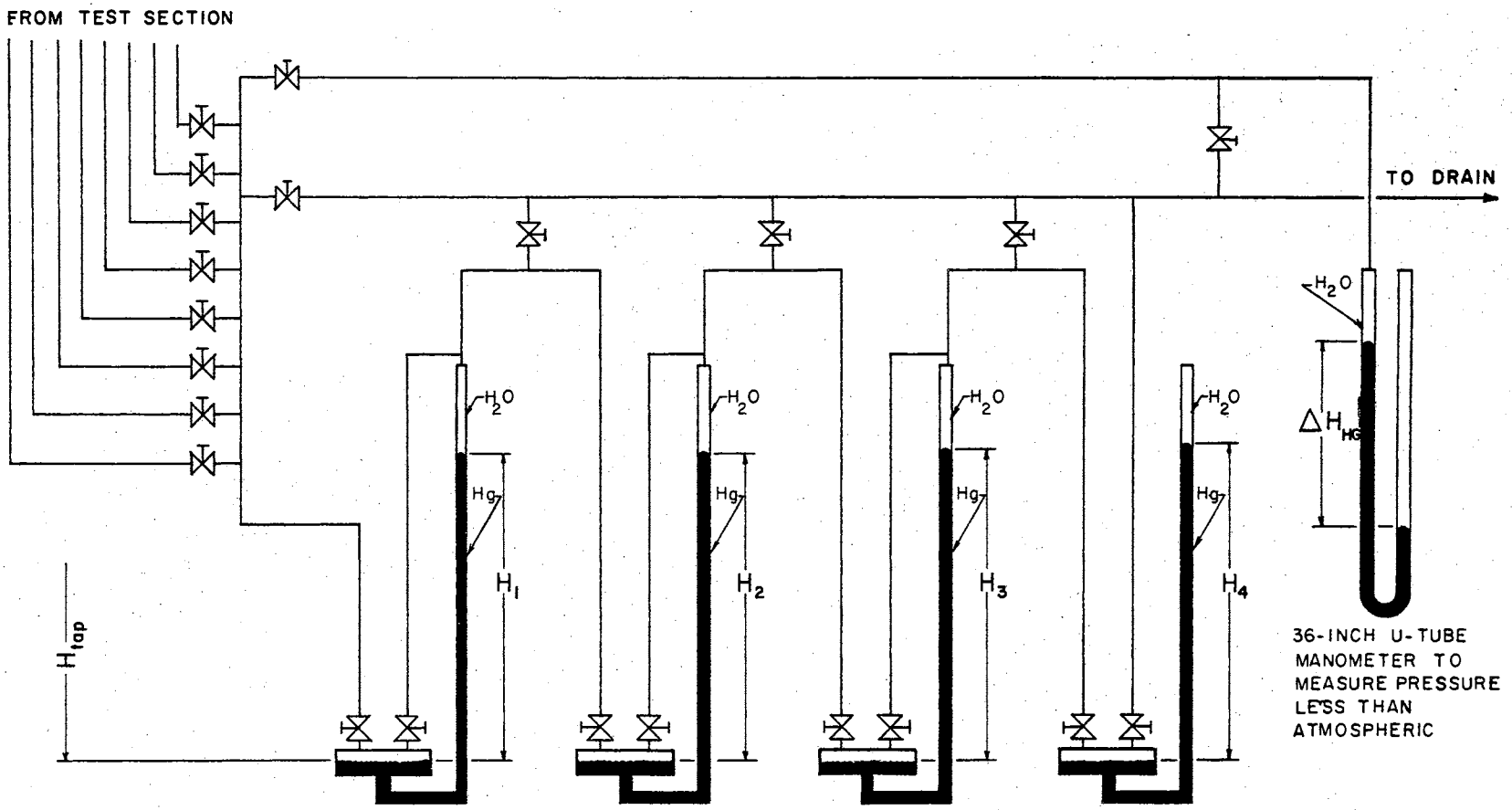

Figure 51. Schematic of Mercury Manometer Hookup Used to Measure Pressures from 0 to 100 psia

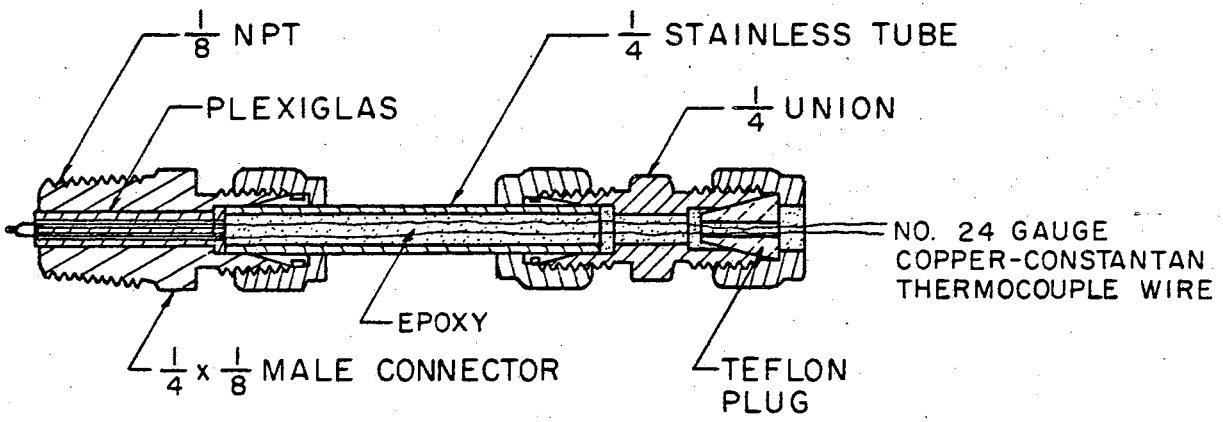

Figure 52. Schematic of Typical Thermocouple

Flow Rate

The flow rate was determined by measuring the pressure drop across a calibrated stainless steel venturi (see Appendix D for calibration). A U-tube mercury manometer was used to measure the pressure drop between the inlet and throat. The diameter of the throat was 0.876-inch. The throat was followed by a conical diffuser of 6 1/2° total angle.

Photographic Equipment

Cavitation was photographed with a high speed (6000 frames per second, maximum) Fastax camera.

CHAPTER V

EXPERIMENTAL PROCEDURE

A definite procedure was followed in preparing the test liquid and filling the tunnel. This same procedure was followed each time the tunnel was filled. Tunnel water was renewed at least once every two days during the testing period. This was done in order to be assured of clean test water during the investigations of limited cavitation.

Preparing Test Liquid

The liquid used in the tunnel studies was commercially available distilled drinking water. This water normally contained about 7 milligrams of oxygen per liter of water (about 85 per cent air-saturated at room temperature) and was degassed prior to tunnel use. Air removal was accomplished by maintaining the water temperature at 205°F for approximately 4 hours. The distilled water was heated by placing the 5-gallon glass containers in a tank of tap water. The tank was equipped with an electric heater. Near the end of the 4-hour heating period the temperature of the distilled water was increased. This increase in temperature caused the distilled water to flow over the top of the glass containers and into the tank. The containers

were then sealed, and the water was cooled to room temperature for storage from 1 to 2 days before transfer to the tunnel.

Filling Tunnel

The treated water was transferred to the tunnel by a low pressure technique to minimize contamination by air. The tunnel and pressure lines were evacuated to about 5 inches of mercury absolute, the glass container was opened, and a pressure difference delivered water to the tunnel by way of the pump housing through 1/4-inch nylon tubing. Some free air was always trapped in the region of highest elevation and in the pressure lines when the tunnel was full of water. The air in the pressure lines was removed by allowing water to flow from the tunnel, through each line, to the drain. The air in the tunnel was removed in 3 to 5 minutes by venting through the cap of the settling chamber while tunnel water was circulated at low speed.

The settling chamber was installed after the tunnel had been in operation for several weeks. Before installing this chamber most of the free air was removed from the tunnel in 30 to 45 minutes by venting through the expansion chamber.

Cavitation Criteria

After the system was filled and the free air removed, the temperature of the water in the tunnel was adjusted and

allowed to reach equilibrium. The temperature was controlled by regulating the flow of cooling fluid through the heat exchanger. Tests were started to study limited cavitation when the tunnel water reached the desired equilibrium temperature.

Limited Cavitation

The degree or amount of cavitation produced in the test section is controllable. The minimum degree of cavitation, herein termed limited cavitation, defines an operating point at which the formation and/or collapse of vapor bubbles on or near the model surface becomes detectable by visible means. It is realized that the limited degree of cavitation is somewhat arbitrary in that subvisible changes may occur in the water. However, for all practical engineering applications, subvisible changes in flowing water do not affect the usual performance parameters such as pump efficiency.

The present investigation is primarily concerned with vaporous cavitation and not the relatively slow diffusion process of gaseous cavitation wherein degassing may occur from water that is locally supersaturated with air. To avoid or minimize degassing effects, no data are reported where supersaturated conditions, based on tunnel temperature and local static pressure, exist in the free-stream approach section. The degree of saturation was calculated from Henry's law, which states that saturation is directly pro-

portional to local pressure.

In this investigation the occurrence of visible cavitation at incipience was readily defined by the abrupt appearance of numerous and sizable cavities (at least 1/8-inch long). The same degree of cavitation was also used to define desinent cavitation. In this investigation no difference was observed between incipient and desinent cavitation. A photograph showing typical incipient cavitation in test section 3 is presented in Figure 53. These definitions of limited cavitation denote only the degree of cavitation and not the method by which it was produced.

Methods of Producing Limited Cavitation

Cavitation experiments in a tunnel are usually conducted by holding the free-stream velocity constant and varying the free-stream static pressure, or by holding the pressure constant and varying the velocity. In this investigation both methods were employed without any noticeable difference in results. Limited cavitation was produced in two ways: (1) by the onset method, and (2) by the suppression method. With the onset method the overall system pressure was gradually reduced or velocity increased until incipient cavitation occurred. With the supperssion method cavitation in excess of limited cavitation was first produced and then was suppressed or reduced to the desinent state by gradually increasing the system pressure or decreasing the velocity (see Table III).

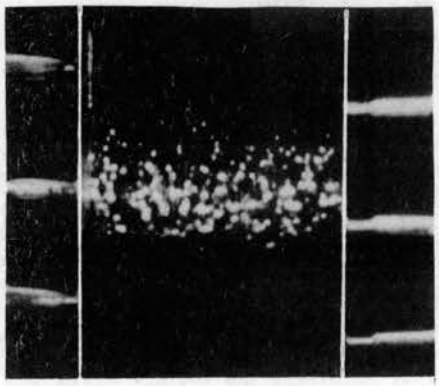

(a). 3600 frames/second

V_{i_t} = 45.67 fps

K_{i_t} = 0.0072

$\frac{\gamma}{\gamma_s}$ = 0.54

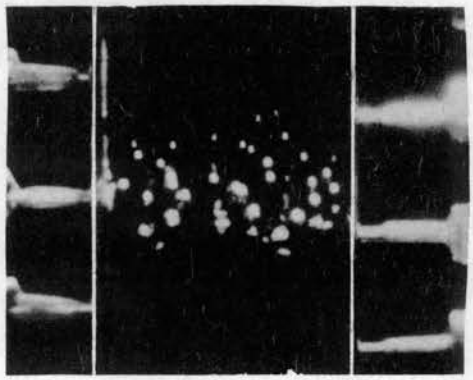

(b). 2900 frames/second

V_{i_t} = 52.11 fps

K_{i_t} = 0.0022

$\frac{\gamma}{\gamma_s}$ = 0.30

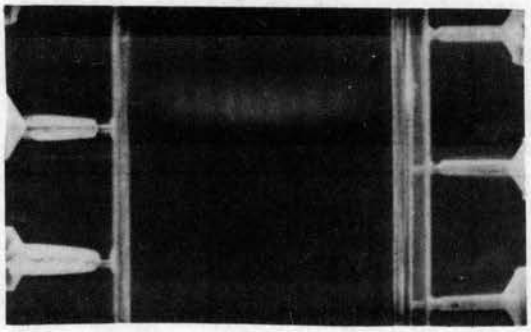

(c). V_{i_t} = 53.57 fps

K_{i_t} = 0.0031

$\frac{\gamma}{\gamma_s}$ = 0.40

Figure 53. Incipient Cavitation Induced on the Walls of Test Section 3 (Flow Direction from Top to Bottom of Page)

TABLE III

METHODS OF PRODUCING LIMITED CAVITATION

Initial Flow Regime In Test Section	Method of Producing Limited Cavitation	Method of Producing Change In Initial Flow Regime		Desired Condition	Additional Property Change Will Produce	Method Employed To Produce Property Change
		Velocity	Pressure			
Non-cavitating	Onset	Constant	Decrease	Incipient Cavitation	Cavity Flow	Reduce Pressure In Pressurizing Chamber
Non-cavitating	Onset	Increase	Constant	Incipient Cavitation	Cavity Flow	Reduce Throttling With Throttle Valve
Cavity	Suppression	Constant	Increase	Desinent Cavitation	Non-cavitating Flow	Increase Pressure In Pressurizing Chamber
Cavity	Suppression	Decrease	Constant	Desinent Cavitation	Non-cavitating Flow	Increase With Throttle Valve

Oxygen Content of Water

The dissolved oxygen content of the tunnel water was determined by the modified Winkler method. The details of this method are given in Appendix E. Water samples were withdrawn from the bottom of the settling chamber while the tunnel water was circulated at low speed. Samples of 300 milliliters were obtained by extending a tube to the bottom of a 300-milliliter glass bottle. The bottle was allowed to overflow 2 or 3 times its volume before replacing the stopper. Oxygen-content measurements were made at least at the start and end of each operating day and always after intentional change in air content.

Stability of the air content during the 2- to 4-hour operating day was such that the oxygen content generally remained constant. Air was intentionally added for subsequent runs to cover the program range of oxygen content from about 1 to 5 milligrams of oxygen per liter of water. This was accomplished by adding high-air-content water (available from the nonboiled supply) to the tunnel while an equal amount of tunnel water was withdrawn.

CHAPTER VI

RESULTS OF EXPERIMENTAL INVESTIGATION

The experimental investigation was conducted using the small hydrodynamic tunnel described in Chapter IV. Three different test sections were used in this investigation (see Chapter IV for a description of the test sections). Distilled water was used as the test liquid. The distilled water was studied over the following range of variables: throat velocity from 35 to 125 feet per second; temperature from 85° to 99°F; and relative oxygen content from about 0.10 to 0.70.

Pressure Distribution Measured Along the Wall

The pressure distribution (without cavitation present) experienced by a liquid flowing through a test section is important in estimating the minimum pressure within the test section during cavitation. The pressure distribution measured along the wall of each test section is presented in terms of the dimensionless pressure coefficient, C_{p_x}, where

$$C_{p_x} \equiv \frac{p_x - p_t}{\rho_L V_t^2 / 2g_c} \quad . \tag{6-1}$$

The pressures along the wall of each test section were measured with mercury manometers as described in Chapter V. The minimum pressures within each test section were well above the vapor pressure of the distilled water. This was done to ensure cavity free flow. During each test the velocity at the throat was determined by using the continuity equation for steady-incompressible flow together with the cross-sectional area at the throat. This relation is

$$(AV)_2 = (AV)_t \ , \qquad (6\text{-}2)$$

where the subscript 2 designates the throat of the calibrated metering venturi. The term $(AV)_2$ was known for all flow rates encountered in this investigation (see Appendix D). A computer program was written to determine the velocity at any point in the test section (see Appendix F).

The pressure coefficients for test sections 1, 2, and 3 are shown in Figures 55, 56, and 57, respectively. The pressure coefficient should be approximately 1.0 at the entrance to each test section. This can be shown by applying the energy equation for steady-incompressible flow to a typical test section (see Figure 54). Thus, the energy equation becomes

$$\frac{p_x - p_t}{\rho_L V_t^2/2g_c} = 1 - \left[\frac{V_x}{V_t}\right]^2 - 2g\,\frac{z}{V_t^2} - \frac{2g_c q_f}{V_t^2} \ . \qquad (6\text{-}3)$$

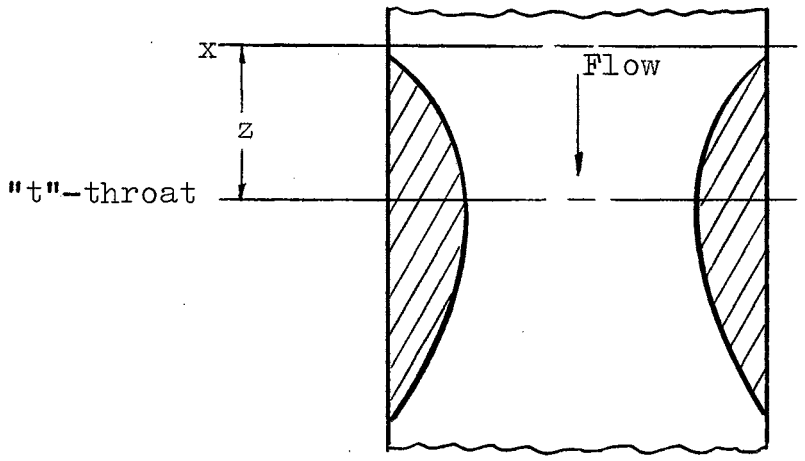

Figure 54. Schematic of Typical Test Section

If the flow area at section "x" is large when compared with the area at section "t", the second term on the right side of equation (6-3) approaches zero. The dimensionless potential energy term, $2g\ z/V_t^2$, is small because z is less than 6 inches. The fourth term on the right side of equation (6-3) represents energy dissipated through friction heating. This term is small for the test sections used in this investigation. Therefore, the pressure coefficient, defined by equation (6-1), should be approximately 1.0 at the entrance to each test section.

The pressure coefficients for test sections 1 and 2 were approximately 1.0 at the entrance to each test section. The maximum and minimum values of C_{p_x}, for 4 test runs, were used to plot Figures 55 and 56. The pressure coefficient for test section 3 was first determined by using the measured

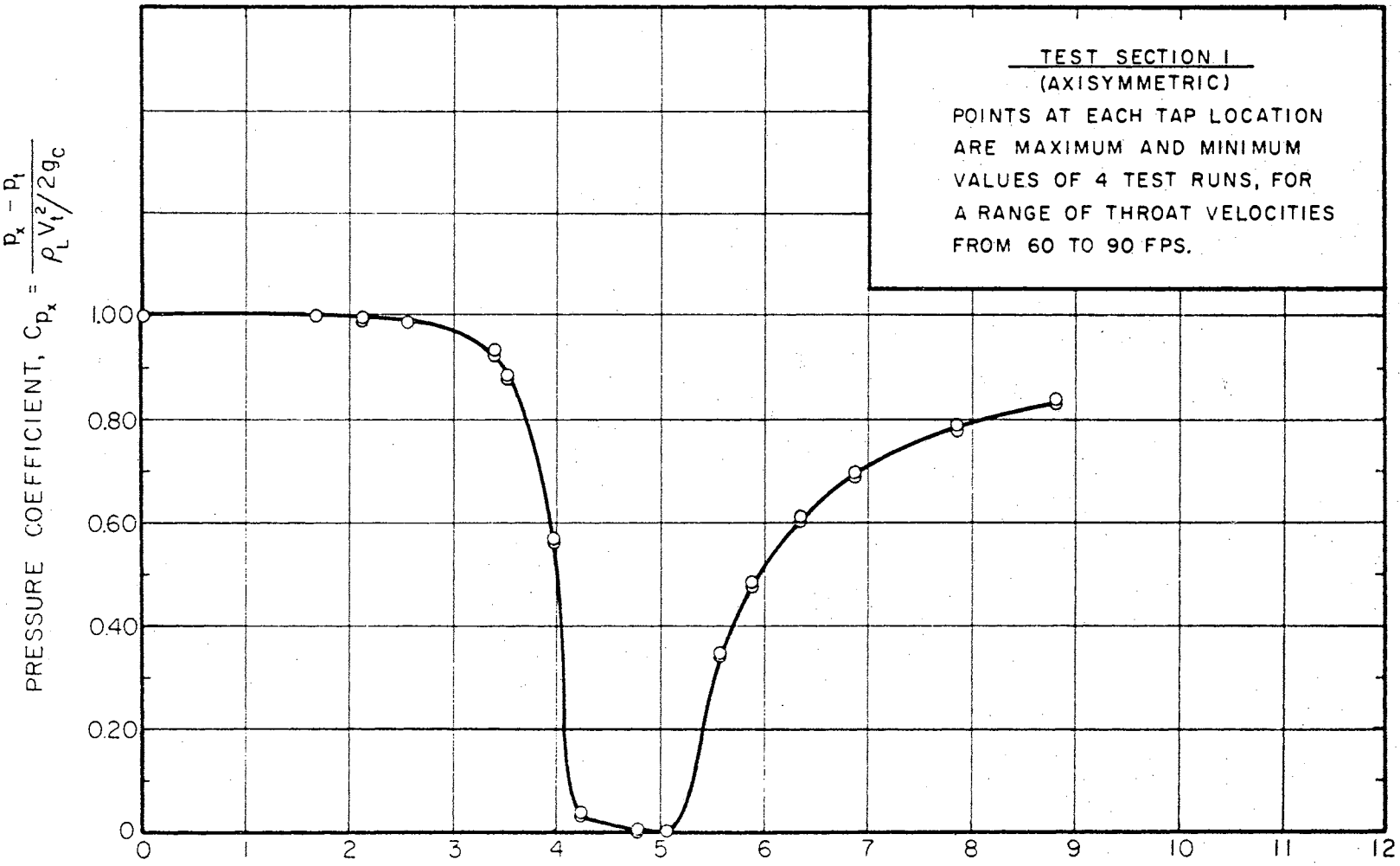

Figure 55. Variation of Pressure Coefficient with Axial Distance for Test Section 1

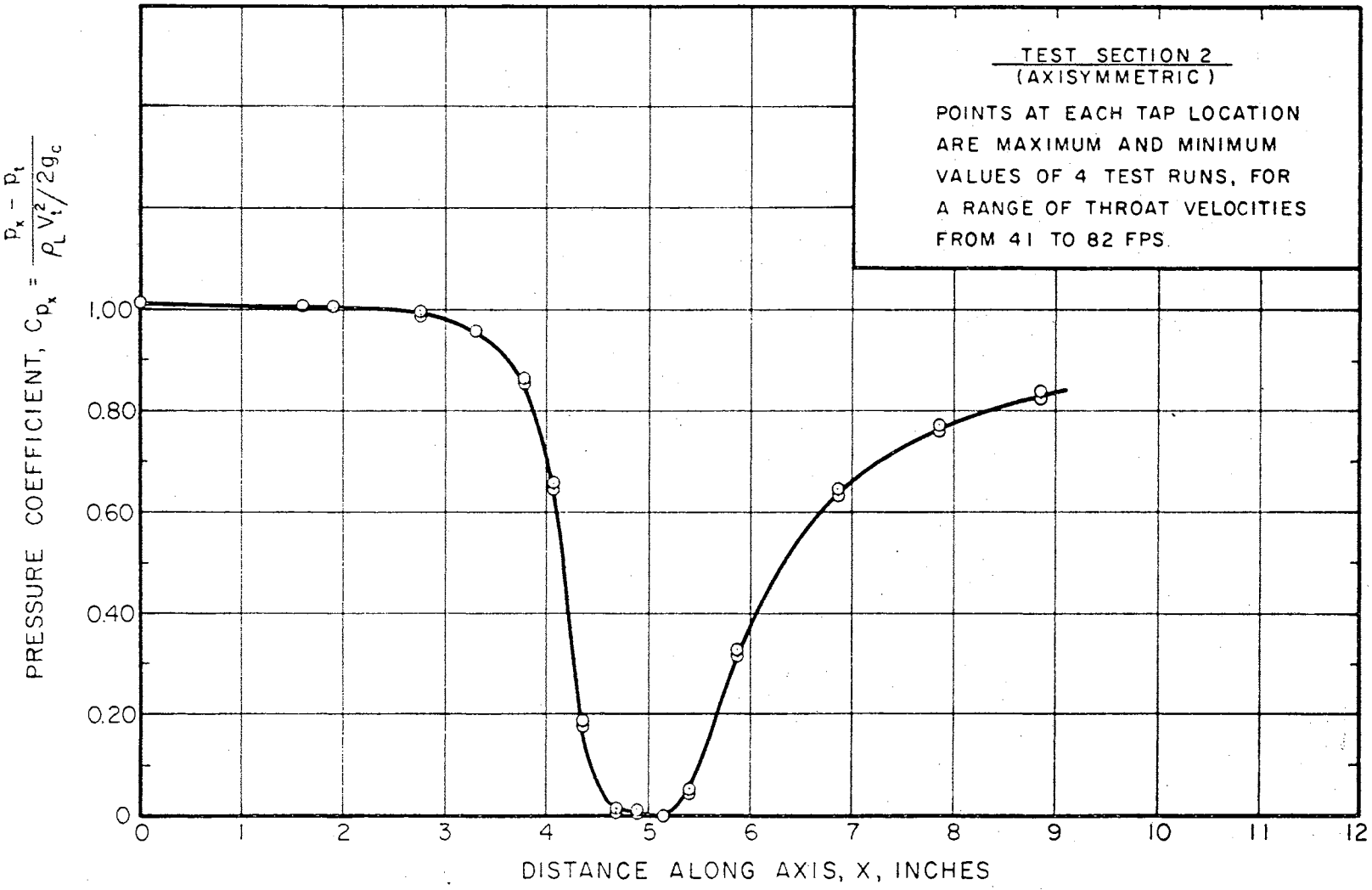

Figure 56. Variation of Pressure Coefficient with Axial Distance for Test Section 2

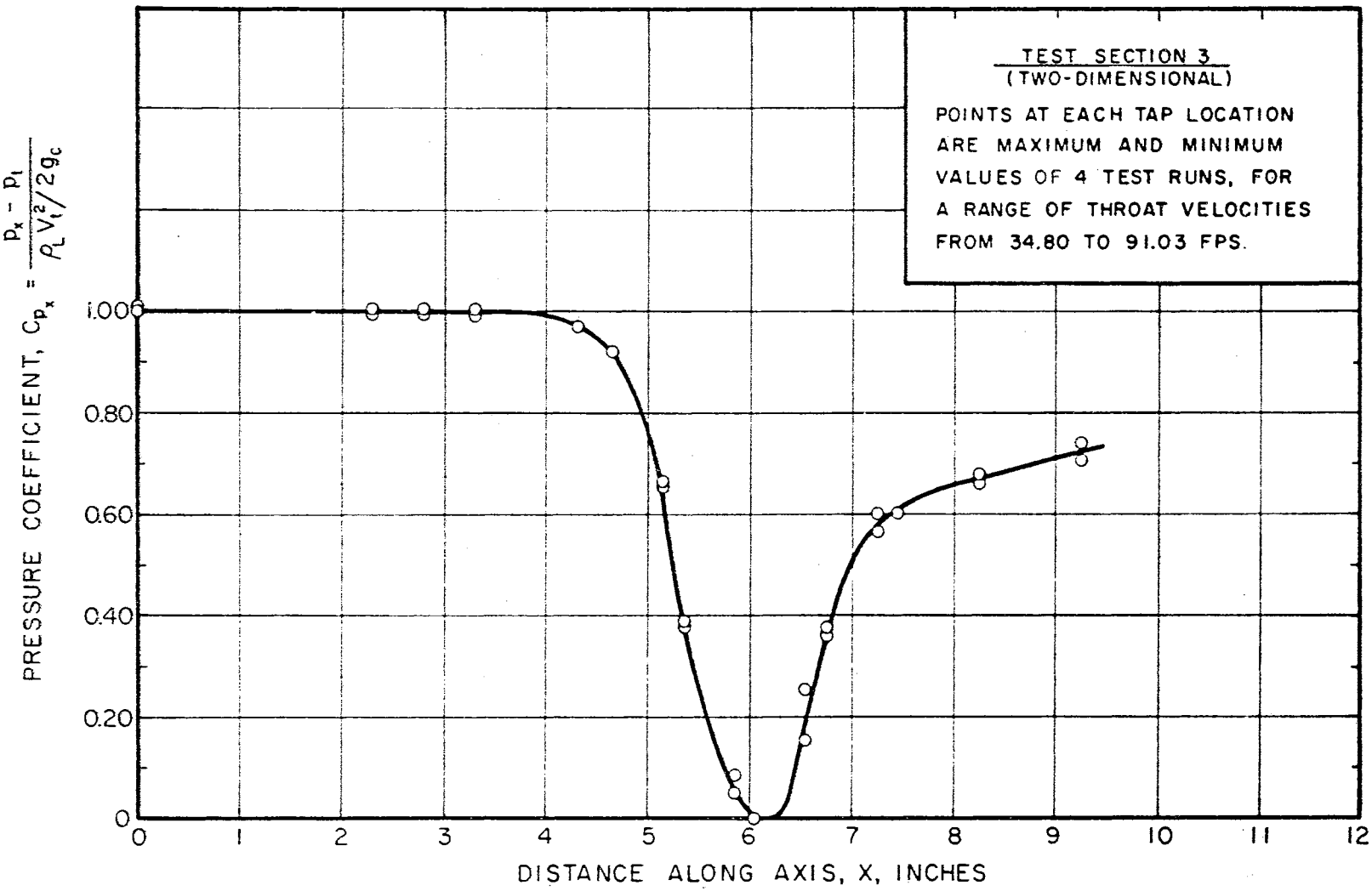

Figure 57. Variation of Pressure Coefficient with Axial Distance for Test Section 3

pressures and the calculated (by equation (6-2)) throat velocities. This resulted in a wall pressure coefficient of 1.24 at the entrance to test section 3. The correct wall pressure coefficient, according to equation (6-3), should have been less than 1.0. This error resulted when the actual area at the throat was used to calculate the throat velocity. The actual throat area was too large. This resulted in a throat velocity which was too small. In order to obtain a wall pressure coefficient of approximately 1.0 at the entrance to test section 3, an effective flow area for the throat was used. The effective area of 0.19109 square inches was used instead of the measured area of 0.21266 square inches.

The difference between the flow area and the measured area at the throat of test section 3 was probably due to boundary layer effects and/or separation. A boundary layer could have had an influence since the parallel sides were 0.140-inch apart. The surface area of test section 3 was approximately twice that of test section 1 or 2; therefore, the boundary layer could have caused some effect upon the flow area.

The major effect was probably due to separation within the diffuser. The diffuser was designed with a total angle of approximately $6\frac{1}{2}$ degrees. However, no separation was observed for various flow rates without cavitation. Nevertheless, this does not eliminate the possibility of separation being present at all flow rates. If separation occurred

within the diffuser, the streamlines near the wall would have been shifted inward (see Figure 58). Thus, the flow area at the throat would have been decreased, which would have caused an increase in the velocity.

The effective area at the throat of test section 3 was calculated so that the wall pressure coefficient was 1.0 at the entrance to test section 3. This was the throat area (0.19109 square inches) used to determine the throat velocity.

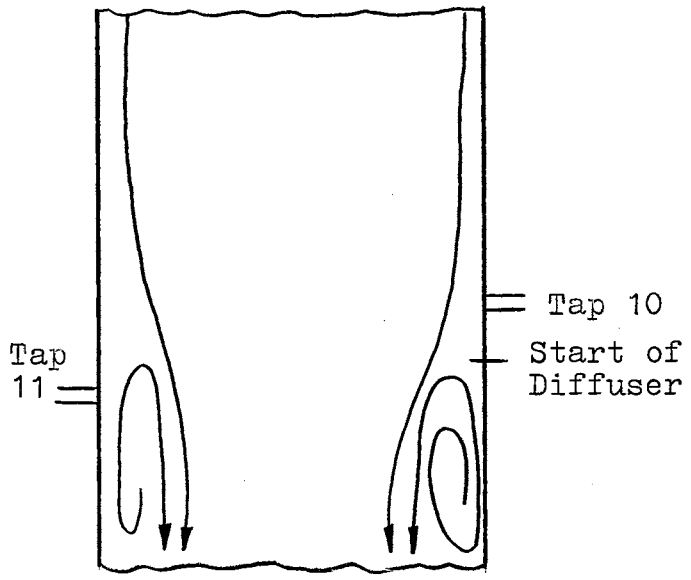

Figure 58. Schematic Showing Flow in Test Section 3 if Separation Occurred

Corrected Minimum Pressure

The minimum pressure coefficient is a function of the local Reynolds number. As the Reynolds number increases

the minimum pressure coefficient usually decreases. Incipient cavitation will alter the flow area within the throat of a test section. This, in turn, will change the minimum pressure coefficient.

Several test runs were made to determine the minimum pressure, during incipient cavitation, by an indirect method. This method was based on the assumption that the minimum pressure coefficient was not altered by the formation of incipient cavitation. A typical test, performed on test section 1, is shown in Figure 59. The corrected minimum pressure p_c was computed by

$$p_c = p_b - (p_b' - p_c'), \qquad (6\text{-}4)$$

where p_b refers to the pressure measured under incipient cavitating conditions and p_b' and p_c' refer to pressures measured at the same locations and at the same velocity but at a higher pressure in the absence of cavitation. The dotted line, shown in Figure 59, was obtained with the use of equation (6-4). Curves A, B, and C were obtained without cavitation being present within the test section. Curve D was obtained with incipient cavitation within the test section.

The method described above was not used to predict the minimum pressure within a test section because it was based on the assumption that incipient cavitation does not alter the minimum pressure coefficient.

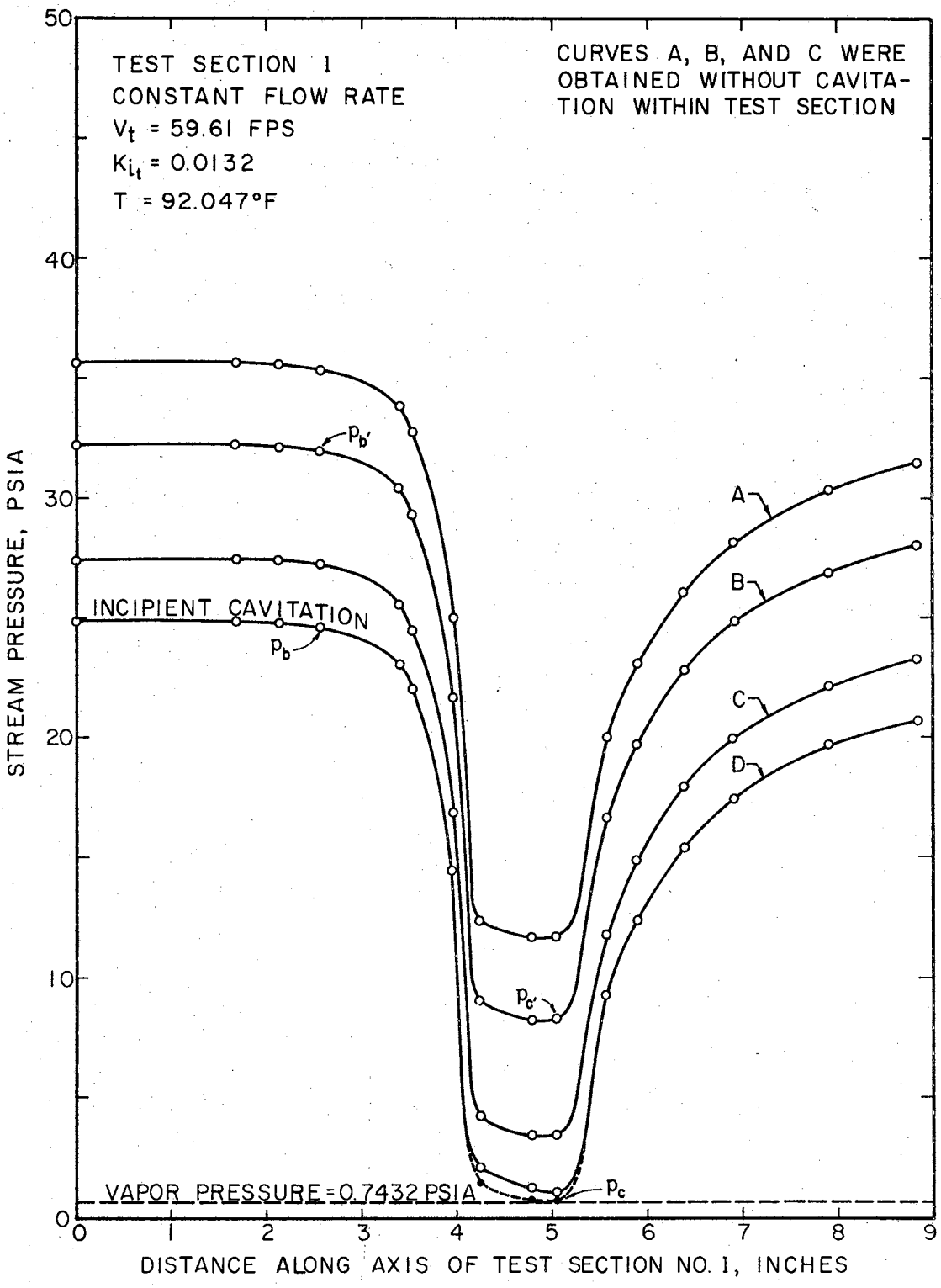

Figure 59. Pressure Distribution in Test Section 1 for Various Pressure Levels and a Constant Flow Rate

Data Reduction

The dynamic flow conditions during cavitation were represented quantitatively by the dimensionless cavitation number, K_t, where

$$K_t \equiv \frac{p_t - p_v}{\rho_L V_t^2/2g_c} . \qquad (6\text{-}5)$$

A body submerged in a flowing liquid has some critical value of K_t. The critical value of K_t is the value at which incipient cavitation occurs on the walls of the test section. For convenience it is given the sumbol K_{i_t}:

$$K_{i_t} \equiv \frac{p_{i_t} - p_v}{\rho_L V_{i_t}^2/2g_c} , \qquad (6\text{-}6)$$

where p_{i_t} was measured when incipient cavitation occurred on the walls of the test section. The velocity V_{i_t} was determined by equation (6-2) when incipient cavitation was present within the test section. During each test the temperature of the water was recorded with a thermocouple which was connected to a digital voltmeter. The method of least squares was used to obtain an equation relating the temperature to the electromotive-force produced by a thermocouple. The method of least squares was also used to obtain equations for density and vapor pressure as functions of temperature. These equations were solved to obtain the density and vapor pressure for use in computing the incipient

cavitation number.

If the flowing liquid cavitates incipiently at the vapor pressure, the minimum pressure equals the vapor pressure; thus,

$$-C_{p_{min}} = K_{i_t} = 0, \quad (p_v = p_x) \; . \tag{6-7}$$

Consequently, a measured value of K_{i_t} less than $-C_{p_{min}}$ indicates incipient cavitation at a local pressure less than the vapor pressure or, as defined herein, a local tensile stress in the liquid. This discussion assumes that the non-cavitating values of C_{p_x} (including $C_{p_{min}}$) are valid at incipient cavitation conditions, since for these conditions only extremely small scale disturbances exist in the flow field. Such disturbances are usually considered to have a negligible effect on the value of $C_{p_{min}}$, at least for conditions just prior to incipient cavitation.

A value of K_{i_t} greater than $-C_{p_{min}}$ indicates incipient cavitation at a local pressure greater than the vapor pressure. Thus, the liquid has not withstood any local tension.

The lower the value of K_{i_t}, the more resistive is the body to cavitation. Thus, K_{i_t} is a useful index for comparing the susceptibility of various conduit shapes to incipient cavitation.

Results and Discussion

The results of the experimental investigation were

presented in terms of the incipient cavitation number and the pressure measured near the plane of incipient cavitation.

Incipient Cavitation Number and Pressure Variation with Velocity

The pressures measured at the various pressure taps (located in the minimum area section of each test section), during incipient cavitation, were the values used in calculating the incipient cavitation numbers and are referred to as the cavitation pressures. Pressure taps 10, 11, and 10 were nearest the location of incipient cavitation for test sections 1, 2, and 3 respectively.

Incipient cavitation numbers and pressures were obtained for a range of throat velocities from 35 to 125 feet per second. The incipient cavitation numbers and pressures were plotted as a function of the velocities at the taps where the cavitation pressures were measured, and are shown in Figures 60, 61, and 62 for test sections 1, 2, and 3, respectively. The pressure near the plane of incipient cavitation increased as the throat velocity was increased.

Effect of Dissolved Oxygen Content

The effect of the dissolved oxygen content on the incipient cavitation number can be seen by examining Figures 61 and 62. As the relative oxygen content was increased the incipient cavitation number increased. This is in agreement with the nucleation theory. As the dissolved gas

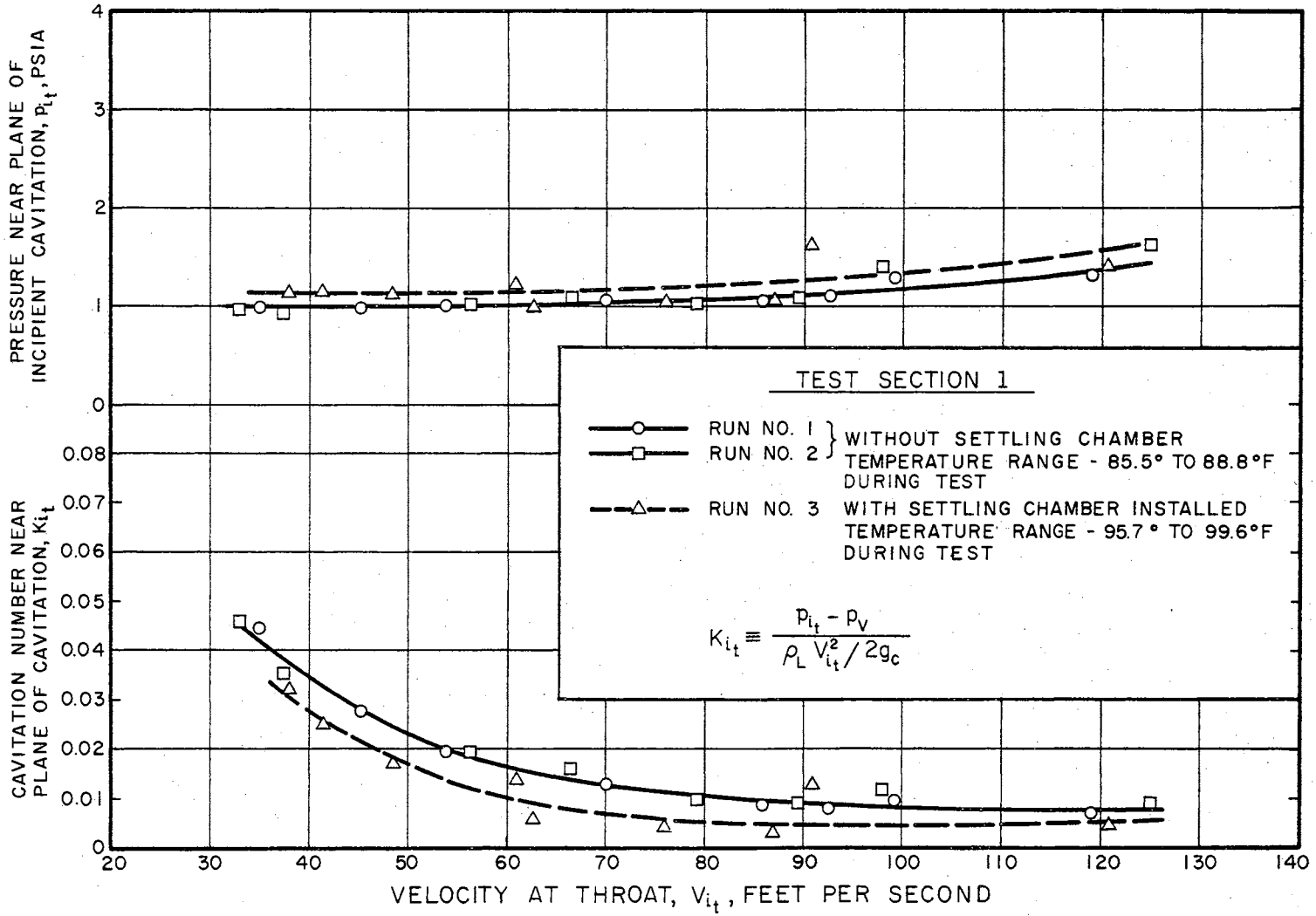

Figure 60. Variation of Cavitation Number and Pressure with Throat Velocity for Distilled Water Flowing Through Test SEction 1

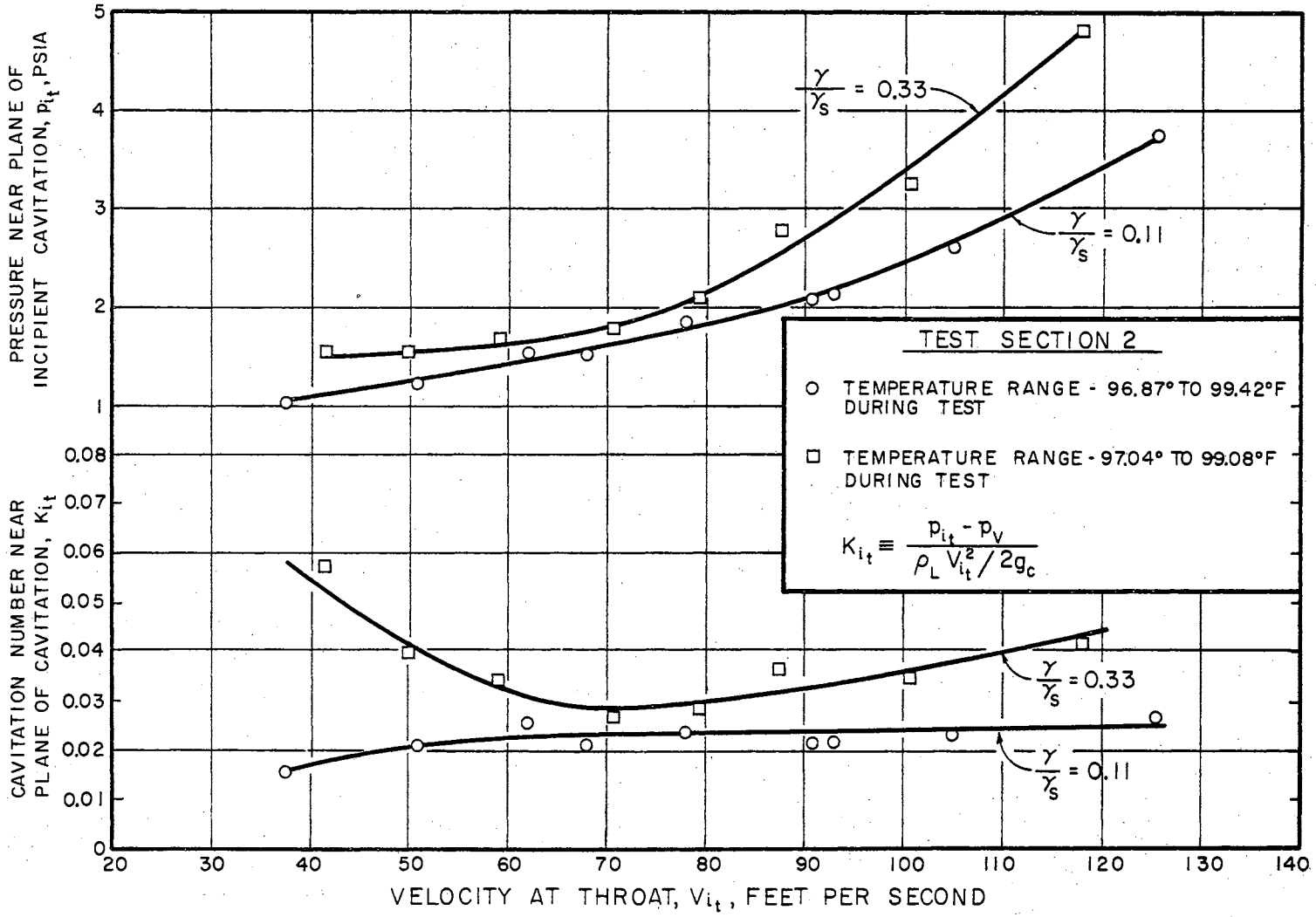

Figure 61. Variation of Cavitation Number and Pressure with Throat Velocity for Distilled Water Flowing Through Test Section 2

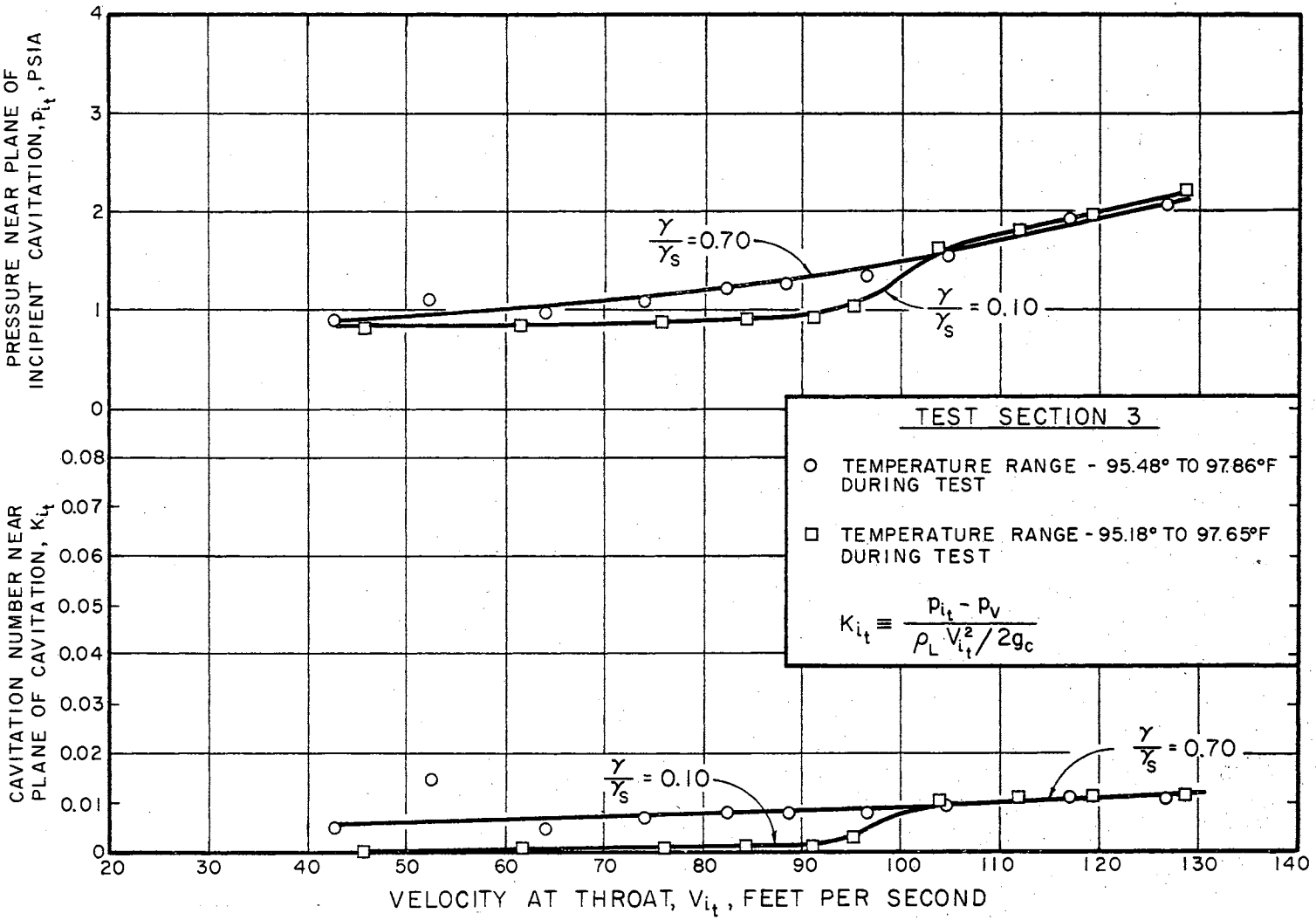

Figure 62. Variation of Cavitation Number and Pressure with Throat Velocity for Distilled Water Flowing Through Test Section 3

content was increased it became easier for a bubble to form.

Lehman and Young [3] were unable to observe any change in the incipient cavitation number over a range of air content from 25 per cent saturated to saturated conditions. Ruggeri and Gelder [33] observed an effect of air content on the incipient cavitation number. However, they used an audible method to detect the occurrence of incipient cavitation. They were unable to observe any effect in the incipient cavitation number when the visible method (method employed in this investigation) was used to detect the occurrence of cavitation.

The incipient cavitation number for test section 1 is shown in Figure 60. During this investigation the dissolved oxygen content was not measured. However, the same procedure was used in preparing the distilled water and filling the tunnel. The test performed after the settling chamber was installed probably had a lower dissolved gas content. The difference in the two incipient cavitation curves was probably due to temperature effects. Temperature has a definite effect on the cavitation pressure.

Effect of Pressure Distribution

The effect of the pressure distribution on the incipient cavitation number can be seen by comparing the magnitudes of the cavitation number shown in Figures 60 and 61 with the cavitation number in Figure 62. A comparison between the pressure distributions can be obtained by examining Figures

55, 56, and 57. The cavitation number for test section 3 was generally lower than for test sections 1 and 2. This was attributed to the fact that a particle of liquid remained within the low pressure region for a shorter period of time. Thus, the pressure distribution had an influence on the conditions at the plane of incipient cavitation.

Tap Effects

The pressure taps located in the minimum area section of test sections 1, 2, and 3 had an effect upon the properties at the plane of incipient cavitation. These tap openings served as weak spots for the formation of cavities. For low throat velocities (30 to 40 fps) no cavitation was observed at the tap openings over the range of dissolved oxygen contents investigated. The incipient cavitation was in the form of a complete ring (see Figure 63). As the throat velocity was increased the complete ring disappeared and incipient cavitation usually stabilized at a few particular locations. These locations usually included one of the tap openings.

As the dissolved oxygen content of the water was increased, the velocity at the disappearance of the complete ring increased. This ring existed for throat velocities as high as 80 feet per second for a relative oxygen content of 0.70. Thus, the dissolved gas content of a liquid has an influence on the appearance (complete ring or local cavities) of incipient cavitation.

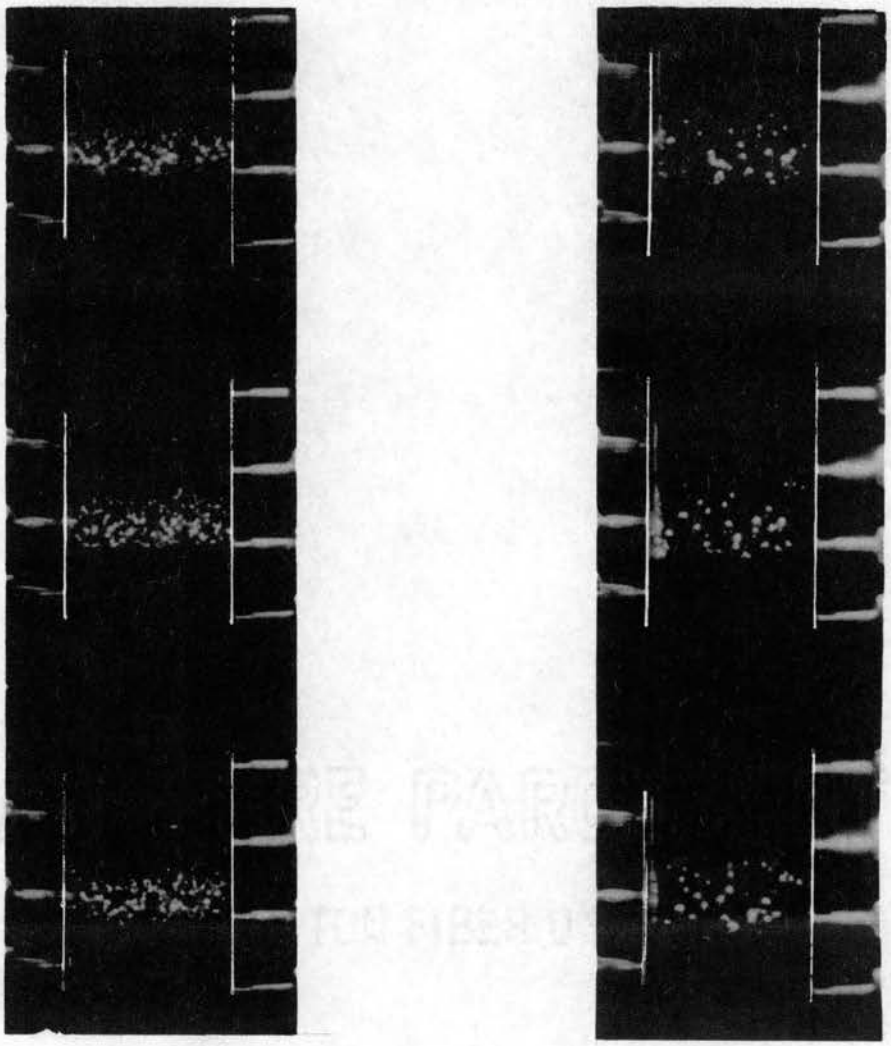

(a). 3600 frames / second

V_{i_t} = 45.67 fps

K_{i_t} = 0.0072

$\frac{\gamma}{\gamma_s}$ = 0.54

(b). 2900 frames/sec

V_{i_t} = 52.11 fps

K_{i_t} = 0.0022

$\frac{\gamma}{\gamma_s}$ = 0.30

Figure 63. Incipient Cavitation in Test Section 3 (Flow Direction from Top to Bottom of Page)

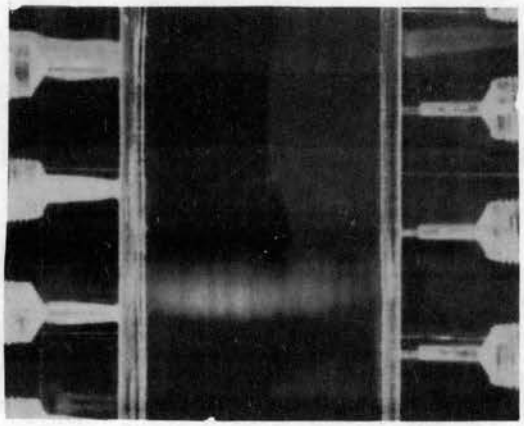

(a). V_{i_t} = 50.9 fps
$T = 92.66^{\circ}F$

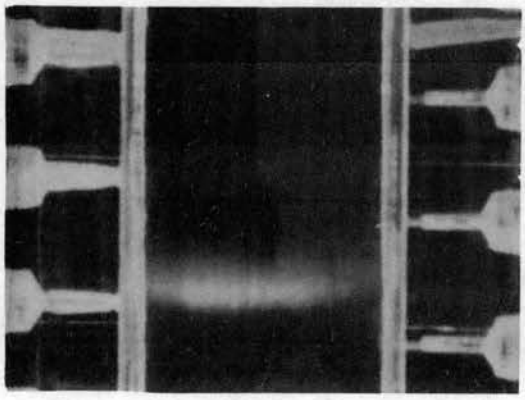

(b). V_{i_t} = 50.9 fps
$T = 93.22^{\circ}F$

Figure 63.— Concluded. Incipient Cavitation in Test Section 3 (Flow Direction from Top to Bottom of Page)

The pressure tap openings within the throat of test section 2 were plugged during a series of incipient cavitation tests. This was done to check the effect of tap openings on incipient cavitation. No consistent effect could be determined. The method used to plug the tap openings was believed to be inadequate.

Local Tension

Several tests were performed to determine the length of time distilled water could flow in the tunnel and withstand tension (occurring in the test section) before cavitation occurred. Before each test the tunnel liquid was allowed to sit for approximately 8 hours. When the tunnel motor was started enough time (15 to 30 minutes) was allowed for the system to reach the desired equilibrium temperature. After the system reached the desired equilibrium temperature, the flow rate was increased until a desired minimum pressure occurred within the test section. When the desired minimum pressure was reached, a timer was started. The timer was stopped when cavitation first appeared.

The time required for the liquid to cavitate appeared to depend on the flow rate, magnitude of minimum pressure, dissolved oxygen content, history prior to test, pressure distribution, and exposure time (time a particle traveling along the wall remained in tension). Figures 64, 65, 66, and 67 show pressures recorded during typical tests. When cavitation occurred, the cavities were in excess of incipient

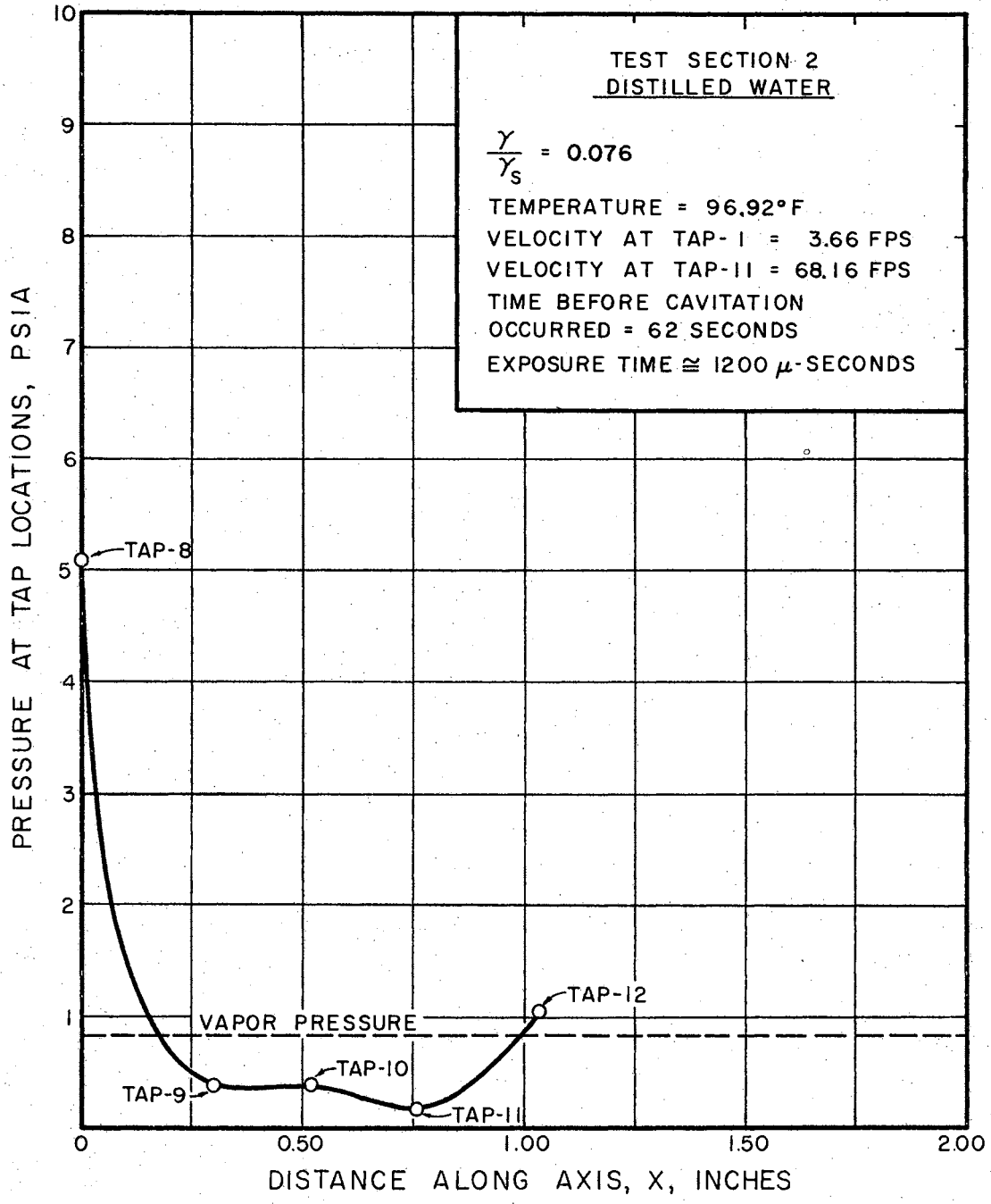

Figure 64. Pressure Distribution in Test Section 2 During A Local Tension Test

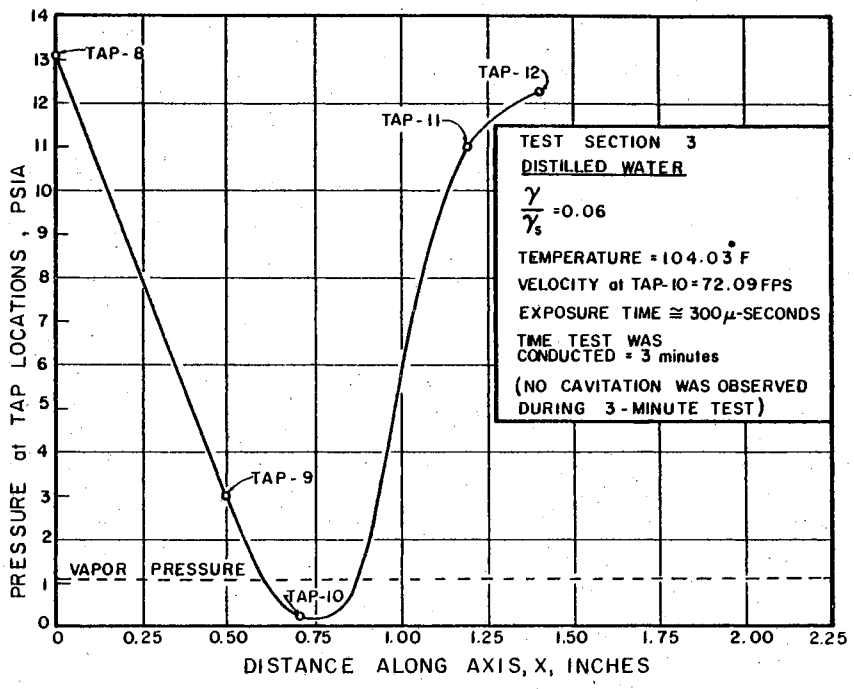

Figure 65. Pressure Distribution in Test Section 3 During A Local Tension Test (No Cavitation Was Observed)

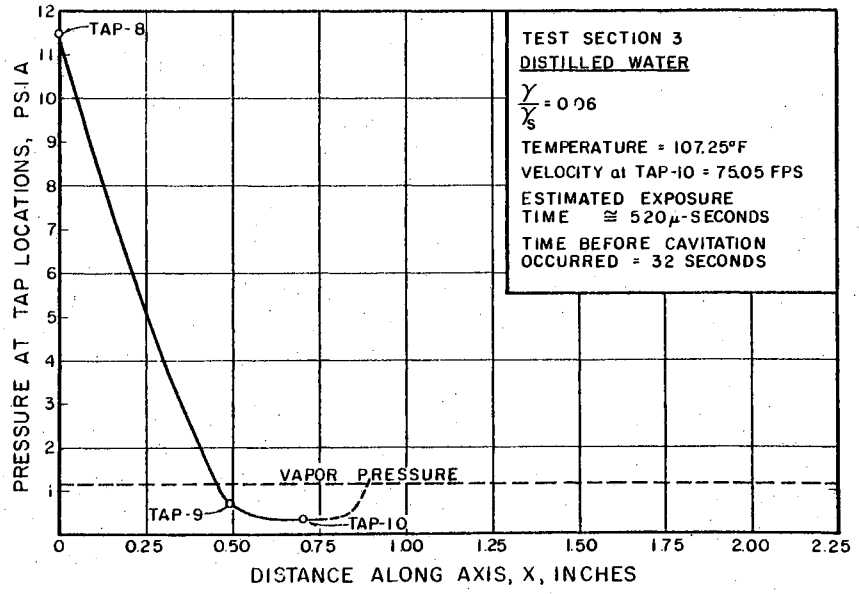

Figure 66. Pressure Distribution in Test Section 3 During A Local Tension Test (Cavitation Was Observed)

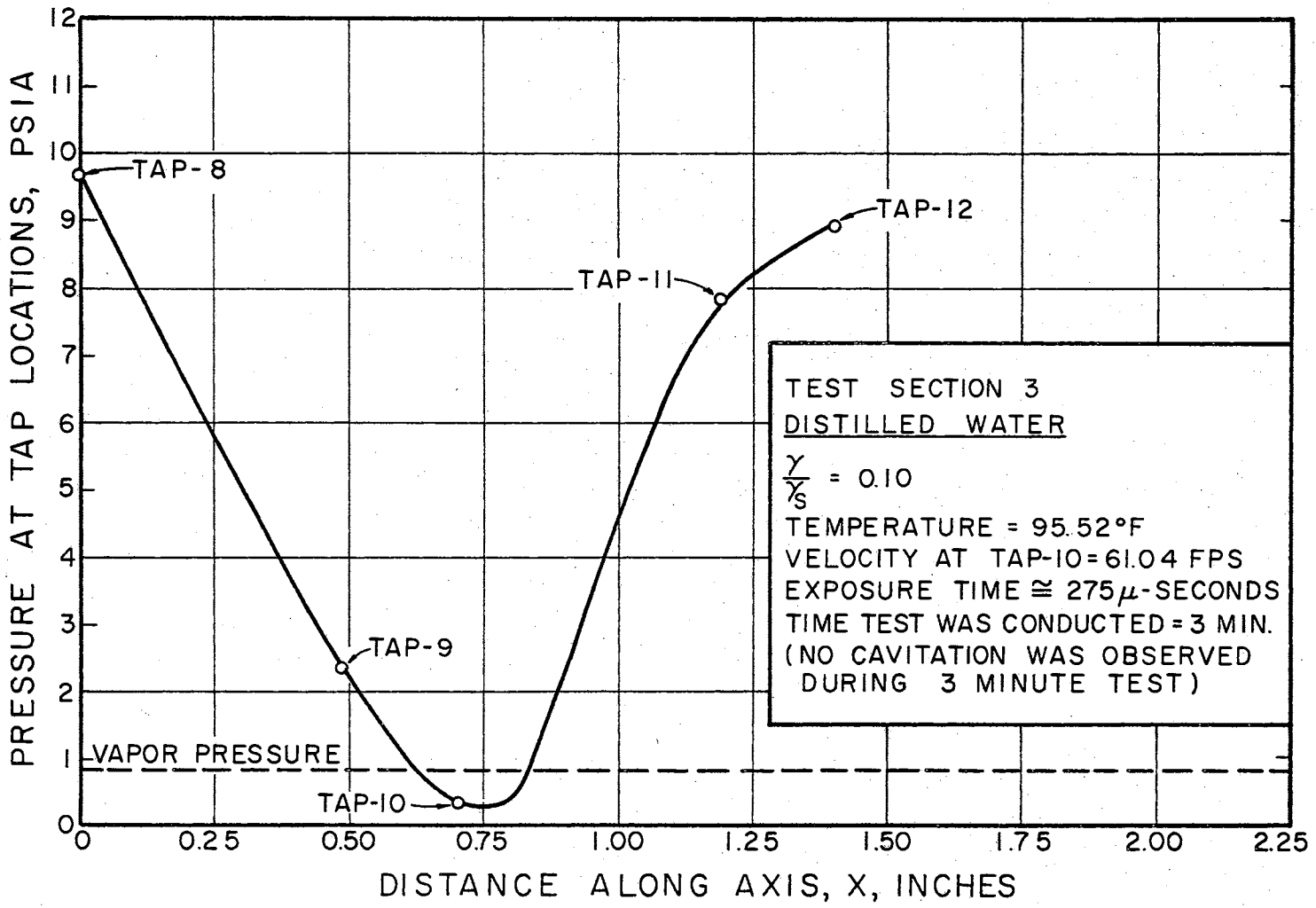

Figure 67. Pressure Distribution in Test Section 3 During A Local Tension Test (No Cavitation Was Observed)

cavitation.

Several tests were performed with various amounts of maximum local tension ($p_{min} - p_v$). As the maximum local tension was decreased, the time required for the water to cavitate increased. The time required for the water to cavitate increased as the dissolved oxygen was decreased. Several tests were performed with the relative oxygen content near 0.85. The water was unable to withstand any local tension during these tests.

After the water had cavitated for a few minutes the local tension could not be obtained until the water was allowed to sit for several hours. Thus, the ability of a liquid to withstand local tension depends on the dissolved gas within the liquid. A further proof of this was reported by Jacobs and Martin [38]. They observed large tensile stresses in liquid hydrogen and nitrogen (low inert gas content liquids) without the occurrence of cavitation. However, they did not measure these pressures directly.

CHAPTER VII

CONCLUSIONS AND RECOMMENDATIONS

The objective of this investigation was twofold. First, a theoretical investigation was conducted to study the effects of viscosity, surface tension, density, pressure distribution, inert gas, polytropic constant, vapor pressure, and initial bubble radius on bubble growth and incipient cavitation. Second, an experimental investigation was performed in order to measure the pressure near the plane of incipient cavitation and to study the effect of different pressure distributions on incipient cavitation. This objective has been accomplished.

The equation of motion of a small bubble served as the starting point for the theoretical investigation. The experimental investigation was conducted using distilled water with a low dissolved gas content.

Conclusions

The conclusions which have been reached as a result of the theoretical investigation are:

1. For the quasistatic behavior of a small bubble, the maximum stable radius is not only a function of $(p_\infty - p_v)/2\sigma$ but is also a function of the

polytropic constant.

2. The viscosity of the liquid can be neglected when studying the growth of small bubbles.
3. The surface tension, density, pressure distribution, inert gas, polytropic constant, vapor pressure, and initial bubble radius must be considered when studying incipient cavitation. All of these variables exhibited an influence on the maximum bubble radius.

The conclusions which have been reached as a result of the experimental investigation are:

1. The experimental investigation reported by Lehman and Young [3] appears to be correct. However, care must be taken in interpreting the results reported by Lehman and Young. The pressures measured near the planes of incipient cavitation are not the minimum pressures within the test sections. Also, separation was possible in the test section having the abrupt contour.
2. Pressure distribution has a pronounced effect on the pressure at the plane of incipient cavitation. For bodies with flat, minimum-pressure profiles, the liquid will cavitate at higher pressures than for bodies with steep, narrow profiles.
3. The inert gas content of a liquid has an important influence on the pressure at the plane of incipient cavitation. This influence appears

to be more important for liquids with low dissolved gas content.

4. The ability of a liquid to withstand a local tension depends on the dissolved gas within the liquid, pressure distribution, exposure time, and history prior to the location where local tension is applied.

Recommendations for Future Study

Areas which it is felt are worthy of future study include:

1. Effects of pressure tap openings on incipient cavitation. This will require the design of new test sections. The pressure taps within the minimum pressure region (taps 6, 7, 8, 9, 10, 11, and 12 in Figures 47, 48, and 49) of each test section should be omitted until the necessary tests of incipient cavitation have been completed.
2. Incipient cavitation characteristics of liquids such as RP-1 and Freon at low dissolved gas content.
3. Tension-time characteristics of liquids other than water. This might be aided by some comprehensive experimental tension-time studies with static liquids.
4. Determine the initial bubble radius and/or radii

needed to satisfy the growth equation. This can be accomplished by solving the equation which describes the growth of small nuclei (equation (3-15)). The initial bubble radius should be selected so that the bubble radius and velocity, $\dot{R}$, are satisfied at the plane of incipient cavitation. Several tests should be conducted so that a correlation between initial bubble radius, pressure distribution, and inert gas content can be obtained.

SELECTED BIBLIOGRAPHY

1. Strasberg, M. "Undissolved Air Cavities as Nuclei." Cavitation in Hydrodynamics (Proc. Nat. Phys. Lab. Symposium), Paper 6, Her Majesty's Stationery Office, London, 1956.

2. Holl, J. W. "An Effect of Air Content on the Occurrence of Cavitation." Trans. ASME, Series D, Journal of Basic Engineering, Vol. 82, pp. 941-946, 1960.

3. Lehman, A. F. and J. O. Young. "Experimental Investigations of Incipient and Desinent Cavitation." Trans. ASME, Series D, Journal of Basic Engineering, Vol 86, 1964, pp. 275-284.

4. Kermeen, R. W. "Some Observations of Cavitation on Hemispherical Head Models." Report E-35.1, Hydrodynamics Laboratory, California Institute of Technology.

5. Eisenberg, P. "On the Mechanism and Prevention of Cavitation." The David W. Taylor Model Basin Report 712, July, 1950.

6. Harvey, E. N., Wm. D. McElroy, and A. H. Whiteley. "On Cavity Formation in Water." Journal of Applied Physics, Vol. 18, February, 1947, pp. 162-172.

7. Johnson, V. E., Jr. "Mechanics of Cavitation." Journal of the Hydraulics Division. ASCE, Vol. 89, No. HY 3, Proc. Paper 3530, May, 1963, pp. 251-275.

8. Noltingk, B. E., and E. A. Neppiras. "Cavitation Produced by Ultrasonics." Proceedings Physical Soc. (B)., London, Vol. 63, 1950, pp. 674-685.

9. Neppiras, E. A. and B. E. Noltingk. "Cavitation Produced by Ultrasonics: Theoretical Conditions for the Onset of Cavitation." Proceedings Physical Society (B)., London, Vol. 64, 1951, pp. 1032-1038.

10. Schweitzer, P. H. and V. G. Szebehely. "Gas Evolution in Liquids and Cavitation." Journal of Applied Physics, Vol. 21, December, 1950, pp. 1218-1224.

11. Knapp, R. T. "Cavitation and Nuclei." Transactions of the ASME, Vol. 80, 1958, pp. 1215-1324.

12. Kermeen, R. W., J. T. McGraw, and B. R. Parkin. "Mechanism of Cavitation Inception and the Related Scale-Effects Problem." Trans. ASME, Vol. 77, 1955, pp. 533-541.

13. Robertson, J. M. "Cavitation in Hydraulic Structures: Scale Effects Involved in Cavitation Experiments." Journal of the Hydraulics Division, ASCE, Vol. 89, No. HY 3, Proc. Paper 3520, May, 1963, pp. 167-180.

14. Holl, J. W. and G. F. Wislicenus. "Scale Effects on Cavitation." Trans. ASME, Series D, Journal of Basic Engineering, Vol. 83, 1961, pp. 385-398.

15. Schlichting, H. Boundary Layer Theory. McGraw-Hill Book Company, Inc., 1960.

16. Knapp, R. T. and A. Hollander. "Laboratory Investigations of the Mechanism of Cavitation." Trans. ASME, Vol. 70, 1948, pp. 419-435.

17. Daily, J. W. and V. E. Johnson, Jr. "Turbulence and Boundary-Layer Effects on Cavitation Inception from Gas Nuclei." Trans. ASME, Vol. 78, 1956, pp. 1695-1706.

18. Parkin, B. R. "Scale Effects in Cavitation Flow." Ph.D. Dissertation, California Institute of Technology, 1952.

19. Holl, J. W. "The Effect of Surface Irregularities on Incipient Cavitation." Ph.D. Dissertation or TM 5.3410-03, Ordnance Research Laboratory, The Pennsylvania State University, 1958.

20. Calehuff, G. L. and G. F. Wislicenus. "ORL Investigations of Scale Effects on Hydrofoil Cavitation." TM 19.4212-03, Ordnance Research Laboratory, The Pennsylvania State University, February, 1956.

21. Abbott, I. H., A. E. von Doenhoff, and L. S. Stivers, Jr. "Summary of Airfoil Data." NACA Report 824, 1945.

22. Parkin, B. R. and J. W. Holl. "Incipient-Cavitation Scaling Experiments for Hemispherical and 1.5 Caliber Ogive-Nosed Bodies." Report NOrd 7958-264, Ordnance Research Laboratory, The Pennsylvania State University, May, 1954.

23. Oshima, R. "Theory of Scale Effects on Cavitation Inception on Axially Symmetric Bodies." Trans. ASME, Series D, Journal of Basic Engineering, Vol. 83, 1961, pp. 379-384.

24. Knapp, R. T. "Cavitation Mechanics and Its Relation to the Design of Hydraulic Equipment." Engineering, Vol. 173, 1952, pp. 566.

25. Holl, J. W. "The Inception of Cavitation on Isolated Surface Irregularities." Trans. ASME, Series D, Journal of Basic Engineering, Vol. 82, 1960, pp. 169-183.

26. McCormick, B. W., Jr. "On Cavitation Produced by a Vortex Trailing From a Lifting Surface." Trans. ASME, Series D, Journal of Basic Engineering, Vol. 84, 1962, pp. 369-379.

27. Kermeen, R. W. and B. R. Parkin. "Incipient Cavitation and Wake Flow Behind Sharp-Edged Disks." Report 85-4, Hydrodynamics Laboratory, California Institute of Technology, August, 1957.

28. Robertson, J. M., J. H. McGinley, and J. W. Holl. "On Several Laws of Cavitation Scaling." La Housille Blanche, September, 1957, p. 540.

29. Numachi, F. and T. Kurokawa. "Uber den Einfluss des Luftgehaltes auf die Kavitationsentstehung." [On the Effect of Air Content on the Appearance of Cavitation] Werft-Reederei-Hafen, Vol. 20, 1939.

30. Crump, S. F. "Determination of Critical Pressures For The Inception of Cavitation in Fresh and Sea Water as Influenced by Air Content of the Water." The David W. Taylor Model Basin, Report 575, October, 1949.

31. Crump, S. F. "Critical Pressures For The Inception of Cavitation in a Large-Scale Numachi Nozzle as Influenced by Air Content of the Water." The David W. Taylor Model Basin, Report 770, July, 1951.

32. Williams, E. E. and P. McNulty. "Some Factors Affecting the Inception of Cavitation." Cavitation in Hydrodynamics (Proc. Nat. Phys. Lab. Symposium) Paper 2, Her Majesty's Stationery Office, London, 1956.

33. Ruggeri, R. S. and T. F. Gelder. "Effects of Air Content and Water Purity on Liquid Tension at Incipient Cavitation in Venturi Flow." National Aeronautics and Space Administration, TN D-1459, March, 1963.

34. Ruggeri, R. S. and T. F. Gelder. "Cavitation and Effective Liquid Tension of Nitrogen in a Tunnel Venturi." National Aeronautics and Space Administration, TN D-2088, February, 1964.

35. Gelder, T. F., R. D. Moore, and R. S. Ruggeri. "Incipient Cavitation of Freon-114 in a Tunnel Venturi." National Aeronautics and Space Administration, TN D-2722, March, 1965.

36. Ruggeri, R. S., R. D. Moore, and T. F. Gelder. "Incipient Cavitation of Ethylene Glycol in a Tunnel Venturi." National Aeronautics and Space Administration, TN D-2722, March, 1965.

37. Hammitt, F. G. "Observation of Cavitation Scale and Thermodynamic Effects in Stationary and Rotating Components." Trans. ASME, Series D, Journal of Basic Engineering, Vol. 85, 1963, pp. 1-16.

38. Jacobs, R. B. and K. B. Martin. "Cavitation Problems in Cryogenics." Trans. ASME, Series D, Journal of Basic Engineering, Vol. 82, 1960, pp. 756-757.

39. Numachi, F., M. Yamabe, and R. Ōba. "Cavitation Effect on the Discharge Coefficient of the Sharp-Edged Orifice Plate." Trans. ASME, Series D, Journal of Basic Engineering, Vol. 82, 1960, pp. 1-11.

40. Ball, J. W. and W. P. Simmons. "Progress Report on Hydraulic Characteristics of Pipeline Orifices and Sudden Enlargements Used for Energy Dissipation." Bureau of Reclamation, Hydraulics Branch, Report No. Hyd.-519, December, 1963.

41. Mikol, E. P. and J. C. Dudley. "A Visual and Photographic Study of the Inception of Vaporization in Adiabatic Flow." Trans. ASME, Series D, Journal of Basic Engineering, Vol. 86, 1964, pp. 257-264.

42. Fauske, H. K. and T. C. Min. "A Study of the Flow of Saturated Freon-11 Through Apertures and Short Tubes." ANL-6667, January, 1963.

43. Eisenberg, P. "A Brief Survey of Progress on the Mechanics of Cavitation." The David W. Taylor Model Basin Report 842, June, 1953.

44. Lienhard, J. H. "Some Generalizations of the Stability of Liquid-Gas-Vapor Systems." Int. Journal of Heat Mass Transfer, Vol. 7, 1964, pp. 813-817.

45. Hord, J., R. B. Jacobs, C. C. Robinson, and L. L. Sparks. "Nucleation Characteristics of Static Liquid Nitrogen and Liquid Hydrogen." Trans. ASME, Journal of Engineering for Power, Vol. 86, 1964, pp. 485-494.

46. Hildebrand, F. B. Introduction to Numerical Analysis. McGraw-Hill Book Company, Inc., 1956.

47. Salvadori, M. G. and M. L. Baron. Numerical Methods in Engineering. Prentice-Hall, Inc., 1961.

48. Stonemetz, R. E. "Liquid Cavitation Studies in Circular Pipe Bends." National Aeronautics and Space Administration, TM X-53278, June 14, 1965.

49. Standard Methods for the Examination of Water and Waste-water. American Public Health Association, Inc., 1790 Broadway, New York 19, New York, 1960.

50. Landau, L. D. and E. M. Lifshitz. Fluid Mechanics. Pergamon Press, Oxford, 1959.

ADDITIONAL REFERENCES*

51. Ball, J. W. "Cavitation Characteristics of Gate Valves and Globe Valves Used as Flow Regulators Under Heads Up to About 125 Feet." Trans. ASME, Vol. 79, 1957, pp. 1275-1283.

52. Ball, J. W. "Hydraulic Characteristics of Gate Slots." ASCE, Journal of the Hydraulics Division, Vol. 85, No. HY10, 1959, pp. 81-114.

---

* Those references which helped in understanding the problem, but were not referred to directly in the text.

53. Briggs, J. L. "The Maximum Superheating of Water as a Measure of Negative Pressure." Journal of Applied Physics, Vol. 26, 1955, pp. 1001-1003.

54. Briggs, J. L. "Limiting Negative Pressure of Water." Journal of Applied Physics, Vol. 21, 1950, pp. 721-722.

55. Brown, F. R. "Cavitation in Hydraulic Structures: Problems Created by Cavitation Phenomena." Journal of the Hydraulics Division, ASCE, Vol. 89, January, 1963, pp. 99-115.

56. "Cavitation in Hydrodynamics." Proc. Symposium Natl. Phys. Lab., London, 1956.

57. "Cavitation in Hydraulic Structures: A Symposium." Proc. Amer. Soc. Civ. Engrs., Vol. 71, September, 1945, pp. 999-1068.

58. "Cavitation in Hydrodynamics." Proceedings, Symposium of the National Physical Laboratory, London, September 14-17, 1955.

59. Daily, J. W. "Cavitation Characteristics and Infinite-Aspect - Ratio Characteristics of a Hydrofoil Section." Trans. ASME, Vol. 71, 1949, pp. 269-284.

60. Dean, R. B. "The Formation of Bubbles." Journal of Applied Physics, Vol. 15, 1944, pp. 446-451.

61. Eisenberg, P. "Modern Developments in the Mechanics of Cavitation." Applied Mechanics Reviews, Vol. 10, 1957, pp. 85-89.

62. Eisenberg, P. "Cavitation." International Science and Technology, February, 1963, pp. 72-84.

63. Eisenberg, P. and M. P. Tulin. "Cavitation." Handbook of Fluid Dynamics, McGraw-Hill Book Company, Inc., 1961.

64. Fisher, J. C. "The Fracture of Liquids." Journal of Applied Physics, Vol. 19, 1948, pp. 1062-1067.

65. Fox, F. E. and K. F. Herzfeld. "Gas Bubbles With Organic Skil as Cavitation Nuclei." Journal of The Acoustical Society of America, Vol. 26, 1954, pp. 984-989.

66. Harvey, E. N., K. W. Cooper, and A. H. Whiteley. "Bubble Formation from Contact of Surfaces." Journal of the American Chemical Society, Vol. 68, Part 2, 1946, pp. 2119-2120.

67. Harvey, E. N., D. K. Barnes, W. D. McElroy, A. H. Whiteley, D. C. Pease, and K. W. Cooper. "Bubble Formation in Animals." Journal of Cellular and Comparative Physiology, Vol. 24, 1944, pp. 23-44.

68. Harvey, E. N., D. K. Barnes, W. D. McElroy, A. H. Whiteley, and D. C. Pease. "Removal of Gas Nuclei From Liquids and Surfaces." Journal of the American Chemical Society, Vol. 67, 1945, pp. 156-157.

69. Hunsaker, J. C. "Cavitation Research." Mechanical Engineering, Vol. 57, 1935, pp. 211-216.

70. Jakobsen, J. K. "On the Mechanism of Head Breakdown in Cavitating Inducers." Trans. ASME, Series D, Journal of Basic Engineering, Vol. 86, 1964, pp. 291-305.

71. Jarman, P. D. and K. J. Taylor. "Light Emission from Cavitating Water." Brit. Journal of Applied Phys., Vol. 15, 1964, pp. 321-322.

72. Kamiyama, S. "Cavitation Tests in Pipe Bends." ASME Paper No. 65-FE-7, June, 1965.

73. Numachi, F., R. Kobayashi, and S. Kamiyama. "Effect of Cavitation on the Accuracy of Herschel - Type Venturi Tubes." Trans. ASME, Series D, Journal of Basic Engineering, Vol. 84, 1962, pp. 351-362.

74. Pease, D. C. and L. R. Blinks. "Cavitation From Solid Surfaces in the Absence of Gas Nuclei." Journal of Phys. Colloid Chem., Vol. 51, 1947, pp. 556-567.

75. Robertson, J. M. "Water Tunnels for Hydraulic Investigations." Trans. ASME, Vol. 78, 1956, pp. 95-104.

76. Rouse, H. "Cavitation in the Mixing Zone of a Submerged Jet." La-Houille Blanche, 1953, pp. 9-19.

77. Rouse, H. and J. S. McNown. "Cavitation and Pressure Distribution: Head Forms at Zero Angle of Yaw." State University Iowa Studies in Engr. Bull. 32, 1948.

78. Rouse, H. "Cavitation and Pressure Distribution: Head Forms at Angles of Yaw." State University Iowa Studies in Engr. Bull. 42, 1962.

79. Sarosdy, L. R. and A. J. Acosta. "Note on Observations of Cavitation in Different Fluids." Trans. ASME, Series D, Journal of Basic Engineering, Vol. 83, 1961, pp. 399-400.

80. Stahl, H. A. and A. J. Stepanoff. "Thermodynamic Aspects of Cavitation in Centrifugal Pumps." Trans. ASME, Vol. 78, 1956, pp. 1691-1693.

81. Stepanoff, A. J. "Cavitation Properties of Liquids." Trans. Asme, Series A, Journal of Engineering for Power, Vol. 86, 1964, pp. 195-200.

82. Stiles, G. F. "Cavitation in Control Valves." Instruments and Control Systems, Vol. 34, 1961, pp. 2086-2093.

83. Strasberg, N. "The Influence of Air-Filled Nuclei on Cavitation Inception." David W. Taylor Model Basin Report 1078, May, 1957.

84. Temperley, H. V. N. and L. L. G. Chambers. "The Behavior of Water Under Hydrostatic Tension." Proc. Physical Society, (London), Vol. 58, 1946, pp. 420-443.

85. Thomas, H. A. and E. P. Schuleen. "Cavitation in Outlet Conduits of High Dams." Trans. of the ASCE, Vol. 107, 1942, pp. 421-493.

86. Wang, P. K. C. and J. T. S. Ma. "Cavitation in Valve-Controlled Hydraulic Actuators." Trans. ASME, Series E, Journal of Applied Mechanics, Vol. 85, 1963, pp. 537-546.

87. Ziegler, G. "Tensile Stresses in Flowing Water." Cavitation in Hydrodynamics, (Proc. Nat. Phys. Lab. Symposium), Paper 3, Her Majesty's Stationery Office, London, 1956.

Ultrasonic Cavitation

88. Akulichev, V. A. and V. I. Il'ichev. "Spectral Indication of the Origin of Ultrasonic Cavitation in Water." Soviet Physics - Acoustics, Vol. 9, 1963, pp. 128-130 (English Translation).

89. Bondy, C. and K. Sollner. "On the Mechanism of Emulsification by Ultrasonic Waves." Trans. Faraday Society, Vol. 31, Part I, 1935, pp. 835-846.

90. Brown, B. "Ultrasonic Cavitation in Water." British Communications and Electronics, Vol. 9, Part 2, 1962, pp. 918-920.

91. Connolly, W. and F. E. Fox. "Ultrasonic Cavitation Thresholds in Water." Journal of the Acoustical Society of America, Vol. 26, 1954, pp. 843-848.

92. Gabrielli, I. and G. Iernetti. "Cavitation and Chemical Effects in Ultrasonic Stationary Fields." Acustica, Vol. 13, 1963, pp. 165-174.

93. Gaertner, W. "Frequency Dependence of Ultrasonic Cavitation." Journal of the Acoustical Society of America, Vol. 26, 1954, pp. 977-980.

94. Gallant, H. "Untersuchungen uber Kavitationsblasen." Osterreichische Ingenieur Zeitschrift, Vol. 5, 1962, pp. 74-83.

95. Galloway, W. J. "An Experimental Study of Acoustically Induced Cavitation in Liquids." Journal of the Acoustical Society of America, Vol. 26, 1954, pp. 849-857.

96. Goldsmith, H. A. and R. C. Heim. "New Way to Measure Ultrasonic Cavitation Intensity." Metal Engineering Quarterly, Vol. 2, No. 1, 1962, pp. 62-66.

97. Kozyrev, S. P. "Ultrasonic Apparatus for Testing Materials for Cavitation - Abrasive Wear." Industrial Laboratory, Vol. 29, No. 2, 1963, pp. 216-218.

98. Mellen, R. H. "Ultrasonic Spectrum of Cavitation Noise in Water." Journal of the Acoustical Society of America, Vol. 26, 1954, pp. 356-360.

99. Messino, D., D. Sette, and F. Wanderlingh. "Statistical Approach to Ultrasonic Cavitation." Journal of the Acoustical Society of America, Vol. 35, 1963, pp. 1575-1583.

100. Numachi, F. "Transitional Phenomena in Ultrasonic Shock Waves Emitted by Cavitation on Hydrofoils." Trans. ASME, Series D, Journal of Basic Engineering, Vol. 81, 1959, pp. 153-166.

101. Sette, D. and F. Wanderlingh. "Nucleation by Cosmic Rays in Ultrasonic Cavitation." Physical Review, Vol. 125, No. 2, 1962, pp. 409-417.

102. Weissler, A. "A Chemical Method for Measuring Relative Amounts of Cavitation in an Ultrasonic Cleaner." IRE International Convention Record, Vol. 10, Part 6, 1962, pp. 24-30.

103. Willard, G. W. "Ultrasonically Induced Cavitation in Water: A Step-by-Step Process." Journal of the Acoustical Society of America, Vol. 25, 1953, pp. 669-686.

104. Wilson, R. W. "Influence of Physical Properties of Liquids on Severity of Cavitation Damage." Compressed Air and Hydraulics, Vol. 27, No. 319, 1962, pp. 382-385.

APPENDIX A

DERIVATION OF EQUATION OF MOTION FOR A SPHERICAL BUBBLE

DERIVATION OF EQUATION OF MOTION FOR A SPHERICAL BUBBLE

The equation of motion for a growing bubble can be derived by applying the continuity and momentum equations to the liquid surrounding the bubble. The assumptions introduced to simplify the derivation will be discussed as they appear.

The system will consist of the viscous, incompressible liquid surrounding a spherical bubble of radius R. The bubble will be filled with a mixture of inert gas and vapor. This growing bubble generates a velocity field within the liquid which, in turn, generates a stress field tending to retard the bubble's growth.

The spherical symmetry of the situation makes it convenient to choose a spherical coordinate system with its origin at the center of the bubble, as illustrated in Figure 68. The velocity field generated in the liquid will have only a radial component, $V_r(r, t)$. The pressure at any point in the liquid is also a function of r and t. Under the above assumptions the continuity and momentum equations reduce to

$$\frac{\partial V_r}{\partial r} + 2\,\frac{V_r}{r} = 0, \qquad \text{(A-1)}$$

and

$$\rho_L\left[\frac{\partial V_r}{\partial t} + V_r \frac{\partial V_r}{\partial r}\right] = -\frac{\partial p}{\partial r} + \mu_L\left[\frac{1}{r}\frac{\partial^2}{\partial r^2}(rV_r) - 2\frac{V_r}{r^2}\right]. \quad \text{(A-2)}$$

In equation (A-2), ρ_L is the density and μ_L the viscosity of the liquid. Both are assumed uniform and constant.

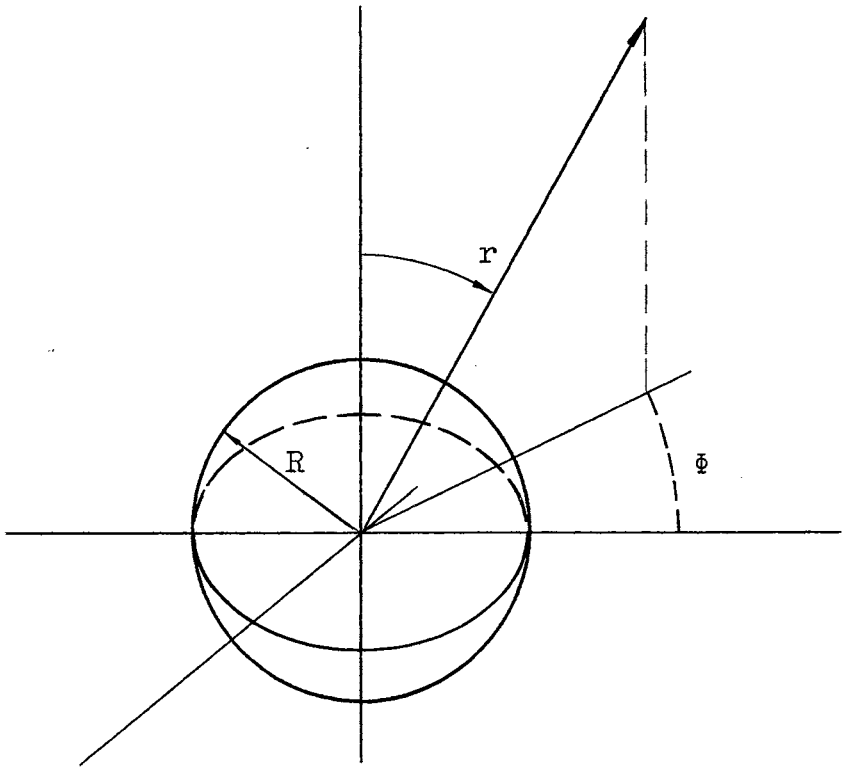

Figure 68. Spherical Coordinate System

By integrating equation (A-1) with respect to r with t held fixed, we find that

$$V_r\, r^2 = \Psi(t), \quad \text{(A-3)}$$

where $\Psi(t)$ is an arbitrary function of t. At the bubble wall, the liquid velocity must equal $\dot{R}(t)$ where a superimposed dot denotes ordinary differentiation with respect to time. Thus, the function $\Psi(t)$ can be expressed in terms of the radius and velocity of the liquid in contact with the bubble wall. This expression is

$$\Psi(t) = \dot{R}\, R^2. \tag{A-4}$$

An expression for the velocity of the liquid can be obtained by substituting equation (A-4) into equation (A-3). The resulting equation is

$$V_r(r,\ t) = \frac{\dot{R}\, R^2}{r^2}\ ,\quad r \geq R\ . \tag{A-5}$$

Equation (A-2) can be reduced to a simpler form by using equation (A-5). The resulting equation is

$$\frac{\partial p}{\partial r} = -\ \rho_L \left[\frac{1}{r^2}\left(R^2\, \ddot{R} + 2\, \dot{R}^2\, R\right) - \frac{2}{r^5}\, R^4\, (\dot{R})^2\right]\ . \tag{A-6}$$

By integrating equation (A-6) with respect to r with t held fixed, we find that

$$p(r,\ t) = -\ \rho_L\left[-\ \frac{1}{r}\left(R^2\, \ddot{R} + 2\, \dot{R}^2\, R\right) + \frac{1}{2r^4}\, R^4\, (\dot{R})^2\right] + Z\ (t), \tag{A-7}$$

where Z (t) is an arbitrary function of t. The boundary conditions are

$$p(r,\ t) = p(R + 0,\ t) \qquad \text{at the bubble wall}$$

and

$$p(r, t) = p_\infty (t) \qquad \text{as } r \longrightarrow \infty.$$

Thus, equation (A-7) reduces to

$$p(R + 0, t) - p_\infty(t) = \rho_L \left[\ddot{R} R + \frac{3}{2} (\dot{R})^2\right]. \qquad \text{(A-8)}$$

The stress components for the velocity field given by equation (A-5) are [50] (for the liquid)

$$\sigma_{rr} = - p(r, t) - \frac{4\mu_L R^2 \dot{R}}{r^3},$$

$$\sigma_{\theta\theta} = \sigma_{\Phi\Phi} = - p(r, t) + \frac{2\mu_L R^2 \dot{R}}{r^3},$$

$$\sigma_{\theta\Phi} = \sigma_{\Phi r} = \sigma_{r\theta} = 0. \qquad \text{(A-9)}$$

Within the bubble,

$$\sigma_{rr} = \sigma_{\theta\theta} = \sigma_{\Phi\Phi} = - (p_g + p_v),$$

$$\sigma_{\theta\Phi} = \sigma_{\Phi r} = \sigma_{r\theta} = 0, \qquad \text{(A-10)}$$

where p_v is the partial pressure of the vapor and p_g is the partial pressure of an inert gas.

The stress components $\sigma_{\Phi r}$ and $\sigma_{r\theta}$ must be continuous across the bubble surface. A comparison of equations (A-9) and (A-10) reveals that this requirement is automatically satisfied. The stress component σ_{rr} must experience a jump of magnitude $2\sigma/R$ at the bubble surface. σ is the coefficient of interfacial tension. Comparing the first of equations

(A-9) with the first of equations (A-10), we find that the pressure just outside the bubble wall is given by

$$p(R + 0, t) = p_g (t) + p_v (T) - \frac{2\sigma + 4\mu_L \dot{R}}{R} . \qquad (A-11)$$

If we substitute equation (A-11) into equation (A-8) we obtain an ordinary differential equation for the bubble radius as a function of the pressures inside and outside the bubble. The resulting equation of motion is

$$\rho_L [R \ddot{R} + \frac{3}{2} (\dot{R})^2] + \frac{2\sigma}{R} + \frac{4\mu_L \dot{R}}{R}$$

$$= p_g(R) + p_v(T) - p_\infty (t) . \qquad (A-12)$$

APPENDIX B

7040 COMPUTER PROGRAM FOR ISOTHERMAL BUBBLE GROWTH

7040 COMPUTER PROGRAM FOR ISOTHERMAL BUBBLE GROWTH

This computer program is the solution to equation (3-22). Equation (3-22) was written in the following form to facilitate programming.

$$\ddot{R} = -\frac{3}{2}\frac{(\dot{R})^2}{R} + C9\left[-\frac{C1}{R^2} - C7\frac{\dot{R}}{R^2} + [C2 + C3 + C1/C5 - C8]\cdot \frac{C6}{R^4} + C8/R - C2/R - C3/R \cos(C4 \cdot \text{Time})\right], \quad (B\text{-}1)$$

where

$C1 = 2\sigma$,

$C2 = p_A$

$C3 = p_o$,

$C4 = \omega$,

$C5 = R_o$,

$C6 = R_o^3$,

$C7 = 4\mu_L$,

$C8 = p_v$,

$C9 = 1/\rho_L$.

The initial conditions were

$$R(0) = R_o = R1,$$

and

$$\dot{R}(0) = R01 = 0.0.$$

Several additional terms must be defined before the reader can follow the program with ease. These terms are read in as input data. They are

TI4 = Initial Time = 0.0,

DR = ΔR = 0.0,

DRO = $\Delta \dot{R}$ = 0.0,

DT1 = Δt,

DT2 = $\Delta t/2$.

```
C     SOLUTION TO EQUATION OF MOTION FOR ISOTHERMAL BUBBLE GROWTH

  100 FORMAT(1X,8(E14.6,1X))
  200 FORMAT(D24.16)
  202 FORMAT(6X,3HTI1,12X,2HR1,12X,3HRO1,12X,4HROO1,12X,3HTR1,12X,
     13HTR3,12X,3HTR4,12X,4HPRES)
      DOUBLE PRECISION TI1,TI2,TI3,TI4,R1,R2,R3,R4,RO1,RO2,RO3,RO4,
     1RO01,RO02,RO03,RO04,TR1,TR2,TR3,TR4,TR5,TR6,TR7,TR8,TR9,TR10,
     1TM1,TM2,TM3,TM4,TM5,TM6,TM7,TM8,TM9,TM10,TE1,TE2,TE3,TE4,TE5,
     1TE6,TE7,TE8,TE9,TE10,TRM1,TRM2,TRM3,TRM4,TRM5,TRM6,TRM7,TRM8,
     1TRM9,TRM10,DT1,DT2,DR,DRO,C1,C2,C3,C4,C5,C6,C7,C8,C9,PRES,
     1TR81,TM81,TE81,TRM81
    5 READ(5,200)TI4,R1,RO1,DR,DRO,DT1,DT2,C1,C2,C3,C4,C5,C6,C7,C8,C9
      WRITE (6,200) R1,DT1,DT2,C1,C2,C3,C4,C5,C6,C7,C8,C9
      Z=0.0
      ZN=12.0
      WRITE(6,202)
    6 TI1=TI4
      R1=R1+DR
      RO1=RO1+DRO
      TR1=-(3.*RO1**2)/(2.*R1)
      TR2=R1**2
      TR3=-C1/TR2
      TR31=(-C7*RO1)/R1**2
      TR4=C2+C3+C1/C5-C8
      TR5=R1**4
      TR6=(TR4*C6)/TR5
      TR7=-C2/R1
      TR8=-C3/R1
      TR81=C8/R1
      TR9=C4*TI1
      TR10=TR8*DCOS(TR9)
      ROO1=TR1+C9*(TR3+TR31+TR6+TR7+TR81+TR10)
      PRES=C2+C3*DCOS(TR9)
      Z=Z+1.
      IF(Z-4500.) 1,1,5
    1 CONTINUE
      TI2=TI1+DT2
      R2=R1+RO1*DT2
      RO2=RO1+ROO1*DT2
      TM1=-(3.*RO2**2)/(2.*R2)
      TM2=R2**2
      TM3=-C1/TR2
      TM31=(-C7*RO2)/R2**2
      TM4=C2+C3+C1/C5-C8
      TM5=R2**4
      TM6=(TM4*C6)/TM5
      TM7=-C2/R2
      TM8=-C3/R2
      TM81=C8/R2
      TM9=C4*TI2
      TM10=TM8*DCOS(TM9)
      ROO2=TM1+C9*(TM3+TM31+TM6+TM7+TM81+TM10)
      TI3=TI1+DT2
      R3=R1+RO2*DT2
```

```
      R03=R01+R002*DT2
      TE1=-(3.*R03**2)/(2.*R3)
      TE2=R3**2
      TE3=-C1/TE2
      TE31=(-C7*R03)/R3**2
      TE4=C2+C3+C1/C5-C8
      TE5=R3**4
      TE6=(TE4*C6)/TE5
      TE7=-C2/R3
      TE8=-C3/R3
      TE81=C8/R3
      TE9=C4*TI3
      TE10=TE8*DCOS(TE9)
      R003=TE1+C9*(TE3+TE31+TE6+TE7+TE81+TE10)
      TI4=TI1+DT1
      R4=R1+R03*DT1
      R04=R01+R003*DT1
      TRM1=-(3.*R04**2)/(2.*R4)
      TRM2=R4**2
      TRM3=-C1/TRM2
      TRM31=(-C7*R04)/R4**2
      TRM4=C2+C3+C1/C5-C8
      TRM5=R4**4
      TRM6=(TRM4*C6)/TRM5
      TRM7=-C2/R4
      TRM8=-C3/R4
      TRM81=C8/R4
      TRM9=C4*TI4
      TRM10=TRM8*DCOS(TRM9)
      R004=TRM1+C9*(TRM3+TRM31+TRM6+TRM7+TRM81+TRM10)
      DR=(DT1/6.)*(R01+2.*R02+2.*R03+R04)
      DR0=(DT1/6.)*(R001+2.*R002+2.*R003+R004)
      ZN=ZN+1.
      IF(ZN-10.) 6,3,4
    3 WRITE(6,100)TI1,R1,R01,R001,TR1,TR6,TR81,PRES
      ZN=0.0
      GO TO 6
    4 WRITE(6,100)TI1,R1,R01,R001,TR1,TR6,TR81,PRES
      ZN=0.0
      GO TO 6
   25 STOP
      END
```

APPENDIX C

7040 COMPUTER PROGRAM FOR POLYTROPIC CHANGES DURING BUBBLE GROWTH

7040 COMPUTER PROGRAM FOR POLYTROPIC CHANGES DURING BUBBLE GROWTH

This computer program is the solution to equation (3-15) for polytropic changes within a bubble. Equation (3-15) was written in the following form to facilitate programming.

$$\ddot{R} = -\frac{3}{2}\frac{(\dot{R})^2}{R} + C9 \cdot \left[-\frac{2\sigma}{R^3} - C7\,\frac{\dot{R}}{R^2} + [C2 + C3 + C1/C5 - C8]\cdot \frac{R_o^{3PN}}{R^{3PN+1}} + \frac{p_v}{R} - \frac{C2}{R} - \frac{C3}{R}\,\mathrm{Cos}\,(C4 \cdot \mathrm{Time})\right], \quad (C\text{-}1)$$

where

$C1 = 2\sigma(T_o)$, PN = Polytropic Constant,

$C2 = p_A$, $C7 = 4\mu_L$,

$C3 = p_o$, $C8 = p_v(T_o)$,

$C4 = \omega$, $C9 = 1/\rho_L$.

$C5 = R_o$,

The initial conditions were

$$R(0) = R_o,$$

and

$$\dot{R}(0) = \ddot{R}(0) = 0.$$

Thus, $R1 = R_o$ and $R01 = \dot{R}(0) = 0$.

Several additional terms must be defined before the reader

can follow the program. These terms are read in as input data. They are

TI4 = 0.0 = Initial Time,

DR = 0.0 = ΔR,

DRO = 0.0 = $\Delta \dot{R}$,

DT1 = Δt,

DT2 = $\Delta t/2$,

and

TO = Temperature at time of zero in ^{o}K.

```
C     SOLUTION TO EQUATION OF MOTION FOR NONISOTHERMAL BUBBLE GROWTH

  100 FORMAT(1X,8(E14.6,1X))
  200 FORMAT(D24.16)
  202 FORMAT(6X,3HTI1,12X,2HR1,12X,3HR01,12X,4HR001,12X,2HT1,12X,
     13HCX1,12X,3HPV1,12X,4HPRES)
      DOUBLE PRECISION TI1,TI2,TI3,TI4,R1,R2,R3,R4,R01,R02,R03,R04,
     1R001,R002,R003,R004,TR1,TR2,TR3,TR4,TR5,TR6,TR7,TR8,TR9,TR10,
     1TM1,TM2,TM3,TM4,TM5,TM6,TM7,TM8,TM9,TM10,TE1,TE2,TE3,TE4,TE5,
     1TE6,TE7,TE8,TE9,TE10,TRM1,TRM2,TRM3,TRM4,TRM5,TRM6,TRM7,TRM8,
     1TRM9,TRM10,DT1,DT2,DR,DRO,C1,C2,C3,C4,C5,C6,C7,C8,C9,PRES,
     1TR81,TM81,TE81,TRM81,TX1,TX2,TX3,TX4,TX5,PN,TO,T1,T2,T3,T4,CX1,
     1CX2,CX3,CX4,PV1,PV2,PV3,PV4,T1X,T2X,T3X,T4X,PVX1,PVX2,PVX3,PVX4,
     1DT3,DT4
    5 READ(5,200)TI4,R1,R01,DR,DRO,DT1,DT2,C1,C2,C3,C4,C5,PN,C7,C8,C9,
     1TO,DT3,DT4
      WRITE(6,200)TI4,R1,R01,DR,DRO,DT1,DT2,C1,C2,C3,C4,C5,PN,C7,C8,C9
      Z=0.0
      ZN=12.0
      RN=0.0
      WRITE(6,202)
      TX1=DEXP(3.0*PN*(DLOG(C5)))
      TX2=3.0*PN
      TX3=3.0*(1.0-PN)
      TX4=C2+C3+(C1/C5)-C8
      TX5=TX1*TX4
    6 TI1=TI4
      R1=R1+DR
      R01=R01+DRO
      T1=TO*(DEXP(TX3*(DLOG(R1/C5))))
      TR1=-(3.*R01**2)/(2.*R1)
      TR2=R1**2
      CX1=237.5280000000-0.3142340000*T1
      TR3=-CX1/TR2
      TR31=(-C7*R01)/R1**2
      TR5=R1*(DEXP(TX2*(DLOG(R1))))
      TR6=TX5/TR5
      TR7=-C2/R1
      TR8=-C3/R1
      T1X=T1-273.161111000000
      PVX1=4.47388000+0.39396000*T1X+0.00382000*(T1X**2)+
     10.00045000*(T1X**3)
      PV1=1333.25511*PVX1
      TR81=PV1/R1
      TR9=C4*TI1
      TR10=TR8*DCOS(TR9)
      R001=TR1+C9*(TR3+TR31+TR6+TR7+TR81+TR10)
      PRES=C2+C3*DCOS(TR9)
      RN=RN+1.0
      IF(RN-2000.) 9,9,8
    8 DT1=DT3
      DT2=DT4
    9 Z=Z+1.
      IF(Z-6000.) 1,1,5
    1 CONTINUE
```

```
      TI2=TI1+DT2
      R2=R1+RO1*DT2
      RO2=RO1+ROO1*DT2
      T2=TO*(DEXP(TX3*(DLOG(R2/C5))))
      TM1=-(3.*RO2**2)/(2.*R2)
      TM2=R2**2
      CX2=237.5280000000-0.3142340000*T2
      TM3=-CX2/TM2
      TM31=(-C7*RO2)/R2**2
      TM5=R2*(DEXP(TX2*(DLOG(R2))))
      TM6=TX5/TM5
      TM7=-C2/R2
      TM8=-C3/R2
      T2X=T2-273.161111000000
      PVX2=4.47388000+0.39396000*T2X+0.00382000*(T2X**2)+
     10.00045000*(T2X**3)
      PV2=1333.255110*PVX2
      TM81=PV2/R2
      TM9=C4*TI2
      TM10=TM8*DCOS(TM9)
      ROO2=TM1+C9*(TM3+TM31+TM6+TM7+TM81+TM10)
      TI3=TI1+DT2
      R3=R1+RO2*DT2
      RO3=RO1+ROO2*DT2
      T3=TO*(DEXP(TX3*(DLOG(R3/C5))))
      TE1=-(3.*RO3**2)/(2.*R3)
      TE2=R3**2
      CX3=237.5280000000-0.3142340000*T3
      TE3=-CX3/TE2
      TE31=(-C7*RO3)/R3**2
      TE5=R3*(DEXP(TX2*(DLOG(R3))))
      TE6=TX5/TE5
      TE7=-C2/R3
      TE8=-C3/R3
      T3X=T3-273.161111000000
      PVX3=4.47388000+0.39396000*T3X+0.00382000*(T3X**2)+
     10.00045000*(T3X**3)
      PV3=1333.255110*PVX3
      TE81=PV3/R3
      TE9=C4*TI3
      TE10=TE8*DCOS(TE9)
      ROO3=TE1+C9*(TE3+TE31+TE6+TE7+TE81+TE10)
      TI4=TI1+DT1
      R4=R1+RO3*DT1
      RO4=RO1+ROO3*DT1
      T4=TO*(DEXP(TX3*(DLOG(R4/C5))))
      TRM1=-(3.*RO4**2)/(2.*R4)
      TRM2=R4**2
      CX4=237.5280000000-0.3142340000*T4
      TRM3=-CX4/TRM2
      TRM31=(-C7*RO4)/R4**2
      TRM5=R4*(DEXP(TX2*(DLOG(R4))))
      TRM6=TX5/TRM5
      TRM7=-C2/R4
      TRM8=-C3/R4
```

```
      T4X=T4-273.161111000000
      PVX4=4.47388000+0.39396000*T4X+0.00382000*(T4X**2)+
     10.00045000*(T4X**3)
      PV4=1333.255110*PVX4
      TRM81=PV4/R4
      TRM9=C4*TI4
      TRM10=TRM8*DCOS(TRM9)
      R004=TRM1+C9*(TRM3+TRM31+TRM6+TRM7+TRM81+TRM10)
      DR=(DT1/6.)*(R01+2.*R02+2.*R03+R04)
      DR0=(DT1/6.)*(R001+2.*R002+2.*R003+R004)
      ZN=ZN+1.
      IF(ZN-10.) 6,3,4
    3 WRITE(6,100)TI1,R1,R01,R001,T1,CX1,PV1,PRES
      ZN=0.0
      GO TO 6
    4 WRITE(6,100)TI1,R1,R01,R001,T1,CX1,PV1,PRES
      ZN=0.0
      GO TO 6
   25 STOP
      END
```

APPENDIX D

CALIBRATION OF METERING VENTURI

CALIBRATION OF METERING VENTURI

Tap water was used to calibrate the metering venturi over a range of flow rates from 5 to 95 gallons per minute. The pressure drop between the inlet and throat was measured with a U-tube manometer. Two different manometer fluids were used. Mercury was used as the manometer fluid when the pressure drop was greater than 2 inches of mercury. "Meriam" 1.75 specific gravity manometer fluid was used when the pressure drop was less than about 2 inches of mercury. The system used to calibrate the venturi is shown in Figure 69.

The metering venturi was calibrated in the actual position with respect to other parts of the tunnel. This was done to eliminate any error that might occur due to a change in the flow pattern at the entrance to the venturi.

The calibration tests were performed by measuring the time required for 800 pounds of water to enter a weighing tank. A Fairbanks Morse balance was set so that it became balanced a few seconds after flow was switched into the measuring tank. The timer was started when the balance passed through the equilibrium point. The necessary weights were then added to the balance to allow 800 pounds of water to enter the weighing tank. When the balance reached the

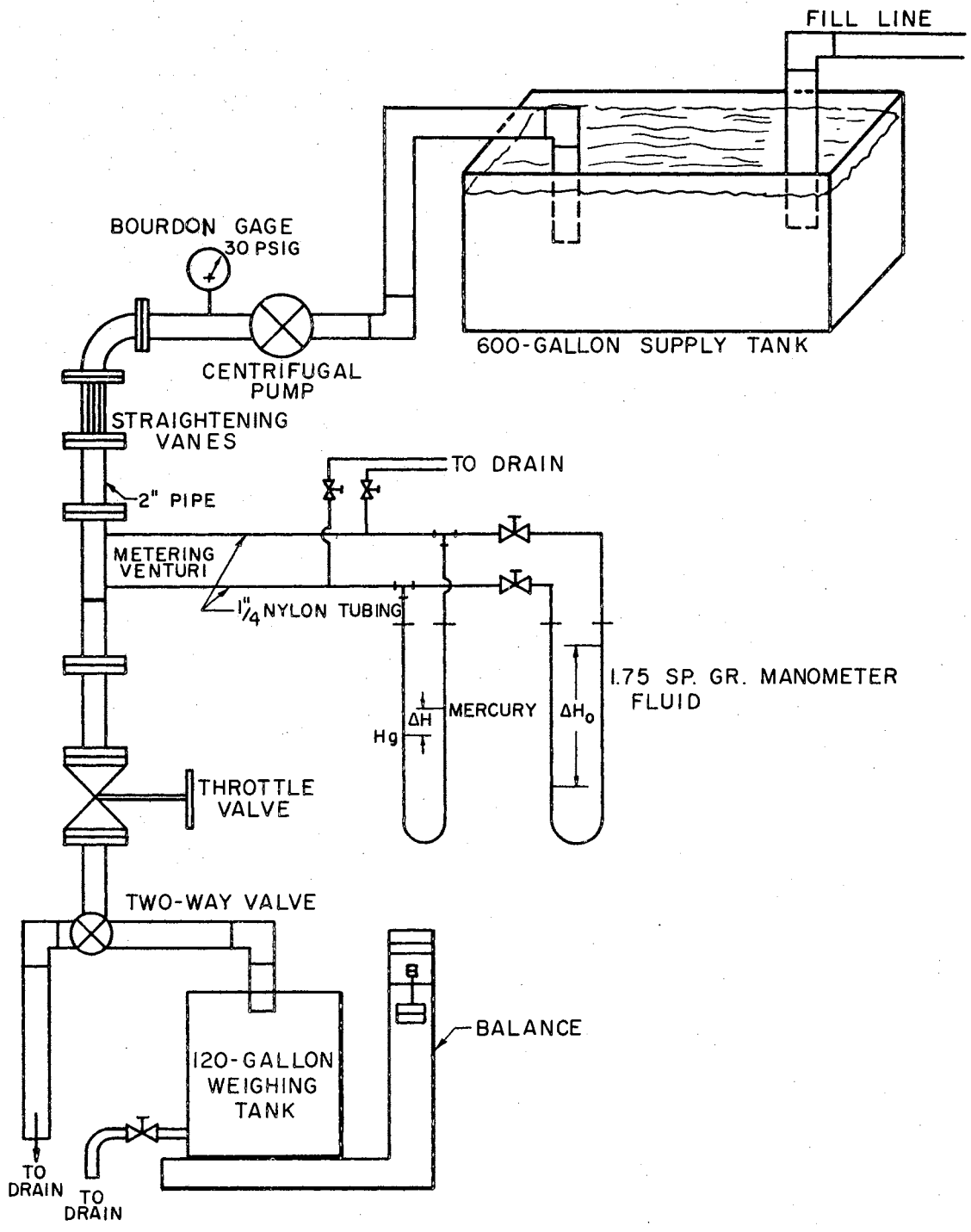

Figure 69. Schematic of Facility Used to Calibrate Metering Venturi

equilibrium position for the second time, the timer was stopped.

During each run the pressure drop across the metering venturi and the temperature of the water were recorded. The temperature was measured with a calibrated mercury thermometer to within one tenth of a degree.

The pump suction head was maintained constant by maintaining a constant level in the supply tank. A Bourdon-tube pressure gage was mounted on the downstream side of the centrifugal pump. The discharge pressure was constant for any given run. However, this pressure varied about 5 psi over the range of flow rates used to calibrate the venturi.

Figure 70 shows the variation of pressure drop across the venturi with flow rate. This curve indicates the repeatability of the data.

The effect of changes in fluid properties upon the actual velocity can be taken into account by a relationship between the discharge coefficient, C_D, and the Reynolds number, R_E. Thus, the experimental data shown in Figure 70 were reduced and plotted in Figure 71. The method of least squares was used to obtain a relationship between the discharge coefficient and the Reynolds number. This relationship is

$$C_D = 0.41509 + 0.19480\ (\log_{10} R_E) - 0.01671\ (\log_{10} R_E)^2. \quad \text{(D-1)}$$

The maximum deviation between the predicted and actual discharge coefficients was less than 0.005. Thus, the actual velocities, calculated through the use of equation (D-1), are in error by less than 1 per cent.

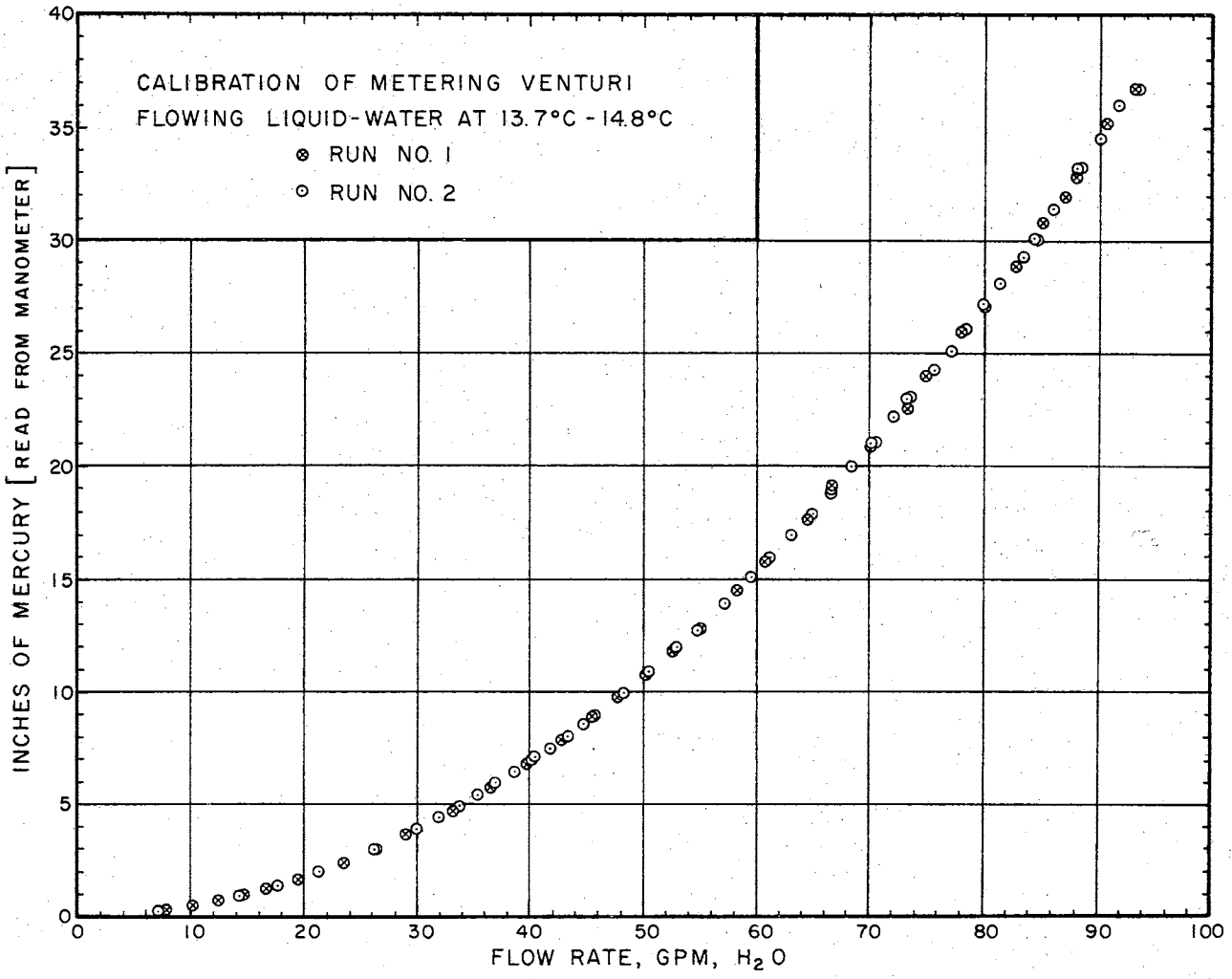

Figure 70. Variation of Pressure Drop With Flow Rate

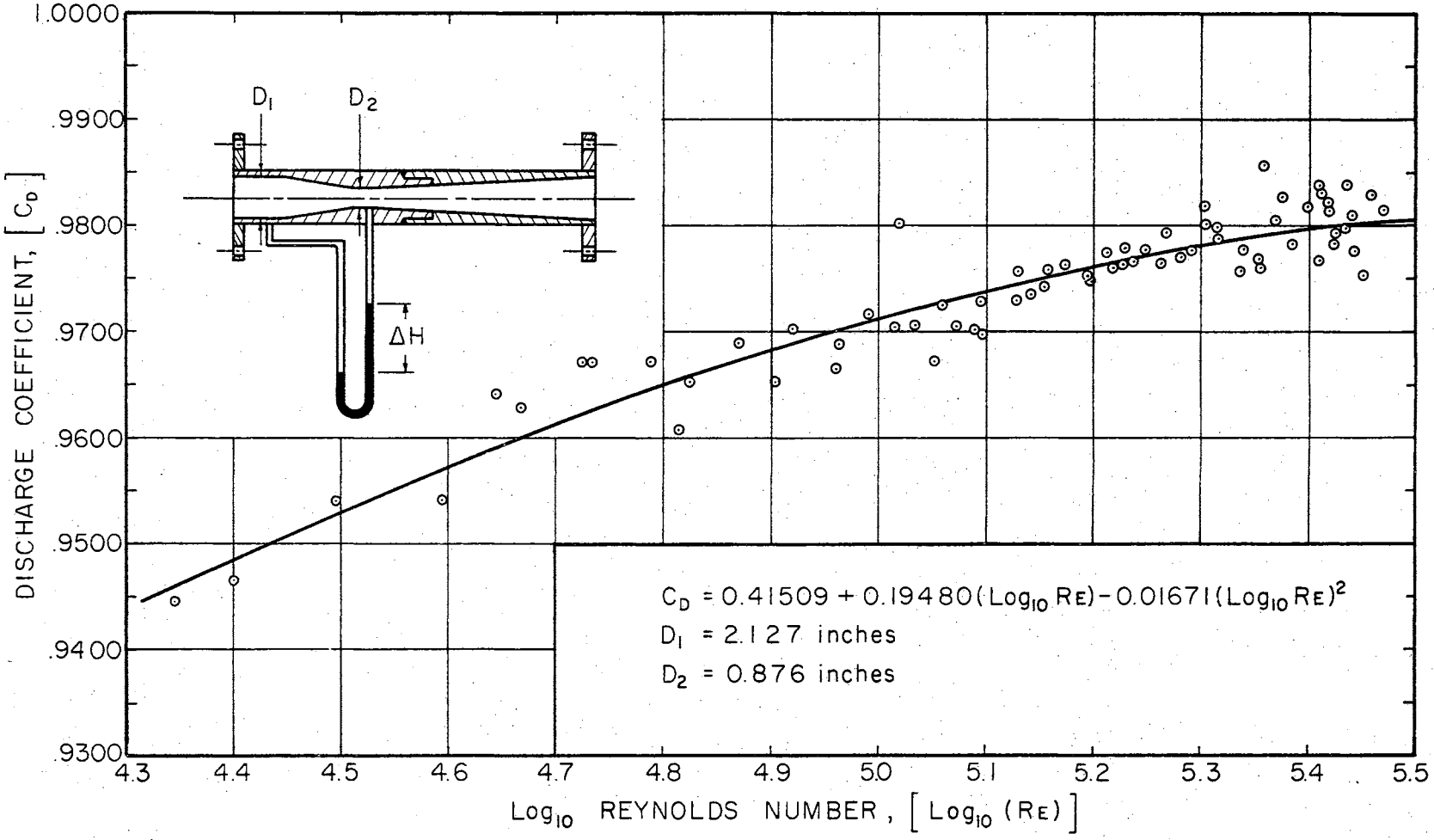

Figure 71. Calibration Curve for Metering Venturi

APPENDIX E

METHOD USED TO DETERMINE THE DISSOLVED OXYGEN CONTENT OF WATER

METHOD USED TO DETERMINE THE DISSOLVED OXYGEN CONTENT OF WATER

The Alsterberg modification of the Winkler method was used to determine the dissolved oxygen content of the tunnel water [49]. The details of preparing the reagents and running the test are reported below.

Reagents

Manganous Sulfate Solution

This solution was prepared by dissolving 364 grams of $MnSO_4 \cdot H_2O$ in distilled water, filtering, and diluting to 1 liter. When uncertainty exists regarding the water of crystallization, a solution of equivalent strength may be obtained by adjusting the specific gravity of the solution to a value of 1.270 at 20°C. The manganous sulfate solution should liberate not more than a trace of iodine when added to an acidified solution of potassium iodide.

Alkali-Iodide-Azide Reagent

This reagent was prepared by dissolving 500 grams of NaOH and 135 grams of NaI in distilled water and diluting to 1 liter. A solution of 10 grams of NaN_3 dissolved in 40 milliliters (ml) of distilled water was added to the above

solution.

Concentrated Sulfuric Acid

The strength of this acid is about 36N.

Starch Solution

This reagent was prepared by mixing 5 to 6 grams of soluble potato starch with a small quantity of distilled water. This emulsion was poured into 1 liter of boiling distilled water, and the mixture was allowed to boil for a few minutes. The mixture was allowed to cool and settle overnight before the clear supernatant was removed. The clear supernatant was preserved by the addition of a few drops of toluene.

Standard Sodium Thiosulfate Solution, 0.025N

This solution was prepared by dissolving 6.205 grams of $Na_2S_2O_3 \cdot 5H_2O$ in freshly boiled and cooled distilled water and diluting to 1,000 ml. The solution was preserved by adding 0.4g of NaOH per liter.

Testing Procedure

The samples of tunnel water were collected in 300-ml glass bottles. Two milliliters of the $MnSO_4$ solution, followed by two milliliters of the alkali-iodide-azide reagent, were added to the samples by placing the end of the pipettes well below the surface of the liquid. The

300-ml bottles were restoppered with care so that no air bubbles would be trapped. The bottles were inverted several times to obtain a homogeneous mixture. These samples were allowed to settle until at least 100 ml of clear supernatant could be observed. At this point the stoppers were removed from the bottles and 2 ml of concentrated H_2SO_4 were immediately added to each by allowing the acid to run down the neck of each bottle. The bottles were restoppered, and the acid was mixed by gentle inversion until dissolution was complete. The iodine was uniformly distributed throughout the bottles before the amount needed for titration was decanted. This corresponds to 200 ml of the original sample. Thus, the volume taken for titration was 203 ml.

The 203 ml sample was titrated with 0.025N thiosulfate to a pale straw color. Then, approximately 2 ml of freshly prepared starch solution was added, and the titration was continued until the first disappearance of the blue color.

Oxygen Content

Since 1 ml of 0.025N $Na_2S_2O_3$ is equivalent to 0.2 mg of dissolved oxygen (DO), each milliliter of sodium thiosulfate used is equivalent to 1 mg/liter of DO if a volume of 200 ml of original sample is titrated.

APPENDIX F

VELOCITY AT ANY POINT IN TEST SECTION

```
C     VELOCITY AT ANY POINT IN TEST SECTION, FT/SEC

C     N = NUMBER OF DIAMETERS
C     DD(I) = AREA IN SQUARE INCHES
C     GELL = READING IN INCHES OF LEFT LEG
C     RLEG = READING IN INCHES OF RIGHT LEG
C     VOLTM = READING OF DIGITAL VOLTMETER IN MILLIVOLTS
   50 FORMAT(I2)
  100 FORMAT(F16.8)
  200 FORMAT(I2,2X,F14.6,2X,F14.6,2X,F14.6)
  300 FORMAT(1H0,11H RUN NUMBER,4XI2)
  301 FORMAT(1H0,25X,5HTEMPF,12X,4HROWL,12X,4HDELT,12X,5HCDACT)
  400 FORMAT(1H0,1HV,I2,1H=,F12.4,6X,F12.4,4X,F12.4,4X,F12.4,4X,F12.4)
      DIMENSION DD(2),V(2)
      READ(5,50) N
      DO 4 I=1,N
      READ(5,100) DD(I)
    4 CONTINUE
    5 READ(5,200) NORUN,GELL,RLEG,VOLTM
      IF(NORUN.EQ.0) GO TO 40
      WRITE(6,300) NORUN
      WRITE(6,301)
      TEMPF=35.64092900+39.17030700*VOLTM+3.82124360*(VOLTM**2)
     1-1.09680340*(VOLTM**3)
      SPVOL=15.99722900-0.00037980*TEMPF+0.00001744*(TEMPF**2)
      ROWL=(1000.0000)/(SPVOL)
      TEMPC=(TEMPF-32.0000)/(1.8000000)
      C=TEMPC-8.43500
      D=(8078.400+(C**2))**0.50
      VSCOS=14.8800*(2.14820*(C+D)-120.000)
      CDASU=0.97000
      DELT=GELL+RLEG
      DELTH=DELT/12.0000
    6 VELOC=CDASU*((832.81500*DELTH)**0.50)
      REY=ROWL*VELOC*VSCOS*0.073000
      X=ALOG10(REY)
      CDACT=0.415090+0.19480*X-0.016710*(X**2)
      B=CDACT-CDASU
      B=ABS(B)
      IF(B-0.000010) 20,20,10
   10 CDASU=CDACT
      GO TO 6
   20 I=1
      DO 30 I=1,N
      V(I)=(0.602695190/DD(I))*VELOC
      WRITE(6,400) I,V(I),TEMPF,ROWL,DELT,CDACT
   30 CONTINUE
      GO TO 5
   40 STOP
      END
```

VITA

GLENNON MAPLES

Candidate for the Degree of

Doctor of Philosophy

Thesis: THEORETICAL AND EXPERIMENTAL INVESTIGATIONS OF THE INCEPTION OF CAVITATION

Major Field: Mechanical Engineering

Biographical:

Personal Data: Born August 24, 1932, in Broom, Mississippi, the son of George and Betty Maples.

Education: Attended elementary school in Broom, Mississippi and graduated from Broom High School in April, 1950; received the Associate of Arts degree in May, 1952, from Perkinston Junior College, Perkinston, Mississippi; received the Bachelor of Science degree in May, 1955, and the Master of Science degree in August, 1961, from Mississippi State University, State College, Mississippi; attended the University of Florida (1962-63), Gainesville, Florida; completed the requirements for the Degree of Doctor of Philosophy in September, 1966.

Professional Experience: Employed from June, 1955, to August, 1958, by Shell Oil Company, as a Mechanical Engineer; from September, 1958, to June, 1961, employed by the Drawing Department at Mississippi State University as an Instructor; employed by the Mechanical Engineering Department at Mississippi State University, as an Assistant Professor, from September, 1961, to June, 1962; from September, 1962, to July, 1963, employed by the Mechanical Engineering Department at the University of Florida as a Research Associate; employed by the Mechanical Engineering Department at Oklahoma State University as a Graduate Assistant, from September, 1963, to June, 1964; employed by the Mechanical Engineering Department at Oklahoma State University, as a Research Assistant, from September, 1964, to September, 1966.